Platinum and Gold Species on Non-Reducible Oxides as Active and Stable Catalysts for the Low-Temperature Water-Gas Shift Reaction

A thesis

Submitted by

Yuan Wang

In partial fulfillment of the requirements

for the degree of

Master of Science

in

Chemical Engineering

TUFTS UNIVERSITY

August 2012

Advisor: Professor Maria Flytzani-Stephanopoulos

This thesis is dedicated to my Mom,

for her love, endless support and trust in me.

Acknowledgements

First and foremost, I would like to thank my advisor Professor Maria Flytzani-Stephanopoulos for her guidance and support throughout this thesis research. Professor Stephanopoulos has shown the passion, erudition and insight in the chemical engineering research, which drive and encourage me to this point. A special thank goes to Professor Howard Saltsburg for his critical inputs and honest suggestions. I would also like to thank my thesis committee members Professor Terry Haas and Professor Hyunmin Yi for their valuable insights and commentary.

I am appreciative of all my colleagues in the Nano Catalysis & Energy Lab at Tufts University, for their friendship and help in these years. I gratefully acknowledge Dr. Yanping Zhai who served as my mentor throughout this project; She shared the experience in experiments, provided instrumental assistance and was patient to all my questions in study and research. Additionally, I am very thankful to Chongyang Wang, Branko Zugic and Dr. Herui Dou, for their help in sample analysis at the MIT and Brookhaven National Lab.

Finally, I especially appreciate my Mom and my husband for their love, support and trust; I would not be here without you. I also want to thank all my new friends at Tufts; you bring me the happiest time in study abroad.

I acknowledge the financial support of this work from the U.S. Department of Energy/Basic Energy Sciences (grant no. DE-FG02-05ER15730) and AFOSR (MURI) (grant No. FA9550-08-1-0309). I also thank the Micromeritics Corporation for supplying the AutoChem II 2920 as part of their Instrument Grant Program.

Abstract

Hydrogen is of interest because it is a clean, safe and efficient energy source. For the low-temperature fuel cell application, the water-gas shift (WGS) reaction is an important step in upgrading hydrogen streams produced from fuel reforming operations. It has been challenging to develop low-temperature WGS catalysts that are both highly active and stable at the operation conditions of proton exchange membrane (PEM) fuel cell systems. The current catalysts used in industrial WGS reactors, $Cu/ZnO/Al_2O_3$, are unsuitable for fuel cell systems because they are pyrophoric, lack thermal stability, and require activation procedures. Noble metal (Au, Pt, Pd etc.) on oxide support (CeO_2, TiO_2, FeO_x etc.) catalysts have emerged as attractive catalyst alternatives possessing high activity and stability for the low-temperature WGS reaction. These have to be designed with trace amounts of valuable metals to be economical.

In this thesis, platinum and gold species on non-reducible silica and alumina supports were investigated as novel catalysts for the low-temperature WGS reaction. In particular, encapsulated platinum in the form of core-shell $Pt@SiO_2$ material was prepared by a reverse microemulsion technique, while supported gold was prepared by deposition on modified γ-alumina supports with OH-rich surfaces through various hydrothermal treatments. Addition of alkali ions, associating Pt and Au species with the OH-rich oxide support surfaces, rendered the corresponding $Pt\text{-}Na@SiO_2$ and $Na\text{-}Au/Al_2O_3$-OH samples active and stable catalysts for the low-temperature WGS reaction, whereas their alkali-free counterparts showed low activity and poor stability.

Samples were characterized by BET surface area, UV-Visible Spectroscopy (UV-Vis), X-ray diffraction (XRD), X-ray photoelectron spectroscopy (XPS), high resolution transmission electron microscopy (HRTEM) and CO chemisorption. Temperature-programmed reduction (TPR) measurements and cyclic TPR tests were conducted using the reactant CO as the reductant. Catalytic activities of the samples were evaluated for the WGS reaction under various gas conditions in temperature-programmed surface reaction (TPSR) and steady-state modes, and compared with other Pt- and Au-based catalysts prepared on various oxides supports by different methods.

The Pt-O_x(OH)-M or Au-O_x(OH)-M species, where M denotes an alkali ion, are concluded to be very promising for further development of low-temperature WGS reaction catalysts. The apparent activation energy, E_{app}, for the reaction is the same for these new catalysts and for other Pt- or Au-based catalysts previously reported. For the Pt-based catalysts, $E_{app} = 70 \pm 5$ kJ/mol, and for Au-based catalysts, $E_{app} = 45 \pm 5$ kJ/mol. This is true whether a reducible or a non-reducible support is used, the latter stabilized only with the help of alkali promoters. Hence, the active site comprises oxygen and hydroxyl groups, but is independent of the type of the support used.

Keywords: Pt catalyst, Au catalyst, encapsulation, core-shell, reverse microemulsion, hydrothermal treatment, alkali promotion, hydroxyl regeneration, water-gas shift reaction

Table of Contents

List of Tables

List of Figures

Chapter 1

Introduction

1.1 Background

Coal, petroleum, petroleum byproducts and natural gas are the main sources of energy in today's world economies. The growth of industrial economies and the consumption rate of natural resources lead to rapid depletion of conventional fossil fuels, estimated for petroleum in a few decades. Currently, we are facing the inefficiencies in fossil fuel utilization and atmospheric pollution adverse effects, especially in the developing world. As we step into the future, a major concern is the development of cleaner, safer and more efficient methods of generating energy. Converting over to a hydrogen-based economy has been a vision for several decades, and perhaps the 21st century will witness the realization of the hydrogen economy. While many elements needed for this realization are still untenable, one important link, i.e. the generator technology, is moving ahead at a faster pace, and is penetrating various market segments. This is the fuel cell technology, briefly considered below.

1.1.1 Proton exchange membrane fuel cell

A fuel cell is an electrochemical device that converts chemical energy directly into electrical energy. When oxidized by oxygen, hydrogen releases the highest amount of energy per unit mass of any fuel without generating greenhouse gases, thus achieving a

significant reduction in carbon dioxide emission to the atmosphere, at least at the end use point of the hydrogen gas. This process is most efficiently and cleanly conducted through fuel cells, which are more than twice as energy efficient as the internal combustion engine. A fuel cell consists of two electrodes sandwiched around an electrolyte. Oxygen passes over the cathode and hydrogen passes over the anode, generating electricity, water and heat. Due to its lower operating temperature, high efficiency and compact size, the proton exchange membrane (PEM) fuel cell is most attractive for residential heaters, transportation applications, and portable devices, such as laptop computers, cellular phones and other personal digital equipment.

A major drawback of hydrogen fuel is the fact that it is difficult to store it compactly and safely, so one of the most promising ways to overcome this is to produce H_2 on-site. Bulk hydrogen is usually generated from hydrocarbons, such as natural gas, coal and oil and may be also generated from an alcohol, such as methanol, in a fuel processor by stream reforming at high temperatures (200-900°C) to yield syngas. In another approach, partial oxidation of a fuel occurs when a sub-stoichiometric, fuel-rich fuel-air mixture is used in a reformer, creating a hydrogen-rich syngas. This step generates a gas mixture which contains 8-12% carbon monoxide as well as hydrogen and carbon dioxide. However, fuel processing for PEM fuel cells requires the complete removal of carbon monoxide down to less than 1-10 ppm, because CO is not only a criterion pollutant, but also a poison for the platinum catalyst of the fuel cell anode. Thus, in a second stage, hydrogen is upgraded through the water gas shift reaction to decrease the carbon monoxide level to less than 1%. To finally produce highly pure hydrogen, trace levels of CO could be reached by a preferential oxidation of carbon monoxide

cleanup system downstream. Of course, the identification of a new very active catalyst that can reach equilibrium CO conversions at ~ 100°C, would achieve the trace levels of CO in one stage and that would be preferable.

The overall fuel processing reactions are given below:

Steam Reforming (SR):	$CH_{2n} + H_2O \rightarrow CO + (n+1)\ H_2$	(1)
Partial Oxidation (POX):	$C_mH_n + m/2\ O_2\ (+ N_2) \rightarrow m\ CO + n/2\ H_2\ (+ N_2)$	(2)
Water Gas Shift Reaction (WGS):	$CO + H_2O \rightarrow CO_2 + H_2$	(3)
Preferential CO Oxidation (PROX):	$CO + ½\ O_2\ (+ H_2) \rightarrow CO_2\ (+H_2)$	(4)

1.1.2 Water-gas shift reaction

The water-gas shift (WGS) reaction is an important industrial reaction, in which carbon monoxide reacts with water to form carbon dioxide and hydrogen. It was discovered by the Italian physicist Felice Fontana in 1780, but it was not applied in industry until 1914 when Bosch and Wild began using Fe/Cr catalysts to produce high purity hydrogen via the WGS reaction for ammonia synthesis [1]. The WGS reaction is always used in conjunction with steam reforming of natural gas or naphtha to upgrade hydrogen for the ammonia synthesis reactors, and to control the H_2/CO ratio to 2:1 for direct use in methanol synthesis reactors. Currently, more than 9 million tons H_2 are produced annually in the U.S. for industrial use.

$$\boldsymbol{CO + H_2O \leftrightarrow CO_2 + H_2}$$

$$\Delta H = -41.2\ kJ \cdot mol^{-1}$$

$$\Delta G = -28.6\ kJ \cdot mol^{-1}$$

The water-gas shift reaction is a reversible reaction, mildly exothermic, yielding -41.2 kJ of heat per mole. The equilibrium shifts to the right as temperature is lowered, so highly active catalysts operating in the low convenient temperature range (100-250 ^{o}C) are preferred. The current commercial WGS technology to upgrade hydrogen for chemicals production involves multiple stages/catalysts: (1) a high temperature WGS (HTS) stage is carried out at 310-450 ^{o}C promoted by iron-chromium oxide catalysts (Fe_2O_3/Cr_2O_3), close to equilibrium conditions and (2) a low temperature WGS (LTS) stage is carried out at (160-250 ^{o}C) on copper-zinc ($Cu/ZnO/Al_2O_3$) oxide catalysts; finally, when the feed contains appreciable amounts of sulfur, which can poison catalytic surfaces, Co/MoS catalysts are used, and are called sour gas shift catalysts [2]. While the Fe-Cr and Cu/ZnO have become industry standards for large scale H_2 production, they are not suitable for PEM fuel cell applications. The $Cu/ZnO/Al_2O_3$ itself is very sensitive to temperature excursions and air exposure (pyrophoric), and requires a controlled and elaborate activation, such as in situ pre-reduction [3-5].

For realistic WGS reaction systems applied to fuel cells, the catalyst is still a technological bottle-neck. The designed catalysts should have high activity and good stability in a wide operating temperature window, and during the cyclic shutdown-startup operation. Additionally, they must meet safety requirements of non-pyrophoricity and water-and air-tolerance, and be able to withstand rapid start-up and shut-down cycles without elaborate pre-reduction procedures, and of course be economical.

To meet these requirements, new WGS catalyst systems are under development with the PEM fuel cell operation conditions in mind. Precious metal-based catalysts (mainly platinum and gold), not suffering from the above drawbacks, have been under

intensive investigation during the last decade for their potential use in the upgrade of hydrogen streams for fuel cell applications.

1.2 Literature review

1.2.1 Platinum-based catalysts for the low-temperature WGS reaction

The supported precious metal catalysts are more expensive than the commercially used copper-based catalysts, but they still are being developed as better alternatives to Cu/ZnO, especially in terms of their stability, for PEM fuel cell applications [6]. Pt-based catalysts can be effectively used for the selective removal of carbon monoxide in hydrogen-rich streams feeding fuel cells and there is a lot of experience from the use of Pt/CeO_2 catalysts for the WGS reaction [7, 8] in the automotive three-way catalytic converters. Compared to the commercial Cu/ZnO catalysts, Pt/CeO_x group of catalysts are being developed as more active and stable materials for the low-temperature WGS reaction [9, 10].

The importance of noble metal and oxide support interaction for the WGS reaction has been discussed extensively in the literature [11-15]. Nanoscale ceria is the support of choice because of its high concentration of surface oxygen defects and hence, its ability to atomically disperse and stabilize active noble metal species [7-9, 16-22]. Work done by Fu *et al.* documented the importance of such interaction between the noble metal (Au or Pt) and the oxygen of ceria, by showing that weakly-bound metallic gold or platinum nanoparticles on ceria are spectator species for the reaction, while the

atomically dispersed [Au-O_x]-Ce or [Pt-O_x]-Ce species, strongly bound on ceria, are the active sites [16, 21, 22].

A great deal of research has been devoted to tailor the synthesis of the catalysts in order to maximize such strongly interacting species on supports. Some conventional techniques, i.e. deposition-precipitation, co-precipitation or incipient wetness impregnation (IMP), are widely used to prepare Pt on different oxide supports [4, 23, 24], especially reducible oxides, such as ceria [15, 16]. Moreover, novel synthesis techniques were applied to get a higher level of control required to systematically investigate the metal-support interaction and to maximize the metal-support interface, i.e. ceria-supported Pt, Pd, and Rh catalysts prepared by chemical vapor deposition [25] and ceria-encapsulated nonmetallic Pt species prepared by reverse microemulsion reported by Yeung *et al.* in 2005 [9].

Due to the rising price of the rare earth oxides, and their propensity to forming carbonates at low temperatures in realistic fuel gas mixtures [20], there is interest in finding alternative Earth-abundant oxide supports for the noble metals, potentially using promoters to achieve the kind of stable atomic dispersions afforded by ceria. It is also of fundamental interest to reproduce the type of active metal site on ceria on other supports via the use of alkali and alkaline-earth promoters. The promotion effects of alkali metals have been addressed in the literature to tune the performance of supported metal catalysts for the reactions involved in the fuel processing, such as methanol steam reforming [26], preferential CO oxidation [27-29], and of course the WGS reaction [30-34]. Alkali additives have also been widely used as promoters for Ru catalysts in industrial processes, such as the synthesis of ammonia [35, 36]. The role of additives is understood either as an ensemble

effect in stabilization of the active metal sites or an electronic (ligand) effect.

For the low-temperature WGS reaction, alkali promotion was studied on Pt-based catalysts with reducible or partially reducible oxide supports such as titania [31-33], zirconia [37], and ceria [26]. However, the interpretation of active site is complicated by the non-zero activity of Pt on these (alkali-free) supports. Independently from the work cited above, Pierre in his Master's thesis was first to identify that that alkali ions can also significantly boost the catalytic performance of Pt catalysts on inert oxide supports, such as SiO_2 [38]. Extension of this work by Zhai *et al.* has been published recently to show that alkali-promoted Pt on both silica and alumina supports can be prepared with activity comparable to Pt/CeO_2 catalysts [34]. Moreover, it was proposed that the alkali-promoted $Pt\text{-}(OH)_x$ species were the active sites for the WGS reaction independent of the type of support [34]. The degree of such promotion depends on the amount of the alkali additive, with over-doping having a negative effect [39, 40]. The similarity of the apparent activation energy for all the Pt catalysts tried on all supports is strongly arguing for a common Pt-based active site. The analog to mononuclear metal complexes in homogeneous catalysis is intriguing.

These findings are useful for the design of highly active and stable WGS catalysts that contain only trace amounts of a precious metal without the need for a reducible oxide support such as ceria. Such exciting results have motivated us to investigate further about how the alkali metal influences the catalytic performance of Pt (or Au) catalysts supported on inert oxides for the WGS reaction. The investigation of an alkali effect on gold catalysts for the WGS reaction has not yet been reported in the literature.

1.2.2 Gold-based catalysts for the WGS reaction

For a long time, gold was considered to be one of the chemically inert and catalytically inactive metals due to its poor chemisorptive capacity of the bulk state. However, more than two decade ago, it was established that gold catalysts at the nanoscale exhibit very high catalytic activity, e.g. for the CO oxidation reaction, when the gold particles are smaller than approximately 4 nm and highly dispersed on the oxide supports [41]. Haruta was the first to show that supported nanoscale gold catalysts could be effective for the oxidation of carbon monoxide at ambient temperature, and even below 0 ^{o}C [42]. After this key paper, a large volume of literature appeared in the following ten years investigating the properties of supported gold catalysts [43-47] and a variety of supported nanoscale-gold catalysts have been synthesized and applied to various reactions, including selective hydrogenations in addition to oxidation-type reactions. Gold was also examined as a new catalyst for the water-gas shift reaction. Sakurai et al. reported that Au nanoparticles supported on TiO_2 comprise an active catalyst, exhibiting low-temperature activity both for the forward and the reverse water gas shift reaction [43]. Tabakova et al. examined supported gold catalysts Au/ZrO_2, Au/Fe_2O_3, Au/ZnO for the WGS reaction, and concluded that the catalytic activity of the gold/metal oxide catalysts depends strongly not only on the dispersion of the gold particles but also on the state and the structure of the support [48]. The same conclusion had been reached earlier by Andreeva *et al.* for Au/FeO_x catalysts [44]. The Tufts group was the first to report on the very high activity of Au/CeO_2 catalysts in 2001, and also found that the structure of ceria affected the catalyst activity [49].

A great volume of research has been devoted to understanding the gold-support interaction. Nanostructured Au/CeO_2 was very important for activity as reported by Fu *et al.* [49]: if ceria was annealed and did not have enough "interacting" sites with gold, the catalyst was of low activity. Soon after the Tufts group reported that metallic gold nanoparticles and weakly bound gold species on ceria played no catalytic role[16]. Indeed when the gold nanoparticles and clusters (at 4.5% loading) were removed by a sodium cyanide leaching process, leaving behind only the residual (< 0.5%) cationic gold species associated with ceria, $[Au\text{-}O_x]\text{-}Ce$, both the mass- and area- normalized reaction rates remained the same. This was also true for the Pt/CeO_2 catalysts [16]. Furthermore, Deng *et al.* studied the Au/FeO_x system for WGS reaction [50] and reported that the areal reaction rates were about the same on either the CeO_2- and Fe_2O_3- supported Au catalysts, which indicates that the same, support-independent $Au\text{-}(OH)_x$ species bound onto the Ce or Fe cations through oxygen atoms are the active sites for the low-temperature WGS reaction.

Recent studies have focused on the modification of supports to keep the Au dispersed, primarily for the dry CO oxidation reaction, where Au destabilization, *e.g.* on TiO_2, takes place even with storage [51]. Veith *et al.* found that the surface hydroxyl groups were essential for stabilizing the gold clusters on TiO_2 against coarsening under ambient conditions [52]. This stabilization was not permanent however, disappearing after 10-20 days [51]. Haruta *et al.* found that for the gold supported on lanthanum oxide, a hydroxide, $AuLa_2(OH)_9$, which was prepared by co-precipitation, showed markedly high catalytic activity for CO oxidation (100% conversion) at a temperature as low as 193 K after reduction at 373 K [53]. The catalyst mainly consists of Au^0 clusters smaller than 1.5 nm, which are well-mixed with $La(OH)_3$ containing isolated $Au(OH)_3$ species. So, here

we see that the notion of gold nanoparticles being active for the CO oxidation reaction has evolved over the last two decades. Sub-nm, few-atom clusters and positively charged single gold atoms properly stabilized on the carrier surfaces are now the focus of intensive studies for both the CO oxidation and the WGS reactions.

In the last decade there has been a growing interest in the effect of alkali (earth) metals on the catalytic performance of Au-based catalysts. The addition of alkali (earth) metal oxides may be beneficial for or detrimental to the catalyst performance, according to some reports. Nieuwenhuys and co-workers have used alkali/alkaline-earth metals as structural promoters to stabilize gold clusters in the preferential oxidation of CO in a H_2-rich gas mixture [54]. It was also reported that Au supported on $Mg(OH)_2$, $Be(OH)_2$ or $La(OH)_3$ displays a high catalytic activity in CO oxidation, especially if the average size of the Au particles is around 2 nm [53, 55]. Moreover, the addition of MO_x (M: Rb, Li, Ba) to Au/Al_2O_3 is beneficial for the low-temperature CO oxidation [56]. But a negative effect of alkali ions has been also reported. For example, K was reported to act either as a promoter (low K/Au ratio) or a poison (higher K/Au ratio) for Au-Pt/CeO_2 catalyst for the WGS reaction [57]. If an optimum alkali loading exists, it is envisioned that further addition of the alkali may cover and otherwise mask the beneficial effect. In the work of Nieuwenhuys and his group, the catalytic performance of Au/Al_2O_3 in CO oxidation has been found to improve by using alkali (earth) metal oxides as additives [56]. Part of these studies deal with the influence of the catalyst nature. The study concerning the promoter effect of Li_2O revealed that most probably the beneficial effect of the additive is due to a change of the morphology and size of the Au particles, and their role would be mostly that of a stabilizer of the Au nanoparticles [58, 59].

In other work, the high activity of gold nanoparticles has been attributed to the relatively high abundance of low coordinated Au atoms in these small nanoparticles [60-62]. Another study reports on facilitated reaction kinetics. Accordingly, the high activity of Au-based catalysts in the low-temperature CO oxidation could be due to lowering of the reaction barrier of O_2 adsorption by the alkali (earth) metal oxides additives, which act as structural promoters and help in O_2 activation [56]. The measured similar apparent activation energies of the reaction over Au/Al_2O_3 and $Au/MO_x/Al_2O_3$ catalysts shows that the additives (Li_2O, Rb_2O, MgO and BaO) are not directly responsible for the higher catalytic activity, i.e. they do not change the reaction pathway. Presumably, their role is to increase the concentration of the Au active sites. In summary, alkali (earth) metal oxides inhibit the growth of gold particles during preparation and catalytic reaction, and promote the catalytic activity of the gold species responsible for the CO oxidation reaction. However, attempts to use alkali metals as promoters of the WGS reaction on gold catalysts have failed to date. It is a key objective of this thesis to explore new ways, especially of catalyst preparation that would clearly show the role of alkali, and further investigate the potential promotion of gold by alkali additives for the WGS reaction.

1.2.3 WGS reaction mechanism

More than one mechanism has been proposed for the WGS reaction over the supported noble metal catalysts. The exact nature of the relevant intermediates' formation/ decomposition and the mechanistic routes for the reaction are still a matter of debate. For the WGS reaction mechanism on Pt/CeO_2 catalyst, the regenerative redox mechanism [63-66] and the associative formate mechanism [67-74] are the two prevailing

mechanisms being debated. However, recently it was shown by Mavrikakis and co-workers that a third mechanism, the carboxyl-mediated mechanism, is responsible for the WGS reaction on Cu [75] and other metals, including Pt [76].

The regenerative mechanism involves successive oxidation and reduction of the surface. In this redox mechanism, water dissociates completely to O* and H*, and O* then combines with CO. The possible elementary steps in this scheme are:

$$H_2O\ (g) + * \leftrightarrow H_2O* \quad (5)$$

$$CO\ (g) + * \leftrightarrow CO* \quad (6)$$

$$H_2O* + * \leftrightarrow OH* + H* \quad (7)$$

$$OH* + * \leftrightarrow O* + H* \quad (8)$$

$$2OH* \leftrightarrow H_2O* + O* \quad (9)$$

$$OH* + H* \leftrightarrow O* + H_2* \quad (10)$$

$$CO* + O* \leftrightarrow CO_2* + * \quad (11)$$

$$2H* \leftrightarrow H_2* + * \quad (12)$$

$$CO_2* \leftrightarrow CO_2 + * \quad (13)$$

$$H_2* \leftrightarrow H_2 + 2* \quad (14)$$

where the asterisk signifies a free surface site and X* represents adsorbed species X. This redox mechanism could involve also two different sites, i.e. as appropriate to a bifunctional catalyst, whereby one type of sites would reside on the metal, e.g. for CO adsorption, while the second would be associated with the support, e.g. dissociating the H_2O molecule.

The associative reaction mechanism was proposed by Shido and Iwasawa who

studied the mechanism of the WGS reaction over CeO_2 and Rh/CeO_2 [74]. It involves reaction through adsorbed surface intermediates, such as formate, and the breaking of C-H bond of formate as the limiting step [77, 78]. In the formate mechanism, water dissociates to form OH*, which then reacts with carbon monoxide to produce HCOO*. Decomposition of formate then results in hydrogen and carbon dioxide products. In fact, formate formation from CO* and OH* would involve several bond breaking and bond-making steps, which might involve significant activation energy barriers [76]:

$$CO^* + OH^* \leftrightarrow HCOO^{**} \quad (15)$$

$$HCOO^{**} \leftrightarrow H^* + CO_2^* \quad (16)$$

Recently, a carboxyl-mediated mechanism for the low-temperature WGS reaction on Cu and other metals, including Pt, has been reported by Mavrikakis and coworkers [75, 76]. The detailed DFT analyses of all the elementary steps including the redox and carboxyl mediated steps point to the predominance of the COOH-mediated WGS path, whereby CO is directly oxidized by surface OH*, rather than atomic O*:

$$CO^* + OH^* \leftrightarrow COOH^* + * \quad (17)$$

$$COOH^* + * \leftrightarrow H^* + CO_2^* \quad (18)$$

$$COOH^* + OH^* \leftrightarrow H_2O^* + CO_2^* \quad (19)$$

This model confirmed that the WGS reaction is favored energetically to go through a carboxyl rather than a formate intermediate, and the carboxyl then decomposes via disproportionation with surface hydroxyl groups. All the H_2O and CO adsorption and desorption steps are as same as the above elementary reaction steps (5)-(7) and (12)-(14), respectively.

Although there is no full agreement for the WGS reaction mechanism as yet, the presence of -OH is decisively important for all of the reaction pathways. In all three mechanisms, the activation of H_2O [79], leading to the formation of the species responsible for oxidizing CO, is a kinetically important step. If the activation of OH groups is the rate limiting step, it may be possible to use supports that do not provide their own oxygen to the reaction, but on which adsorption of surface OH can be effective via additives and study the phenomenon. Inert supports, in particular SiO_2, interact very weakly with the metallic Au or Pt particles deposited on their surfaces, and do not have any reducible surface oxygen or OH groups [80-84]. It is not surprising to find lower or even no WGS reaction activity of Pt deposited over these inert oxide supports.

A large promotion effect has recently been reported for the alkali group metal additives on Pt on reducible oxide supports [30, 37] and even non-reducible oxides [34], but this still calls for an explanation. As the reactant of the WGS reaction, CO can be easily absorbed on a Pt atom, but H_2O is more difficult to be activated [85] due to its thermodynamic stability. For the precious metal based-WGS catalysts, a hydrophilic oxide support is essential to adsorb and activate water. If the alkali ion on the surface of inert support is able to dissociate water and continuously supply surface OH groups to the metal ion or cluster, we propose this ensemble could be an active site, similar that of atomic Pt or Au adsorbed on a reducible ceria or iron oxide support. As shown in the schematic illustration of the proposed WGS reaction pathway (see Figure 1.2), we assume that [Pt-O_x(OH)-M] species, where M denotes an alkali ion, is the active site for the low-temperature WGS reaction. In this mechanism, carbon monoxide adsorbs on the metal surface and water easily dissociates to active OH* and H* on the site of metal

associated with alkali ions, then the adsorbed carbon monoxide reacts with active OH* to form carboxyl intermediate following the Mavrikakis analysis for Cu catalysts [75]. Finally, the carboxyl decomposes to carbon dioxide and hydrogen. The primary elementary steps are listed below. This is a hypothesis, as other mechanisms as discussed above could be invoked around this active site. It is worth to examine the mechanisms comparatively using DFT; and to check for relevant intermediates by in situ spectroscopies. This was not possible to do in this Master's thesis because of limited scope.

$$[Pt\text{-}O_x\text{-}M] + CO \leftrightarrow [Pt\text{-}O_x\text{-}M] - \mathbf{CO^*} \quad (20)$$

$$[Pt\text{-}O_x\text{-}M] + H_2O \leftrightarrow [Pt\text{-}O_x\text{-}M] - \mathbf{OH^*} + H^* \quad (21)$$

$$OH^* + CO^* \leftrightarrow \mathbf{COOH}^* \quad (22)$$

$$COOH^* + OH^* \leftrightarrow \mathbf{CO_2}^* + H_2O \quad (23)$$

$$H^* + H^* \leftrightarrow \mathbf{H_2}^* \quad (24)$$

For this thesis, I have examined the alkali-promoted Pt catalyst in more depth, including kinetics studies, and also examined whether the alkali-promotion effect can be extended and realized on suitably prepared gold catalysts. Mechanistic elucidation of the WGS reaction will provide insights on how the alkali-promoted catalyst works, and whether this is a general scheme for all noble metals. The answer to this key question is very important and will impact catalyst formulation for practical applications. This constitutes the overall goal of this thesis.

1.3 Thesis motivation and objectives

Previous work done in our lab has already reported that Au/CeO_2, Pt/CeO_2, Au/FeO_x and $Na\text{-}Pt/SiO_2$ metals show excellent catalytic activity for the low-temperature WGS reaction, and has identified that the oxidized, atomically dispersed gold and platinum species associated with active oxygen or hydroxyls on the surface of the supports are the active sites in reaction [16, 34, 50]. It would be desirable to investigate whether active gold catalyst can be prepared on non-reducible supports, such as silica or alumina, whether surface modification can stabilize metal species with more hydroxyl groups, what catalyst structures can improve the activity and stability of catalysts, and ultimately if there is there a common active site for all the metal catalysts in the WGS reaction. These are the main issues I have considered in this thesis work.

As first mentioned in Pierre's M.S. thesis [38], an inactive Pt/SiO_2 catalyst could be activated dramatically by adding a small amount of sodium in the preparation of the material . This effect has been investigated in more depth by Zhai in her Ph.D. thesis work [86], from which $Pt\text{-}O_x(OH)\text{-}Na$ species have been proposed as the active sites. On irreducible oxide supports, alkali ions are the chemical promoter to activate and regenerate surface oxygen species and hydroxide groups through water dissociation, also they are the structural promoter to keep the metal species in oxidized state and well-dispersed during the heat treatment and reaction at the high end (~ 300 ^oC) of the operating temperature window. In this thesis, I have further investigated whether the catalyst structure affects the catalytic activity and stability of the alkali-modified Pt catalysts in the form of $Pt@SiO_2$ for the low-temperature WGS reaction.

In regard to gold catalysts, the specific activity of Au/CeO_2 and Au/Fe_2O_3 materials in the WGS reaction was found to be the same and was reported to depend only on the number of Au-O-Ce and Au-O-Fe sites [50]. Recent studies have also shown that the modification of supports can improve the gold dispersion, which leads to better activity and stability of the gold catalysts. Meanwhile, the effect of alkali (earth) metals on the catalytic performance of Au-based catalysts has been reported in many reactions, i.e. CO oxidation. In this thesis, I have designed the gold catalyst on irreducible alumina supports and investigated whether the hydrothermal treatment of the support and alkali additives can generate $Au\text{-}O_x(OH)\text{-}Na$ active sites thus rendering the Au/Al_2O_3 system an active and stable catalyst for the low-temperature WGS reaction.

Based on the above description of the evolution of our understanding of the activation of Pt and Au species for the WGS reaction, the aim of this thesis was to investigate the synthesis of gold and platinum species on non-reducible oxide supports as active and stable catalysts for the low-temperature water-gas shift reaction. The thesis is comprised of five chapters: Chapter 1 presents the background introduction and literature review; Chapter 2 outlines the experimental principles and characterization techniques; Chapter 3 provides the results of activity of silica encapsulated Pt-based catalysts in the WGS reaction; Chapter 4 discusses the synthesis and modification of alumina-supported Au-based catalysts in the WGS reaction; and Chapter 5 summarizes the major findings of the thesis and gives recommendations for future work.

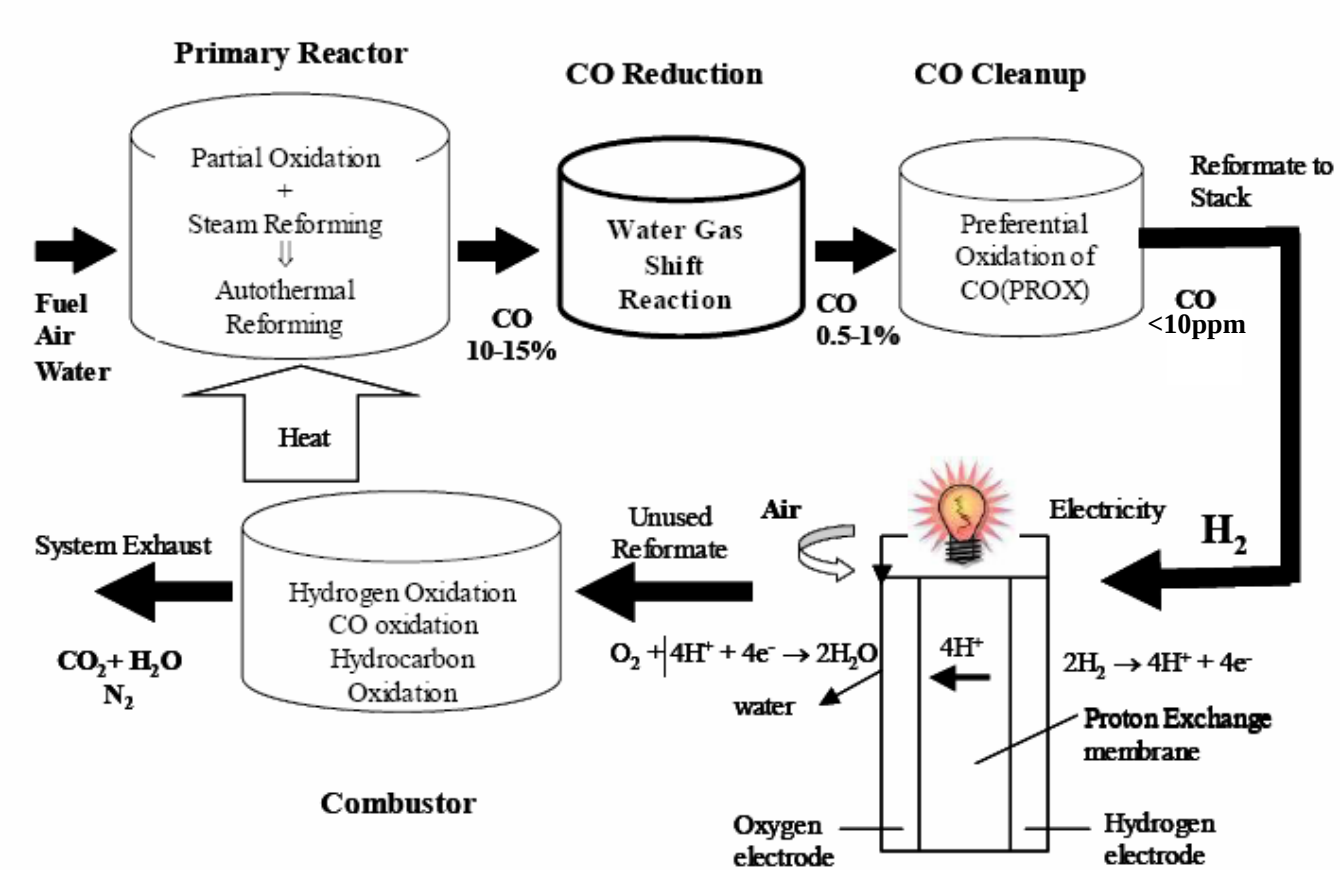

Figure 1.1 Fuel process and fuel cell system for hydrogen generation [87]

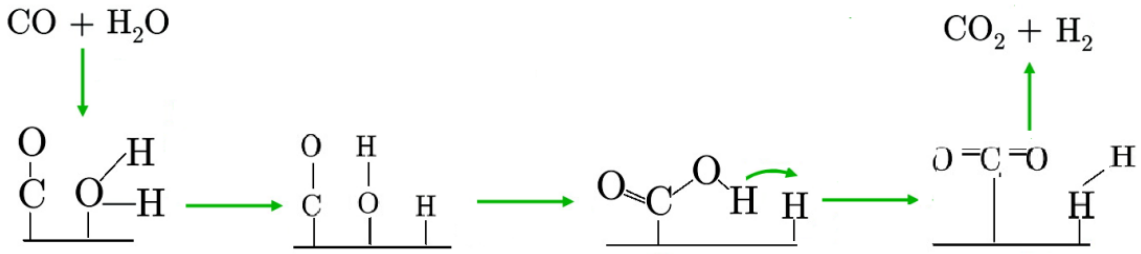

Figure 1.2 Schematic illustration of the carboxylateWGS reaction pathway [75]

References

[1] C. Bosch, W. Wild, ***Canadian Patent 153379*** (1914).

[2] C. Ratnasamy, J.P. Wagner, ***Catalysis Reviews*** 51 (2009) 325-440.

[3] W. Ruettinger, O. Ilinich, R.J. Farrauto, ***Journal of Power Sources*** 118 (2003) 61-65.

[4] K.G. Azzam, I.V. Babich, K. Seshan, L. Lefferts, ***Journal of Catalysis*** 251 (2007) 163-171.

[5] D.S. Newsome, ***Catalysis Reviews-Science and Engineering*** 21 (1980) 275-318.

[6] R. Farrauto, S. Hwang, L. Shore, W. Ruettinger, J. Lampert, T. Giroux, Y. Liu, O. Ilinich, ***Annual Review of Materials Research*** 33 (2003) 1-27.

[7] W. Deng, M. Flytzani-Stephanopoulos, ***Angewandte Chemie International Edition*** 45 (2006) 2285-2289.

[8] D. Pierre, W. Deng, M. Flytzani-Stephanopoulos, ***Topics in Catalysis*** 46 (2007) 363-373.

[9] C.M.Y. Yeung, K.M.K. Yu, Q.J. Fu, D. Thompsett, M.I. Petch, S.C. Tsang, ***Journal of the American Chemical Society*** 127 (2005) 18010-18011.

[10] W. Ruettinger, X. Liu, R.J. Farrauto, ***Applied Catalysis B: Environmental*** 65 (2006) 135-141.

[11] D. Tibiletti, A. Goguet, F.C. Meunier, J.P. Breen, R. Burch, ***Chemical Communications*** (2004) 1636-1637.

[12] K.G. Azzam, I.V. Babich, K. Seshan, L. Lefferts, ***Journal of Catalysis*** 251 (2007) 163-171.

[13] Y. Sato, K. Terada, S. Hasegawa, T. Miyao, S. Naito, ***Applied Catalysis A: General*** 296 (2005) 80-89.

[14] H. Iida, A. Igarashi, ***Applied Catalysis A: General*** 303 (2006) 48-55.

[15] Y. Bi, W. Zhang, H. Xu, W. Li, ***Catalysis Letters*** 119 (2007) 126-133.

[16] Q. Fu, H. Saltsburg, M. Flytzani-Stephanopoulos, ***Science*** 301 (2003) 935-938.

[17] C.M.Y. Yeung, F. Meunier, R. Burch, D. Thompsett, S.C. Tsang, ***Journal of Physical Chemistry B*** 110 (2006) 8540-8543.

[18] M. Hatanaka, N. Takahashi, N. Takahashi, T. Tanabe, Y. Nagai, A. Suda, H. Shinjoh, ***Journal of Catalysis*** 266 (2009) 182-190.

[19] J.M. Zalc, V. Sokolovskii, D.G. Loffler, ***Journal of Catalysis*** 206 (2002) 169-171.

[20] X. Liu, W. Ruettinger, X. Xu, R. Farrauto, ***Applied Catalysis B: Environmental*** 56 (2005) 69-75.

[21] Q. Fu, W. Deng, H. Saltsburg, M. Flytzani-Stephanopoulos, ***Applied Catalysis B: Environmental*** 56 (2005) 57-68.

[22] W. Deng, A.I. Frenkel, R. Si, M. Flytzani-Stephanopoulos, ***The Journal of Physical Chemistry C*** 112 (2008) 12834-12840.

[23] G. Jacobs, L. Williams, U. Graham, D. Sparks, B.H. Davis, ***Journal of Physical Chemistry B*** 107 (2003) 10398-10404.

[24] H. Iida, A. Igarashi, ***Applied Catalysis A: General*** 298 (2006) 152-160.

[25] T. Bunluesin, R.J. Gorte, G.W. Graham, ***Applied Catalysis B: Environmental*** 15 (1998) 107-114.

[26] H. Evin, G. Jacobs, J. Ruiz-Martinez, U. Graham, A. Dozier, G. Thomas, B. Davis, ***Catalysis Letters*** 122 (2008) 9-19.

[27] N. Pavlenko, P.P. Kostrobij, Y. Suchorski, R. Imbihl, ***Surface Science*** 489 (2001) 29-36.

[28] I.N. Yakovkin, G.A. Katrich, A.T. Loburets, Y.S. Vedula, A.G. Naumovets, ***Progress in Surface Science*** 59 (1998) 355-365.

[29] Y. Minemura, M. Kuriyama, S.-i. Ito, K. Tomishige, K. Kunimori, ***Catalysis Communications*** 7 (2006) 623-626.

[30] A. Hagemeyer, R.E. Carhart, K. Yaccato, A. Lesik, C.J. Brooks, ***United States Patent Application*** 20040175325 (2004).

[31] X. Zhu, M. Shen, L.L. Lobban, R.G. Mallinson, ***Journal of Catalysis*** 278 (2011) 123-132.

[32] P. Panagiotopoulou, D.I. Kondarides, ***Applied Catalysis B: Environmental*** 101 (2011) 738-746.

[33] P. Panagiotopoulou, D.I. Kondarides, ***Journal of Catalysis*** 267 (2009) 57-66.

[34] Y. Zhai, D. Pierre, R. Si, W. Deng, P. Ferrin, A.U. Nilekar, G. Peng, J.A. Herron, D.C. Bell, H. Saltsburg, M. Mavrikakis, M. Flytzani-Stephanopoulos, ***Science*** 329 (2010) 1633-1636.

[35] K.-i. Aika, H. Hori, A. Ozaki, ***Journal of Catalysis*** 27 (1972) 424-431.

[36] Z. Kowalczyk, J. Sentek, S. Jodzis, E. Mizera, J. Góralski, T. Paryjczak, R. Diduszko, ***Catalysis Letters*** 45 (1997) 65-72.

[37] J.M. Pigos, C.J. Brooks, G. Jacobs, B.H. Davis, ***Applied Catalysis A: General*** 319 (2007) 47-57.

[38] D. Pierre, ***M.S. Thesis, Department of Chemical and Biological Engineering, Tufts University*** (2006).

[39] H. Tanaka, M. Kuriyama, Y. Ishida, S.-i. Ito, K. Tomishige, K. Kunimori, ***Applied Catalysis A: General*** 343 (2008) 117-124.

[40] H. Tanaka, M. Kuriyama, Y. Ishida, S.-i. Ito, T. Kubota, T. Miyao, S. Naito, K. Tomishige, K. Kunimori, ***Applied Catalysis A: General*** 343 (2008) 125-133.

[41] M. Haruta, H. Kobayashi, H. Sano, N. Yamada, ***Chemical Letters*** (1987) 405.

[42] M. Haruta, N. Yamada, T. Kobayashi, S. Iijima, ***Journal of Catalysis*** 115 (1989) 301-309.

[43] S. Hiroaki, U. Atsushi, K. Tetsuhiko, H. Masatake, ***Chemical Communications*** 3 (1997) 271-272.

[44] D. Andreeva, V. Idakiev, T. Tabakova, A. Andreev, ***Journal of Catalysis*** 158 (1996) 354-355.

[45] W. Liu, M. Flytzanistephanopoulos, ***Journal of Catalysis*** 153 (1995) 304-316.

[46] W. Liu, M. Flytzanistephanopoulos, ***Journal of Catalysis*** 153 (1995) 317-332.

[47] M. Haruta, S. Tsubota, T. Kobayashi, H. Kageyama, M.J. Genet, B. Delmon, ***Journal of Catalysis*** 144 (1993) 175-192.

[48] T. Tabakova, V. Idakiev, D. Andreeva, I. Mitov, ***Applied Catalysis A: General*** 202 (2000) 91-97.

[49] Q. Fu, A. Weber, M. Flytzani-Stephanopoulos, ***Catalysis Letters*** 77 (2001) 87-95.

[50] W. Deng, C. Carpenter, N. Yi, M. Flytzani-Stephanopoulos, ***Topics in Catalysis*** 44 (2007) 199-208.

[51] G.M. Veith, A.R. Lupini, N.J. Dudney, ***The Journal of Physical Chemistry C*** 113 (2008) 269-280.

[52] G.M. Veith, A.R. Lupini, S.J. Pennycook, N.J. Dudney, ***ChemCatChem*** 2 (2010) 281-286.

[53] T. Takei, I. Okuda, K.K. Bando, T. Akita, M. Haruta, ***Chemical Physics Letters*** 493 (2010) 207-211.

[54] A.C. Gluhoi, B.E. Nieuwenhuys, ***Catalysis Today*** 122 (2007) 226-232.

[55] S. Tsubota, M. Haruta, T. Kobayashi, A. Ueda, Y. Nakahara, P.A.J.P.G. G. Poncelet, B. Delmon, ***Studies in Surface Science and Catalysis***, Elsevier, 1991, pp. 695-704.

[56] A.C. Gluhoi, X. Tang, P. Marginean, B.E. Nieuwenhuys, ***Topics in Catalysis*** V39 (2006) 101-110.

[57] Y. Li, Q. Yu, X. Zou, H. Zhuo, Y. Yao, Z. Suo, ***Chinese Journal of Catalysis (Chinese Version)*** 31 (2010) 671.

[58] A.C. Gluhoi, M.A.P. Dekkers, B.E. Nieuwenhuys, ***Journal of Catalysis*** 219 (2003) 197-205.

[59] A.C. Gluhoi, S.D. Lin, B.E. Nieuwenhuys, ***Catalysis Today*** 90 (2004) 175-181.

[60] N. Lopez, T.V.W. Janssens, B.S. Clausen, Y. Xu, M. Mavrikakis, T. Bligaard, J.K. Nørskov, ***Journal of Catalysis*** 223 (2004) 232-235.

[61] N. Lopez, J.K. Nørskov, T.V.W. Janssens, A. Carlsson, A. Puig-Molina, B.S. Clausen, J.D. Grunwaldt, ***Journal of Catalysis*** 225 (2004) 86-94.

[62] B.E. Nieuwenhuys, A.C. Gluhoi, E.D.L. Rienks, C.J. Weststrate, C.P. Vinod, ***Catalysis Today*** 100 (2005) 49-54.

[63] C.V. Ovesen, B.S. Clausen, B.S. Hammershoi, G. Steffensen, T. Askgaard, I. Chorkendorff, J.K. Norskov, P.B. Rasmussen, P. Stoltze, P. Taylor, ***Journal of Catalysis*** 158 (1996) 170-180.

[64] R.J. Gorte, S. Zhao, ***Catalysis Today*** 104 (2005) 18-24.

[65] G.C. Chinchen, P.J. Denny, J.R. Jennings, M.S. Spencer, K.C. Waugh, ***Applied Catalysis*** 36 (1988) 1-65.

[66] Y. Li, Q. Fu, M. Flytzani-Stephanopoulos, ***Applied Catalysis B: Environmental*** 27 (2000) 179-191.

[67] G. Jacobs, U.M. Graham, E. Chenu, P.M. Patterson, A. Dozier, B.H. Davis, ***Journal of Catalysis*** 229 (2005) 499-512.

[68] A. Goguet, S.O. Shekhtman, R. Burch, C. Hardacre, F.C. Meunier, G.S. Yablonsky, ***Journal of Catalysis*** 237 (2006) 102-110.

[69] G. Jacobs, S. Ricote, U.M. Graham, P.M. Patterson, B.H. Davis, ***Catalysis Today*** 106 (2005) 259-264.

[70] G. Jacobs, E. Chenu, P.M. Patterson, L. Williams, D. Sparks, G. Thomas, B.H. Davis, ***Applied Catalysis A: General*** 258 (2004) 203-214.

[71] T. van Herwijnen, W.A. de Jong, ***Journal of Catalysis*** 63 (1980) 83-93.

[72] D.C. Grenoble, M.M. Estadt, D.F. Ollis, ***Journal of Catalysis*** 67 (1981) 90-102.

[73] T. Salmi, R. Hakkarainen, ***Applied Catalysis*** 49 (1989) 285-306.

[74] T. Shido, Y. Iwasawa, ***Journal of Catalysis*** 141 (1993) 71-81.

[75] A.A. Gokhale, J.A. Dumesic, M. Mavrikakis, ***Journal of the American Chemical Society*** 130 (2008) 1402-1414.

[76] L.C. Grabow, A.A. Gokhale, S.T. Evans, J.A. Dumesic, M. Mavrikakis, ***Journal of Physical Chemistry C*** 112 (2008) 4608-4617.

[77] G. Jacobs, S. Ricote, P.M. Patterson, U.M. Graham, A. Dozier, S. Khalid, E. Rhodus, B.H. Davis, ***Applied Catalysis A: General*** 292 (2005) 229-243.

[78] S. Ricote, G. Jacobs, M. Milling, Y. Ji, P.M. Patterson, B.H. Davis, ***Applied Catalysis A: General*** 303 (2006) 35-47.

[79] C.T. Campbell, ***Journal of Catalysis*** 204 (2001) 520-524.

[80] L. Guczi, G. Peto, A. Beck, K. Frey, O. Geszti, G. Molnar, C. Daroczi, ***Journal of the American Chemical Society*** 125 (2003) 4332-4337.

[81] M. Haruta, ***CatTech*** 6 (2002) 102-115.

[82] R. Zanella, L. Delannoy, C. Louis, ***Applied Catalysis A: General*** 291 (2005) 62-72.

[83] A. Wolf, F. Schuth, ***Applied Catalysis A: General*** 226 (2002) 1-13.

[84] S.D. Lin, M. Bollinger, M.A. Vannice, ***Catalysis Letters*** 17 (1993) 245-262.

[85] M.A. Henderson, ***Surface Science Reports*** 46 (2002) 1-308.

[86] Y. Zhai, ***Ph.D. Dissertation, Department of Chemical and Biological Engineering, Tufts University*** (2011).

[87] Q. Fu, ***Ph.D. Dissertation, Department of Chemical and Biological Engineering, Tufts University*** (2004).

Chapter 2

Experimental Procedures

2.1 Catalyst preparation

This section describes in detail the chemicals, materials and preparation methods used in this work. The analysis and results of these catalysts will be discussed in following chapters. First, is the description of metal precursors and oxide supports with hydrothermal treatments, followed by the methods used to prepare Pt/SiO_2, $Pt@SiO_2$ and Au/Al_2O_3 catalysts. These methods are Reverse Microemulsion (ME), Incipient wetness impregnation (IMP) and Deposition-precipitation (DP).

2.1.1 Materials

The major chemicals and reagents used in this work and their sources are listed in Table 2.1. All materials were used as provided from respective suppliers without further purification.

2.1.1.1 Metal precursors

The platinum precursor used was tetraammoniumplatinum (II) nitrate ($(NH_3)_4Pt(NO_3)_2$, Sigma-Aldrich, 99.995% trace metals basis) and the gold precursor was hydrogen tetrachloroaurate (III) hydrate ($HAuCl_4 \cdot 3H_2O$, Alfa-Aesar, 99.99%). The alkali

addition was accomplished from alkali nitrates as the precursor salts (Sigma-Aldrich).

2.1.1.2 Oxide supports

A commercial silica (Sigma-Aldrich, fumed, S_{BET} = 243 m^2/g, V_p = 3 mL/g) was used as the oxide support of the sample Pt/SiO_2. Another oxide support, γ-alumina (Puralox, SBa-200, S_{BET} = 210 m^2/g, V_p = 0.55 mL/g), was modified by hydrothermal treatment with the goal to create a hydroxide-rich surface. The procedure was carried out by the following steps:

1) Immersing the commercial γ-alumina powers in 50 mL of doubly de-ionized water (D.I. water) or 0.5 M sodium hydroxide aqueous solution at room temperature.
2) Transferring the slurry of Al_2O_3 into an autoclave. The mixture was heated up to 100 ^oC and kept at temperature for 20 h.
3) The final mixture was filtered and washed three times by D.I. water to remove any contaminants such as residual sodium ions.
4) The modified alumina supports were dried overnight at 100 °C under vacuum and are denoted as Al_2O_3-OH.

2.1.2 Preparation methods

The preparation of nano-sized noble metal particles and their deposition on metal oxide supports has been attracting strong interest because of the wide spread use of these particles in heterogeneous catalysis (i.e. WGS, CO oxidation, hydrocarbon oxidation).

Methods such as deposition-precipitation, impregnation, and physical vapor deposition are among the most commonly used preparation techniques. In recent years, the focus has shifted toward the use of some new techniques, such as microemulsion and atomic layer deposition, which can control better the dispersion and uniformity/homogeneity of the catalyst structure.

2.1.2.1 Reverse Microemulsion Technique (ME)

Microemulsion syntheses are advantageous over conventional preparation methods due to their ability to control the particle size, metal dispersion, and prepare highly structured materials [1]. Encapsulated nanoparticles can be prepared using a reverse microemulsion technique. In brief, in reverse microemulsion, the bulk phase is oil and the preparation of the material takes place in small water droplets stabilized by surfactants within the oil phase. A typical procedure from the literature [2] was used in this work , comprising the following steps:

1) At room temperature, a certain amount of cationic surfactant, cetyltrimethylammonium bromide (CTAB, ≥98%, Sigma Aldrich) was added to excess dried toluene.
2) An aqueous solution of $(NH_3)_4Pt(NO_3)_2$ was added drop wise to the surfactant-oil mixture. This introduction of an aqueous phase to the surfactant/oil mixture initiates the formation of micelles.
3) After the stabilization of the micelle solution for 1 h, 1M NaOH or 50% NH_4OH aqueous solution was added to adjust the pH of the aqueous micelles in the bulk

toluene and aged for another 2 hours.

4) Hydrazine was added to reduce the platinum and the emulsion was aged for 1 h.
5) To prepare a silica shell over the Pt particles, an amount of tetraethoxysilane (TEOS) was added, and the hydrolysis reaction between the basic solution and TEOS was allowed to proceed overnight.
6) The final mixture was filtered and washed three times in hot ethanol and de-ionized water to remove any contaminants such as residual surfactant.
7) The as-prepared samples were dried overnight at 100 °C and are denoted as Pt-Na@SiO_2 (when NaOH was used to adjust the pH) and Pt@SiO_2 (when NH_4OH was used to adjust the pH). All dried samples were calcined at 400 °C at a heating rate of 2 °C/min in static air for 4 h.

   Figure 2.1 shows a schematic of the ME synthesis.

2.1.2.2 Incipient wetness impregnation (IMP)

Impregnation is a common technique used to prepare precious metal-based catalysts. The incipient wetness impregnation (IMP) is an approach to fill the pore volume of the solid, whereby a measured amount of aqueous solution (the volume of the solution is equal to the pore volume of the oxide support) carrying the required metal ion concentration is added drop wise (or by spray drying industrially) in one step.

Incipient wetness impregnation was used here to prepare Pt/SiO_2 and Pt/Al_2O_3 materials. Typically, the commercial support, γ-Al_2O_3 or SiO_2, was impregnated with an aqueous solution of the metal precursor, tetraammoniumplatinum (II) nitrate. The

solution was added drop wise under vigorous stirring, the volume of the solution being equal to the pore volume of the support. The wet powder was dried under vacuum at 60 ^{o}C overnight to remove water and allow good coating of the metal on the pore surface. All dried samples were calcined at 400 °C at a heating rate of 2 °C/min in static air for 4 h.

Catalyst properties such as dispersion and morphology are influenced by the properties of the impregnating solution (i.e. volume, pH, and temperature). Due to the nature of the synthesis it is difficult to obtain both high loading and high dispersion in one step, and typically the impregnation with excess solution requires several steps. Because of the weak interaction between platinum and SiO_2, this one step preparation technique leads to a low Pt-loading. One disadvantage of the IMP technique is that control of the metal particle size and location on the support is more difficult, which leads to non uniform structures.

2.1.2.3 Deposition-precipitation (DP)

To investigate the influence of the preparation methods and the impregnation sequence on the catalyst performance, a Pt/CeO_2 sample was prepared by deposition–precipitation (DP). The procedure was carried out by the following steps:

1) Pre-made ceria support (prepared by Urea Gelation Coprecipitation method [3]) was suspended in de-ionized water (D.I. water) at room temperature.
2) Adjusting the pH of the suspension at 9 by adding 1 M ammonium carbonate ($(NH_4)_2CO_3$) with vigorous stirring.

3) Dissolving the desired amount of Pt precursor, $Pt(NH_3)_4((NO_3)_2$, in 100 mL D.I. water at room temperature.

4) Adding the solution drop wise into the slurry of CeO_2. The pH 9 was maintained with the aid of 1M $(NH_4)_2CO_3$.

5) Upon completion, aging the mixture at room temperature for 1 h.

6) Filtering and washing the precipitate three times with sufficient amount of D.I. water.

7) Drying the solid sample at 60 ^oC under vacuum overnight to remove water. All dried samples were calcined at 400 °C at a heating rate of 2 °C/min in static air for 4 h.

The deposition-precipitation method has been shown to produce nanometer size gold (< 5nm), sub-nm gold clusters, and gold atoms on ceria [4]. The precursors used in preparing supported gold catalysts are $HAuCl_4$, while the speciation of the gold ions depends strongly on the concentration, pH and temperature of the solution (see Figure 2.2) [5]. Gold is precipitated from an aqueous solution, at pH 8 and electrostatic forces that exist between the support and the gold allow for the deposition of the gold (in hydroxide form, $Au(OH)_3$). A modified DP procedure using urea for the precipitation step according to Zanella's work [6] was carried out to prepare Au/Al_2O_3 by the following steps:

1) Suspending alumina powders in 200 mL of D.I. water at room temperature.
2) Dissolving the gold precursor, $HAuCl_4 \cdot 3H_2O$, in 100 mL of D.I. water at room temperature and the solution was added drop wise into a slurry of Al_2O_3 under constant stirring.

3) Using a certain amount of urea to adjusting the pH of the suspension. The mixture was heated to 80 ^{o}C to allow the slow decomposition of urea.

4) Upon completion, aging the mixture at 80 ^{o}C for 4 h with vigorous stirring.

5) Filtering and washing the precipitate three times with sufficient amount of hot water to remove any contaminants such as chlorine and residual reactants such as excess tetracholorauric acid or any undecomposed urea.

6) Drying the solid sample at 60 ^{o}C under vacuum overnight to remove water, referred as Au/Al_2O_3.

This DP with urea technique was also used to prepare supported gold on the hydrothermally treated alumina supports.

2.1.2.4 Alkali additives and water washing treatment

Na-modified SiO_2 and Al_2O_3 supports were prepared by the IMP method as described above and denoted as Na-SiO_2 (Al_2O_3). Na ions were also added to the dried samples (Pt@SiO_2, Pt/SiO_2 and Au/Al_2O_3) by IMP as well, using sodium nitrate as the precursor (Sigma-Aldrich). The modified samples were dried under vacuum at 60 ^{o}C overnight, further calcined at 400 ^{o}C at a heating rate of 2 ^{o}C/min in static air for 4 h. These samples are denoted as Na-Pt/SiO_2, Na-Pt@SiO_2 and Na-Au/Al_2O_3. The atomic percentage of Pt and Na were calculated by the following equations:

$$Pt\ atomic\ \% = \frac{Pt\ mol}{Pt\ mol + Na\ mol + Si\ mol} \times 100\%$$

$$Au\ atomic\ \% = \frac{Pt\ mol}{Au\ mol + Na\ mol + Al\ mol} \times 100\%$$

$$Na\ atomic\ \% = \frac{Na\ mol}{Pt\ mol + Na\ mol + Si\ (or\ Al)\ mol} \times 100\%$$

Selected, calcined Na-modified samples were washed by D.I. water to remove excess Na from the surface. The samples in powder form were suspended in sufficient amount of D.I. water and stirred at room temperature for 5 min. This was followed by filtering the suspension and drying the solid under vacuum overnight.

2.2 Catalyst characterization

2.2.1 Bulk Composition Analysis

Elemental bulk composition analyses of the catalysts were done by Inductively Coupled Plasma Atomic Emission Spectrometry (ICP-AES). The gold/alumina catalyst powders were dissolved in HCl (36.5-38%, Aldrich) that contained a small amount of H_2O_2 (29-32%, Aldrich) and diluted with de-ionized H_2O. The resulting solutions were analyzed by ICP (Perkin Elmer Plasma 40, Leeman Labs, Inc.) at the Department of Chemistry, Tufts University. Standard ICP solutions of Au, Na and Al were purchased from Alfa Aesar and diluted to produce calibration curves. The platinum/silica samples were tested in EAGLABS (NY), where the Inductively Coupled Plasma Optical Emission Spectrometry (ICP-OES) is equipped with a HF-resistant torch. The silica-supported catalyst powder was dissolved in 30 mL of the diluted HF (A.C.S. reagent) solution containing 4 mL of H_2O_2, 2 mL of HF, 2.5 mL of HNO_3 and 2.5 mL of HCl. The solution was further diluted by 19 mL of H_2O before ICP tests.

2.2.2 Surface area measurements

The BET surface area of each sample was measured by single-point N_2 adsorption-desorption cycles in a Micromeritics AutoChem II 2920 apparatus. In a typical experiment 0.1 g of the sample was loaded between beds of quartz wool and degassed in He at 200 ^{o}C for 30 min before the adsorption. A 30%N_2-He gas mixture was used in the BET measurement. Each measurement was repeated three times, the reported surface areas are the averages of the three repeats.

2.2.3 CO Chemisorption

Pulse CO-chemisorption was carried out in the Micromeritics AutoChem II 2920 instrument equipped with a thermal conductivity detector (TCD). The Pt metal dispersion was measured by CO chemisorption at ambient temperature. Pretreatment was in 10%H_2-Ar at 350 ^{o}C for 2 h, followed by cooling down to room temperature in He. A linear CO adsorption on Pt (CO:Pt = 1:1) was assumed for the dispersion calculation [7].

2.2.4 Electron microscopy

Electron microscopes use a beam of highly energetic electrons to examine objects on a very fine scale. The development of the electron microscopy and related micro-analytical techniques has allowed comprehensive structural analysis of catalysts at a sub-nanometer or even atomic scale. It can also provide information on the elemental composition of the particles by Energy Dispersive x-ray Spectroscopy (EDS) by

detecting the X-rays which are produced by the interaction of electrons with the matter or by analyzing the way the electrons are diffracted [8].

Transmission electron microscopy (TEM) was used to study the structure and morphology of the supported precious metal catalysts. To estimate the particle size distribution in this work, high resolution transmission electron microscopy (HRTEM) was performed. HRTEM is useful to measure the size of supported metal crystallites and changes in their size, shape, and position with catalyst use. In this work, HRTEM data were collected on a JEOL 2010 microscope operating at 200 kV with a lanthanum hexaboride cathode (MIT CSME facility).The sample powder was suspended in ethanol using an ultrasonic bath and deposited on a carbon-coated 200 mesh copper grid.

2.2.5 X-ray photoelectron spectroscopy (XPS)

X-ray photoelectron spectroscopy is a surface analysis technique that is used to determine atomic concentrations, chemical shift and oxidation states of elements in a sample. For XPS, a primary beam of X-ray irradiates the sample and releases core-level electrons. These photoelectrons are collected and analyzed by the detector to produce a spectrum of emission intensity versus electron kinetic energy, which is correlated to the binding energy. Since each element has a unique set of binding energies, the resulting spectrum of intensity plotted against the binding energy can be used to identify the relative composition of a sample, along with the oxidation state of its components due to the chemical shift of any peaks. These peak areas are used to quantify the concentration of the elements. Additionally, the surface sensitivity of this technique is predicated by the

fact that the kinetic energy of the escaping photoelectrons limits the depth from which it can emerge, giving XPS excellent surface sensitivity and a low sampling depth of a few nanometers; the exact value depending on the element.

In this work, a Kratos AXIS Ultra Imaging XPS with a resolution of 0.1 eV (MIT CSME facility) was used to determine the atomic metal ratios of the elements on the surface region and the oxidation state of platinum in selected catalysts. Samples in powder form were pressed on a double-sided adhesive copper tape for analysis (see Figure 2.3). All measurements were carried out at room temperature without any pre-treatment. Unless otherwise noted, the samples were analyzed after the calcination step described above. An Al Kα X-ray source was used and the X-ray generator power was typically set at 15 kV and 10 mA. Both broad survey and detailed scans were performed.

The identification of the oxidation states for the studied element depends primarily on the accurate determination of line energies. In the measurements of silica-supported catalyst, i.e. Pt/SiO_2, $Na\text{-}Pt/SiO_2$, $Pt@SiO_2$ and $Na\text{-}Pt@SiO_2$, the Si_{2p} peak from the support was present in all the samples. Therefore, it was used as internal standard for the charge correction, and all the binding energies were aligned to the Si_{2p} peak at 103.6 eV. For other measurements, i.e. Au/Al_2O_3, since the C_{1s} peak from adventitious hydrocarbons present on the samples was found in all the measurements, it was used as internal standard for the charge correction. Therefore, all the binding energies were aligned to the C_{1s} peaks at 285.0 eV.

2.2.6 X-ray diffraction (XRD)

Powder XRD analysis was used in this work to identify the structure change of the support after hydrothermal treatments based on the diffraction peak position and pattern. XRD analysis was performed on a Rigaku RU300 instrument with a rotating anode X-ray generator and a monochromatic detector (MIT CSME facility). Cu Kα1 radiation (λ = 1.5406 Å) was used with a power setting of the voltage 50 kV and current 300 mA, respectively. Typically, a scan rate of 2 ^{o}/min with 0.02 ^{o} data interval was used.

2.2.7 UV-Visible (UV-Vis) Spectroscopy

UV-visible (UV-Vis) spectroscopy is used to examine the electronic transition states of metals based on the absorption intensity of varying wavelengths of light in the range of 160 – 800 nm. In particular with Au catalysts, the coordination environment can be qualitatively measured based on the shape and position of different absorption bands. In this work, UV-Vis spectra were taken on the HP Diode Array Spectrophotometer 8452A instrument. Au precursor was dissolved in de-ionized water and placed in a quartz cuvette with a path length of 1 cm. Materials were analyzed for absorption in the range of 190 – 590 nm.

2.2.8 Temperature-programmed reduction (TPR)

Temperature Programmed Reduction (TPR) is a technique in which the surface reduction of an oxide is monitored while the temperature of the sample is ramped in a programmed fashion with time. This analysis can yield insight into the type of oxygen

groups present on a support surface.

CO temperature-programmed reduction (CO-TPR) was carried out in the Micromeritics AutoChem II 2920 instrument. Each component in the product gas stream was monitored by an on-line residual gas analyzer (SRS, RGA 200). The sample was first purged at room temperature in a flow of He for 30 min, then heated in 10%CO-He (30 mL/min) from room temperature to the target temperatures (400 °C) at a rate of 10 ^{o}C/min.

If doing cyclic CO-TPR without any treatment in between, after the first reduction run, the sample was cooled down to room temperature in He, and then the next CO-TPR cycle was conducted similar to the first run. If doing cyclic CO-TPR with a water-treatment, after the first reduction run, the sample was cooled down to room temperature in He, then exposed to 3%H_2O-He (30 mL/min) at room temperature and kept for 30 min. For the rehydration step, the He gas stream was passed through a bubbler filled with water at room temperature and saturated with H_2O vapor (~ 3%) before flowing to the reactor. Following a purge in pure He, the next CO-TPR cycle was conducted similar to the first run.

CO-TPR was used to sample the different surface oxygen species by products from the reduction, for example,

$$CO + O^* \rightarrow CO_2$$

$$CO + OH^* \rightarrow CO_2 + \frac{1}{2}H_2$$

The amount of surface hydroxyls was calculated by integrating the peak areas of the CO_2 and H_2 produced. The integrated area was then converted to moles of activated

oxygen using a calibration curve created by performing a series of similar CO-TPRs over the standard reference sample Ag_2O in which the amount of CO_2 is stoichiometrically equivalent to the total oxygen in the sample.

2.3 Catalytic activity tests

2.3.1 Temperature-programmed surface reaction (TPSR)

The temperature-programmed surface WGS reaction (TPSR) was used to probe the surface reactivity of the catalyst dynamically. The experiment was performed in a Micromeritics AutoChem II 2920 apparatus. After any necessary pretreatment, the sample was purged in He at room temperature for 30 min, and then exposed to 10%CO-3%H_2O-He, 30 mL/min. Water was introduced by passing diluted CO gas through a vapor generator, which was set at room temperature. The sample was heated from room temperature to 350-400 ^oC at 10 ^oC/min in 5%CO-3%H_2O-He. In some tests, an isothermal hold was performed after the linear ramp.

The composition of the outlet gas was monitored by an on-line residual gas analyzer (SRS, RGA 200). The onset temperature of the WGS reaction was followed by the first appearance of H_2 product. Prior to this, CO_2 alone was typically eluted (dry CO oxidation by the adsorbed oxygen species), but this is not counted as WGS-derived CO_2. The catalytic activity and conversion of the feed were followed by tracking the CO (m/z = 28), CO_2 (m/z = 44), H_2 (m/z = 2) signals, while the water was trapped after the reactor and not introduced into the mass spectrometer.

2.3.2 Steady-state WGS reaction activity tests

The steady-state performance of a catalyst and reaction kinetics were measured in a quartz-tube microreactor system (see Figure 2.4). The WGS reaction light-off tests and kinetics measurements were conducted at atmospheric pressure in the packed-bed flow microreactor. In each experiment, the sample was loaded in the quartz tube (1/2 in. i.d. × 24 in. long) on a porous quartz frit support. The reactant gases, all certified calibration gas mixtures with helium (Airgas), were controlled by mass flow rate controllers and mixed prior to the reactor inlet. Water was injected into the flowing gas stream by a calibrated syringe pump and vaporized in the heated gas line before entering the reactor. A water condenser in ice bath was installed after the reactor exit. The inlet and outlet gas streams were analyzed on-line by a HP-5890 or SRI 310C gas chromatograph (GC) equipped with a thermal conductivity detector (TCD) and using a Carbosphere (Alltech) packed column (80/100, 6 ft. ×1/8 in.).

Typically, 0.1 g catalyst (particle size ~ 50 μm) was used for each test. Each sample was diluted with 0.2 g inert quartz sand prior to being placed on the frit. The total bed height was less than ½ in. typically. For the steady-state performance tests of catalysts in the WGS reaction, the wet feed gas composition was the product-free gas, 2%CO-10%H_2O-He (70 mL/min, contact time = 0.09 g·s/mL). The catalytic activity of each sample was tested in both the ascending- and descending-temperature mode in 25 or 50 ^oC increments. Steady-state conversions were measured for one hour at each temperature. To conduct the kinetics measurements, the wet feed gas composition was the full reformate gas, 11%CO-26%H_2O-26%H_2-7%CO_2-He (207 mL/min, contact time = 0.03 g·s/mL). The kinetic tests were conducted in a differential mode keeping the CO

conversion below 15%: setting the starting conditions that give ~ 10% conversion at the highest temperature and waiting until no change in the activity took place, then collecting the data in the descending-temperature mode in 25 or 50 ^{o}C increments; while increasing the contact time to keep the conversion at ~ 10%. Steady-state conversions were measured for one hour at each temperature, when there should be no more deactivation due to temperature effect.

The percent CO conversion (X_{CO}) was determined by:

$$X_{CO}(\%) = \frac{CO^{in} - CO^{out}}{CO^{in}} \times 100\%$$

The production rate of CO_2 was used to calculate the reaction rate:

$$Rate = \frac{N_t^{out} \times CO_2^{out} - N_t^{in} \times CO_2^{in}}{W_{cat}} ({}^{mol}/_{g.s})$$

Where N_t^{in} or N_t^{out} was the total molar flow rate (in the unit of mol/s) of the dry feed or product gas stream. CO^{in}, CO^{out}, CO_2^{in}, or CO_2^{out} was the molar fraction of CO or CO_2 in the dry feed or product gas stream, and the W_{cat} was the amount of catalyst loading in grams. Since N_t^{out} can not be monitored continuously, it is expressed based on carbon mass balance as,

$$N_t^{out} = N_t^{in} \times \frac{CO_2^{in} + CO^{in}}{CO_2^{out} + CO^{out}}$$

Where N_t^{in} was constant and measured before reaction, the concentrations of CO and CO_2 were measured by GC. The rate is based on CO consumption being equal to the rate of CO_2 production. There was no methane production observed under the conditions of the experiments performed here.

2.3.3 Catalyst stability tests

Long-term isothermal stability tests of catalysts for the WGS reaction were conducted at atmospheric pressure in a heated quartz tube microreactor containing the catalyst powder as a packed-bed. The feed and product gas streams were analyzed by a HP-5890 GC or SRI 310C equipped with a TCD. The test was performed in WGS reaction system with full reformate gas comprising 11%CO–26%H_2O-26%H_2–7%CO_2-He (207 mL/min, contact time = 0.03 g·s/mL). The stability tests were also conducted with several shutdown-startup operation cycles throughout the experiment.

Table 2.1 Precursors and reagents

Element or Compound	Precursor	Source
Pt	Tetraammoniumplatinum (II) nitrate, 99.995%	Sigma-Aldrich
Au	Hydrogen tetrachloroaurate (III) hydrate, 99.99%	Alfa Aesar
Na	Sodium nitrate, 99.9%	Sigma-Aldrich
Si	Tetraethoxysilane (TEOS), 98%	Alfa Aesar
SiO_2	Silica, fumed	Sigma-Aldrich
Al_2O_3	γ-alumina, Puralox SBa-200	Condea
NaOH	Sodium hydroxide, 1.0N	Alfa Aesar
$NH_3.H_2O$	Ammonium Hydroxide, 50/50 v/v	Alfa Aesar
$(NH_4)_2CO_3$	Ammonium carbonate	Alfa Aesar
$CO(NH_2)_2$	Urea, 99-100.5%	Sigma-Aldrich
N_2H_4	Hydrazine	Alfa Aesar
CTAB	Cetyltrimethylammonium bromide, ≥98%	Sigma-Aldrich
PVP	Polyvinylpirrolidone, MW 8000	Alfa Aesar
C_2H_5OH	Ethanol	Sigma-Aldrich
$C_6H_5CH_3$	Toluene	Alfa Aesar

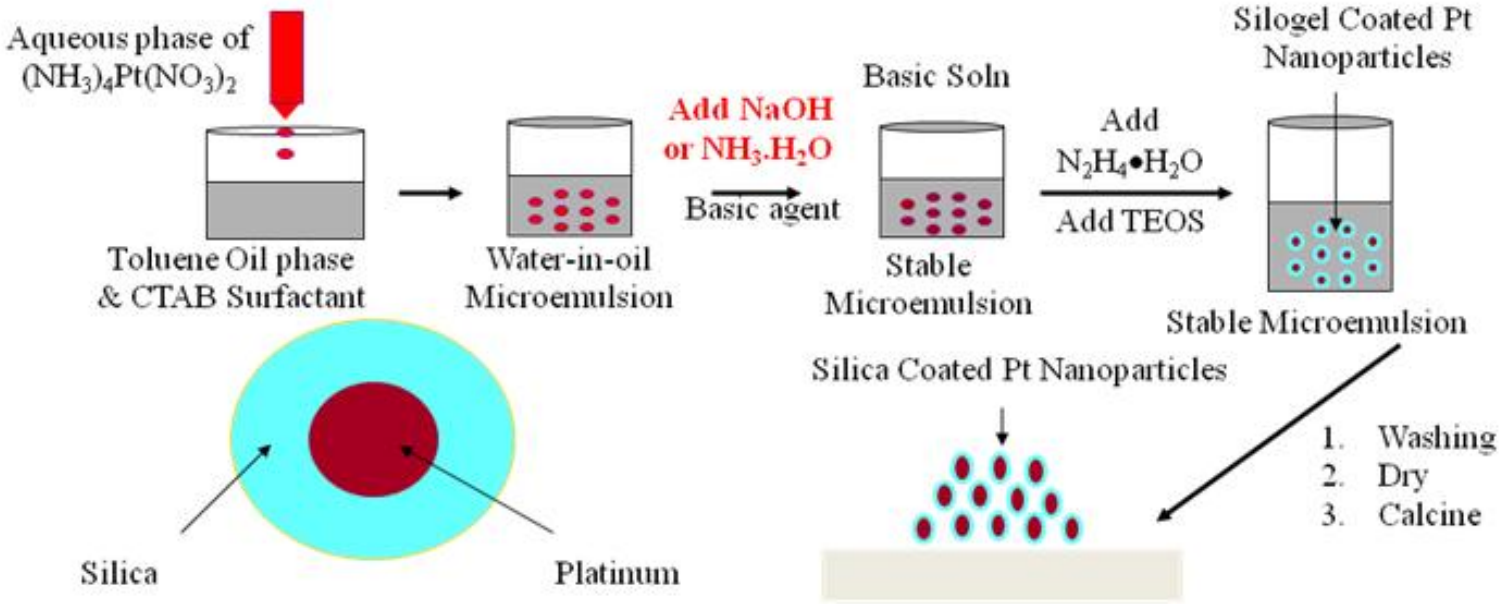

Figure 2.1 Schematic of Reverse Microemulsion synthesis of Pt@SiO_2 sample [9]

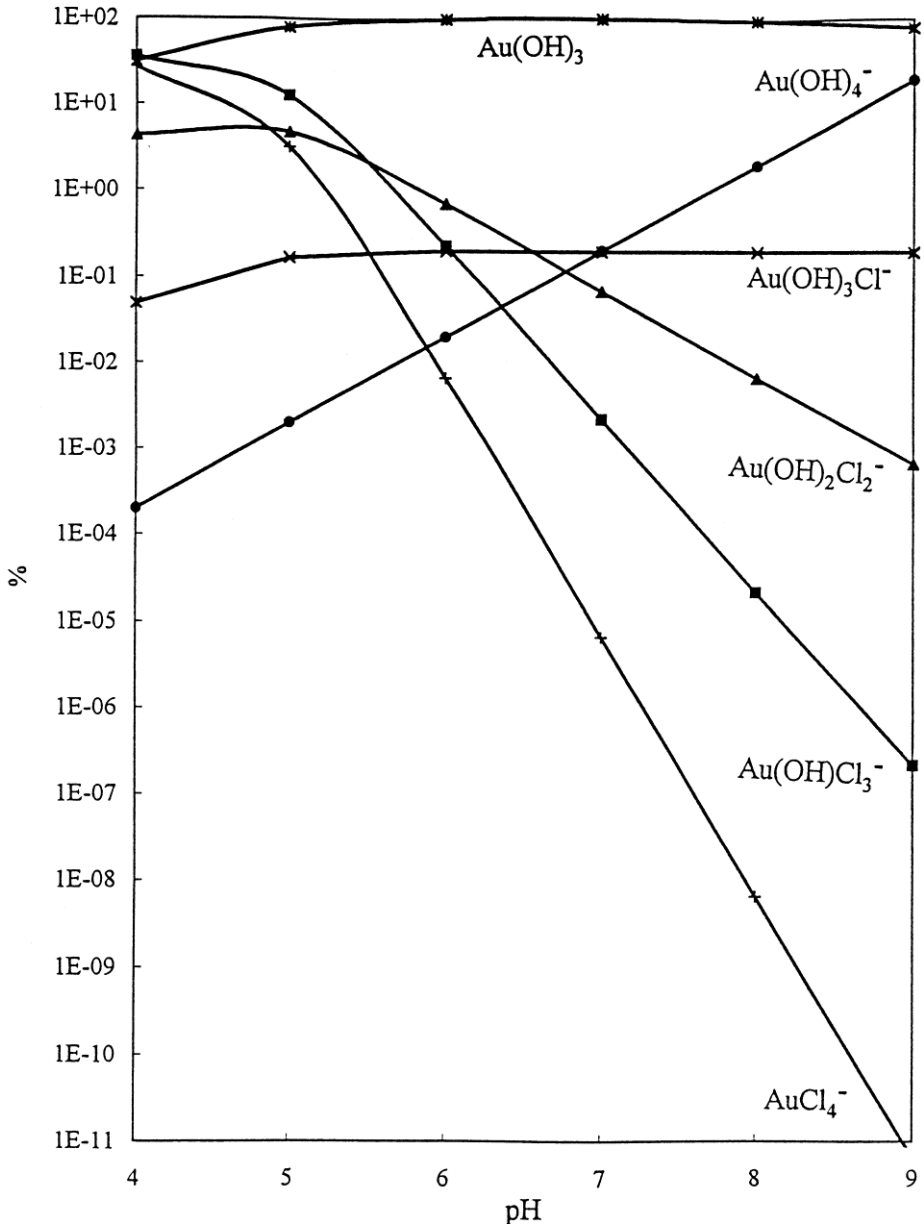

Figure 2.2 The variation in calculated fractions of different gold species in impregnation solution with the pH values at 300 K [5]

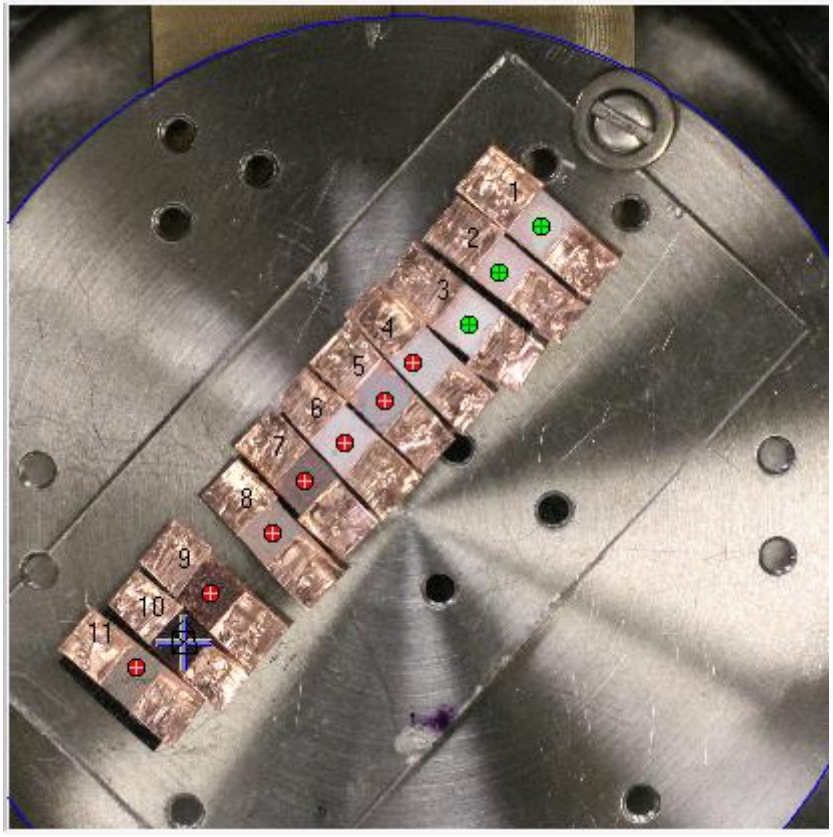

Figure 2.3 Scheme of X-ray photoelectron spectroscopy (XPS) measurement

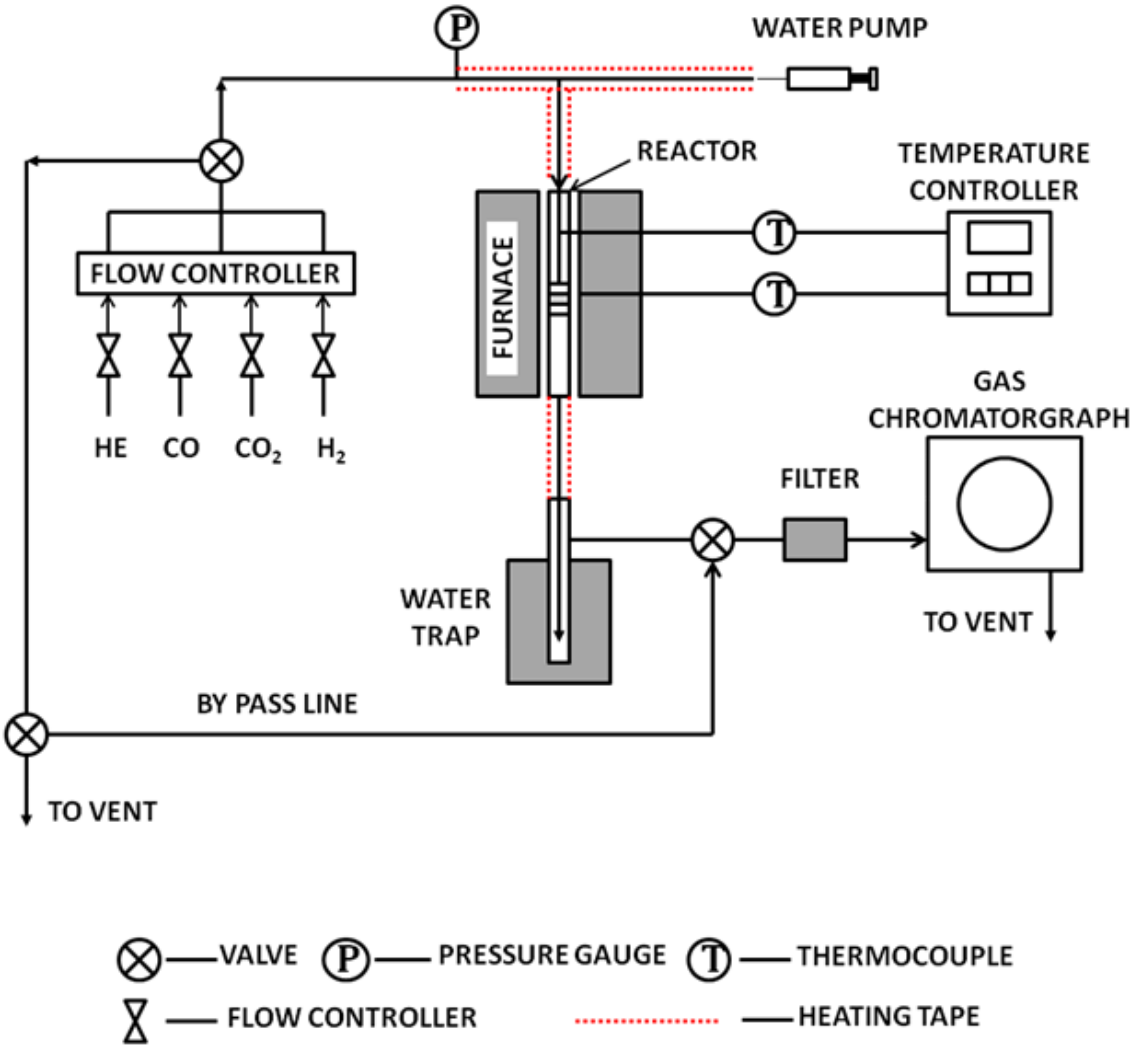

Figure 2.4 Scheme of Water-gas shift reaction system setup

References

[1] S. Eriksson, U. Nylen, S. Rojas, M. Boutonnet, ***Applied Catalysis A: General*** 265 (2004) 207-219.

[2] K.M.K. Yu, C.M.Y. Yeung, D. Thompsett, S.C. Tsang, ***Journal of Physical Chemistry B*** 107 (2003) 4515-4526.

[3] D. Pierre, W. Deng, M. Flytzani-Stephanopoulos, ***Topics in Catalysis*** 46 (2007) 363-373.

[4] Q. Fu, ***Ph.D. Dissertation, Department of Chemical and Biological Engineering, Tufts University*** (2004).

[5] C.-K. Chang, Y.-J. Chen, C.-t. Yeh, ***Applied Catalysis A: General*** 174 (1998) 13-23.

[6] R. Zanella, S. Giorgio, C.R. Henry, C. Louis, ***The Journal of Physical Chemistry B*** 106 (2002) 7634-7642.

[7] S. Derrouiche, P. Gravejat, B. Bassou, D. Bianchi, ***Applied Surface Science*** 253 (2007) 5894-5898.

[8] F. Delannay, ***Characterization of Heterogeneous Catalysts***, Dekker, New York (1984), p. 423.

[9] D. Pierre, ***M.S. Thesis, Department of Chemical and Biological Engineering, Tufts University*** (2006).

Chapter 3

Silica-Encapsulated Platinum Catalysts with Alkali-Promotion for the Low-Temperature Water-Gas Shift Reaction

3.1 Introduction

Preparation methods play a crucial role in catalyst design. Over the past few decades, the preparation of nano-sized noble metal particles and their deposition on metal oxide supports has attracted strong interest because of the widespread use of these particles in heterogeneous catalysis. The importance of noble metal and oxide support interaction for the WGS reaction has been discussed extensively in the literature [1-5]. A great deal of research has been devoted to tailor the synthesis of the catalysts in order to maximize such strongly interacting species on supports. However, conventional techniques like deposition-precipitation or incipient wetness impregnation (IMP), while good for practical applications, cannot give the level of control required to harness and, more so, to systematically investigate the metal-support interaction and to maximize the metal-support interfaces. Novel techniques are thus continually considered and applied. A novel synthesis approach which is demonstrable of nonmetallic Pt species interaction with ceria was reported by Yeung *et al.* in 2005 [6]. Encapsulation of platinum nanoparticles inside a nanoscale shell of ceria was achieved by a reverse microemulsion technique. The resulting material showed excellent activity for the WGS reaction, presumably through atomically dispersed platinum in the ceria shell, while the undesired methanation reaction was suppressed by not exposing the metallic core Pt sites.

Due to the rising price of rare earth oxides, there is interest in finding alternative Earth-abundant oxide supports for the noble metals or using promoters to achieve the kind of stable atomic dispersions afforded by ceria. It is also of fundamental interest to reproduce the type of active metal site on ceria on other supports, and the use of alkali and alkaline-earth ions as promoters has already been investigated for the WGS reaction catalysts [7-11]. The study of alkali promotion was extended to Pt-based catalysts for the low-temperature WGS reaction with reducible or partially reducible oxide supports such as titania [8-10], zirconia [12], and ceria [13]. However, the interpretation of active site is complicated by the non-zero activity of Pt on these (alkali-free) supports. Recently, Pierre, and Zhai *et al.* reported that alkali ions can also significantly boost the catalytic performance of Pt catalysts on inert oxide supports, such as SiO_2 and Al_2O_3, for the low-temperature WGS reaction and proposed that alkali-stabilized Pt-$(OH)_x$ species were the active sites for the reaction [14, 15]. It was also concluded that the same Pt-$(OH)_x$ species catalyze this reaction independent of the type of support [11]. Understanding the alkali promotion would allow rational designs of new low-temperature WGS catalysts using very small amounts of Pt and a wide choice of low-cost supports.

In this chapter, the results of new investigations of catalyst structure-activity effects of alkali-modified Pt catalysts for the low-temperature WGS reaction are presented. Instead of using the conventionally open-structured catalysts, I focused on the encapsulated platinum within a shell of silicon oxide (prepared via the reverse microemulsion technique); and extended the findings reported in Pierre's thesis [14]. Na^+ ions were applied as promoters. Samples were characterized by scanning transmission electron microscopy (STEM), X-ray photoelectron spectroscopy (XPS), BET surface area measurements, and by CO chemisorption. Temperature-programmed reduction (TPR) measurements were conducted using the reactant, CO, as the

reductant. Catalytic activities of core-shell structured $Pt@SiO_2$ were evaluated for the WGS reaction under various gas conditions and compared with Pt catalysts prepared by conventional impregnation methods.

3.2 Materials and Methods

A microemulsion is a surfactant-stabilized oil phase in a bulk water medium. This stabilized minor phase (micelles) is achieved via the inherent properties of the surfactant. A typical surfactant is a molecule that contains a hydrophilic head and a hydrophobic tail. In an extremely diluted oil-in-water (or vice versa) solution the surfactant dissolves and exists as a monomer, but when its concentration exceeds a certain minimum, critical micelle concentration (CMC), the molecules of surfactant orient to form micelles. Within these micelles a noble metal salt can be localized and stabilized for future manipulation (i.e. reduction, reaction, or deposition onto a support, etc.). The benefits of microemulsion-prepared materials include high surface area, thermal stability, nanosized, monodispersed particles, and highly structured materials.

Platinum particles, encapsulated by a silica shell, were prepared here by the reverse microemulsion (ME) method, following the approach described in Figure 2.1. The as-prepared samples were dried overnight at 100 °C and are denoted as $Pt\text{-}Na@SiO_2$ (when NaOH was used to adjust the pH) and $Pt@SiO_2$ (when NH_4OH was used to adjust the pH). A part of the dried $Pt@SiO_2$ was further impregnated to incipient wetness (IMP) final state with a $NaNO_3$ aqueous solution (0.3 mol/L) followed by drying overnight at 100 °C. This is denoted as $Na(IMP)\text{-}Pt@SiO_2$. Another part of $Pt@SiO_2$ was further impregnated with a small amount of cerium after precipitation of the silicon oxide. An amount of dissolved cerium(III) nitrate was added after

TEOS to the basic solution, the pH of the solution being sufficiently basic (pH 10-11, controlled by ammonia) to precipitate cerium hydroxide within the pores of the silica shell. The final mixture was filtered, washed and dried overnight at 100 °C. This is denoted as $Pt@SiO_2$-CeO_2 [a]. All dried samples were calcined at 400 °C at a heating rate of 2 °C/min in static air for 4 h.

For comparison, Pt/SiO_2 and Pt/CeO_2 [a] samples were prepared with open supports. 1 at. % Pt/SiO_2 was prepared by IMP. A certain amount of Na was also added on the dried Pt/SiO_2 sample with an aqueous solution of $NaNO_3$ by the IMP method as well, denoted as Na(IMP)-Pt/SiO_2. 0.8 at.% Pt/CeO_2 [a] sample was prepared by deposition–precipitation (DP) with ammonium carbonate. Pre-made ceria support was prepared by the Urea Gelation Coprecipitation method [16]. All dried samples were calcined at 400 °C at a heating rate of 2 °C/min in static air for 4 h.

Selected, calcined Na-modified samples were washed by D.I. water to remove excess Na ions. This was followed by filtering the suspension and drying the solid at 100 ^oC under vacuum overnight, no further calcination.

Table 3.1 lists the properties of the materials prepared and tested in this work.

---

a. The $Pt@SiO_2$-CeO_2 and Pt/CeO_2 samples were prepared and tested by Pierre in his thesis.

3.3 Results and Discussion

3.3.1 Characterization

3.3.1.1 Surface area and pore volume measurements

The physical properties of the materials prepared and tested in this work were listed in Table 3.1 and 3.2. The commercial silica support has surface area of 210 m^2/g. The core-shell structured samples were all prepared with high surface areas and pore volume, indicating that the silica shell is mesoporous and hence open for facile diffusion of the small reactant molecules of CO and H_2O to the "encapsulated" Pt sites. As shown in Table 3.1, especially high (400 m^2/g) is the shell area of Pt@SiO_2 prepared with ammonia. Surface modification of the samples with subsequent addition of Na ions decreased the surface area significantly, *i.e.* the surface area of Pt-Na@SiO_2 and Na(IMP)-Pt@SiO_2 was 198 m^2/g and 157 m^2/g , respectively. Adding NaOH during the preparation also lowered the pore volume considerably, *i.e.* the pore volume of Pt@SiO_2 and Pt-Na@SiO_2 was 0.55 mL/g and 0.18 mL/g, respectively. This drop in surface area and pore volume is a result of pore collapsing upon the application of NaOH, impregnation and heat treatment. However, as shown in Table 3.2, both Pt@SiO_2 and Pt-Na@SiO_2 samples have pore size of 4-5 nm (diameter). The porosity was adequate for reactant accessibility to the pores of the sample. The Weisz-Prater criterion was used to estimate the influence of pore diffusion on the reaction rates [17]. Here the dimensionless WP number was much less than 0.3, hence diffusion limitations can be excluded [18].

3.3.1.2 Bulk elemental analysis

In recent work with Pt promoted by Na ions on open silica supports, it was reported that well-dispersed Pt-O_x species can associate with Na ions and retain the Na ions during a water-washing step [11]. Absent the Pt, all of Na washes away from the silica surface. A similar result was found here with the Na-modified encapsulated Pt@SiO_2 samples; *i.e.* some Na remained in the sample even after several washings. This is shown in Table 3.1 for both Pt-Na@SiO_2 and Na(IMP)-Pt@SiO_2 samples. No Pt was found in the washing solution as checked by ICP. The residual alkali is then attributed to the interaction of the alkali with the atomically dispersed Pt species, *i.e.* to strong Pt-O_x-Na interaction, resisting washing.

3.3.1.3 Electron microscopy

Around 1 at.% Pt was found in the samples prepared by the reverse microemulsion method and the average Pt particle size at the core as imaged by electron microscopy is around 7 nm. The particle size can also be found by the metal dispersion calculated from the chemisorption measurements. However, as shown in Table 3.3, the Pt dispersion varied in different encapsulated samples, with or without Na addition, both before and after water washing. This is an indication that other than the Pt nanoparticles at the core, there are also dispersed Pt clusters and atoms in the silica shell of these core-shell structured materials. Alternatively, Na-modification and water washing treatment could have affected the chemisorption results which was then checked by further sample characterization.

The STEM image in Figure 3.1 is a reproduction of Figure 4.1 from Pierre's thesis [14]. It confirms the encapsulation of the platinum nanoparticles within the silicon oxide shell in Pt-

Na@SiO_2 sample. The platinum cores are on the order of 7-10 nm with 60 nm thick silica shells. The elemental maps obtained from the EDS analysis of Pt-Na@SiO_2 not only show a high concentration of platinum at the center of the particles, but also the existence of small platinum clusters embedded throughout the pores of the silica shell. This also explains why residual Na was found in the well-washed Pt-Na@SiO_2, since atomically dispersed Pt species stabilize and retain the Na ions even after washing [11]. Particle deposition in the pores of a highly mesoporous material is not uncommon in microemulsion techniques. Calderone *et al.* found that other than being encapsulated by the silica in the center during the silica coating, the Pt species could also be dispersed throughout the shell as demonstrated by TEM images [19]. Thus, it is not surprising to see the dispersed Pt clusters in the 4-5 nm diameter pores of the materials as shown in Figure 3.2 and 3.3. These figures are from Pt@SiO_2 and Pt-Na@SiO_2 samples made in this thesis with the properties shown in Tables 3.2 and 3.3.

3.3.1.4 Metal dispersion and accessibility

Atomically-dispersed Pt-O_x species are reported to be the active sites for the WGS reaction on ceria [20, 21], and for the alkali-promoted Pt on inert, open supports [11]. Here, because of the core-shell structure, the accessibility of these sites was an initial concern. CO chemisorption was used to address the dispersion and accessibility of Pt species in the encapsulated samples. Calculated by CO chemisorption measurements at ambient temperature, the Pt dispersion was 22% in the Pt@SiO_2 sample but a lower value of 5-6% was found for the Pt-Na@SiO_2 and Na(IMP)-Pt@SiO_2 samples, assuming a linear CO adsorption on Pt [22]. With higher alkali loading, the nominal Pt dispersion was further decreased. One possibility with the high coverage of alkali is that some part of the platinum was fully covered, hence inaccessible to

CO. Indeed, the Pt dispersion increased after the water washing treatment due to the removal of excess Na and exposure of more Pt sites to CO, as Table 3.3 shows. Another reason for the different dispersion is that the strength of CO adsorption on the Na-promoted Pt was different. Such weakening has been reported for alkali-modified Pt/Al_2O_3, and the mode of CO-Pt adsorption was partially changed from linear to bridged adsorption [23]. Thus, it is hard to estimate the Pt dispersion in these Na-modified samples by CO chemisorption, because the assumption of CO:Pt = 1:1 may not hold true for the part of Pt that is associated with Na ions. Moreover, the estimated dispersion is distorted also by the presence of platinum as large (7-10 nm size) nanoparticles at the core of these structures. Since we do not know the exact amount of Pt at the core, we cannot use the CO chemisorption measurements to compare to the TEM results. TEM, in turn, is not good to image sub-nm clusters and atoms. For the latter, atomic resolution microscopy is needed, and it is highly recommended for more precise particle size distribution measurements.

When the same amount of Pt was loaded by the IMP method on silica, Pt/SiO_2, a slightly higher Pt dispersion was estimated, as Table 3.3 shows, using the above assumptions. The lower metal dispersion in $Pt@SiO_2$ indicated that part of the Pt is not accessible to CO, mainly the 7 nm platinum particle at the core. The results with the Na-modified $Pt@SiO_2$ are even harder to explain. While the average Pt particle size remained the same with Na addition, as the TEM data in Table 3.3 show, the dispersion values dropped dramatically. Even if we consider bridged CO adsorption on the Na-promoted Pt [23], the values remain too low. So apparently, the scaling factor (all of the Pt) used in estimating the dispersion is inaccurate. Besides the ~ 7 nm -particles at the core, some more platinum must have become totally inaccessible to CO in the Na-containing samples, perhaps through partial collapse of the pores as mentioned above. The pore

surface area is almost half in Na-promoted samples and total pore volume is only one third, as listed in Table 3.1-3.2 and depicted in Figure 3.2-3.3. The lost in surface area and pore volume leads to the block of platinum sites and thus the lower metal dispersion in Na-containing $Pt@SiO_2$ samples.

Overall, it is clear that in the core-shell structured Pt samples, only a minority of the Pt species will exist as clusters and atoms in the pores of the silica shell and be accessible to CO. If reaction is observed, this will be due to the presence of this phase and not the big platinum particles at the core or elsewhere in the mesoporous silica shell. Hence, these core-shell structures can be used to check whether a reaction known to occur on either the metallic or the nonmetallic state of platinum takes place. For example, in ref. [6], the $Pt@CeO_2$ core-shell catalyst was excellent for the WGS reaction, but inactive for the methanation reaction, the latter catalyzed by metallic Pt sites. The activity of the Na-promoted $Pt@SiO_2$ is further investigated in the following sections.

3.3.1.5 Metal oxidation states

The small Pt clusters dispersed throughout the silica shell are interesting to investigate as sites for various reactions. These and attendant Pt atoms (TEM-invisible) have no activity for the water-gas shift reaction as first shown by Pierre [14] and also verified in this work. On the other hand, the Na-promoted $Pt\text{-}Na@SiO_2$ is very active. As shown in Table 3.3 all the Na-containing $Pt@SiO_2$ samples have similar average particle size of Pt as found by TEM. Their TEM-invisible Pt portion may be different, however. More so, the TEM-invisible platinum in the unpromoted sample $Pt@SiO_2$ must be very low, as indicated by the bigger average Pt particle size, and the

good correspondence of the TEM- and CO chemisorption-based estimates of metal dispersion [24] (see Table 3.3).

In recent work, it was reported that atomically-dispersed Pt species can associate with Na ions, and the Na-modified Pt is positively charged and remains so under WGS conditions [8, 11]. XPS measurements were conducted to check the oxidation states of Pt in the samples examined and tested in this work. Initial- and final-state effects have been reported to shift the binding energy of supported Pt clusters [22, 25]. Generally, final-state effects cause a positive shift of the binding energy of metallic nanoparticles as their size is decreased [22], but below a certain cluster size (~ 2 nm), initial-state effects prevail [25], which is determined principally by the electronegativities of the atoms involved. Figure 3.4 shows XP spectra for Pt_{4f}, the binding energy assignments for Pt^0 at 71.1 and 74.5 eV, Pt^{2+} at 72.8 and 76.2 eV, and Pt^{4+} at 74.2 and 77.6 eV, respectively [26]. With the addition of Na ions, the peaks shifted to higher binding energies. The observed large positive shift (by 1.7 eV) shows a clear increase of the fraction of oxidized Pt species in the encapsulated Pt-Na@SiO_2 sample. The same trend was observed in the differently structured material Na-Pt/SiO_2. For the open Pt-Na/SiO_2 sample, the positive energy shift is attributed to the smaller Pt particle sizes and the electron deficiency of Pt species in the presence of Na-O_x species, as reported by Zhai et al. [11].

3.3.2 Reducibility and regeneration

CO-TPR was used here to identify reducible surface oxygen species and probe the onset of the WGS reaction by activation of the surface hydroxyls to produce CO_2 and H_2. As shown in Figure 3.6, there is no CO_2 or H_2 production over the Na-free Pt@SiO_2 sample till 300 ^oC. With

Na in the sample, Pt-Na@SiO_2 showed CO_2 and H_2 production from 150 ^oC. The same was true for the conventionally prepared Na-Pt/SiO_2 sample, consistent with what has been reported before [11]. Hence, the addition of Na introduces both reducible surface oxygen species and active surface hydroxyl groups to the dispersed Pt species. Through strong interaction with Na-O, the Pt-O_x(OH)-Na species shifts the reduction and as shown below, the WGS reaction, to much lower temperatures.

In order to evaluate the regenerability of the hydroxyl groups on Pt-Na@SiO_2, cyclic CO-TPR tests were conducted. If a second cycle of CO-TPR was carried out without any treatment after the first cycle, negligible CO_2 and H_2 productions were detected, as shown in Figure 3.7, which means most of the reducible species had been consumed and surface OH groups were depleted during the first cycle. If a rehydration treatment was introduced between the two cycles, with helium saturated with water vapor (3%H_2O-He) flowing through the reactor at room temperature for an hour, a full recovery of OH groups was found, as shown in Figure 3.8 by the full recovery of H_2 production along with the CO_2. These cyclic CO-TPR tests demonstrate that the activation of water and the regeneration of OH groups take place on the Na-promoted Pt sites at close to ambient temperature. This is the feature that renders the Pt-O_x(OH)-Na cluster active for the low-temperature WGS reaction, as also shown for the open Na-Pt/SiO_2 catalyst [11].

Since no molecular O_2 was used to replenish the adsorbed oxygen, no CO_2 is produced from reaction of CO with the adsorbed oxygen on the active sites, as shown in the second CO-TPR cycle of Figure 3.7 and 3.8. Of course, this was clearly produced in the first CO-TPR cycle of a fully oxidized surface. These catalysts are also very good for the dry CO oxidation reaction. Na-promoted Pt@SiO_2 is shown here to be an active catalyst for the CO oxidation reaction at close to ambient temperatures; a significant finding in its own right. As mentioned in the

introduction, the alkali promotion of the CO oxidation reaction has been demonstrated by Nieuwenhuys and his group for the Au/Al_2O_3 system [27, 28] but not for the Pt/SiO_2.

3.3.3 WGS reaction activity

3.3.3.1 Alkali-promotion effect

Similar to the CO-TPR data, the activity plots, in Figure 3.9, show that sodium addition has the same promotion effect on the activity of the encapsulated platinum catalyst for the WGS reaction as for the open Pt/SiO_2 catalyst. The Na-free samples, $Pt@SiO_2$ and Pt/SiO_2, show no activity for the reaction up to 300 ^oC, while the Na-containing samples are active, perhaps as active in TOF as the Pt/CeO_2 sample, shown in Figure 3.10. As explained by the CO chemisorption results, the open $Pt\text{-}Na/SiO_2$ samples have a larger number of active sites available than the encapsulated core-shell $Pt\text{-}Na@SiO_2$ samples, which accounts for the better total activity of the former. However, the specific activity may be the same, as indicated by the same light-off temperature (100 ^oC) and the same apparent activation energies (see below). Also $Pt\text{-}Na@SiO_2$ may contain active sites that are inaccessible to the gases; e.g. through pore collapse, as mentioned before. Therefore the reactivity difference should be due to the difference of the population and accessibility of the active sites.

Without sodium, the sample $Pt@SiO_2$ is not active for the WGS reaction due to the lack of surface oxygen and hydroxyl groups. To investigate this sample further, Na was added into the $Pt@SiO_2$ by the IMP method (see Table 3.1). CO-TPR showed that Na added this way was still effective in introducing active OH groups and binding through oxygen groups to the dispersed Pt. The enhanced reducibility of the $Pt\text{-}Na@SiO_2$ was manifested also by the Na(IMP)-

$Pt@SiO_2$ sample during the CO-TPR test. As a result, in the CO-TPR data shown in Figure 3.11, the CO activated the OH and produced CO_2 and H_2 similar to the Pt-$Na@SiO_2$ sample. In turn, as shown in Figure 3.9, Na(IMP)-$Pt@SiO_2$ is as active as Pt-$Na@SiO_2$ catalyst for the low-temperature WGS reaction. This series of experiments also shows that the atomically dispersed minority phase of Pt in the core-shell preparations is there (in the shell) even when no Na was used in the preparation, as shown in Table 3.3 and in Figure 3.2. These sites are simply not stabilized and not activated unless Na is added even in a post-preparation step.

Catalytic activity tests of these Na-promoted $Pt@SiO_2$ samples were run in both the ascending- and descending-temperature mode. The well maintained activities of the catalysts indicated the good stabilities of these Na-modified samples. A long-term stability of Pt-$Na@SiO_2$ was evaluated for the WGS reaction in the full reformate gas stream at 350 ^oC for about 60 h, as shown in Figure 3.12. Shutdown to 100 ^oC was examined still in the full reformate gas stream without removing the water from the gas mixture. After several shutdown-startup cycles, the catalyst maintained its activity. This long-term stability is an important property if the catalysts are to be developed for commercial WGS applications.

A single-pot microemulsion procedure was adapted to prepare $Pt@SiO_2$-2%CeO_2 sample, as described in Pierre's thesis [14]. This material had no sodium and a relatively high surface area of 223 m^2/g. The addition of cerium salt took place toward the end of the core-shell synthesis, and this coupled with slow precipitation, allowed for uniform cerium oxide distribution throughout the silica shell. For comparison, a Pt/CeO_2 sample made by deposition–precipitation was examined as well. In the activity measurements, this sample had identical activity to the $Pt@SiO_2$-2%CeO_2 sample containing only 2 at.% ceria. A small amount of ceria additive is thus sufficient to fully interact with the dispersed platinum species in the silica shell and therefore

yield a very active material to catalyze the WGS reaction. It is also clear that sodium promotion of Pt is similar by that of CeO_2, i.e. the sodium addition is as effective as addition of ceria in promoting Pt for the WGS reaction. This finding has very significant implications for practical catalyst design.

3.3.3.2 Kinetic Measurements

The Na-promotion effect on the WGS reaction activity over the Pt-based catalysts is further confirmed in activity tests conducted in the full reformate gas mixture, as depicted in Figure 3.13. The rates measured over the encapsulated samples are much lower than the rates on the Na-promoted Pt/SiO_2, which we attribute to the inaccessibility of much of the Pt in the core-shell sample. However, comparing the apparent activation energy (E_{app}) of the WGS reaction over the different samples, it is clear that the E_{app} over all the Pt-based samples falls into the same range, 70 ± 5 kJ/mol. As already discussed in ref. [11], this demonstrates that the Na-promotion is independent of the support structure and type. Na ions stabilize the Pt ions and facilitate the regeneration of the active OH groups, continuously providing OH to complete the reaction pathway. These OH groups are not present on alkali-free Pt/SiO_2 or $Pt@SiO_2$ surfaces, but they are on ceria. Hence the $Pt\text{-}O_x(OH)$-Ce and the $Pt\text{-}O_x(OH)$-Na clusters are analogs.

Based on the same apparent activation energy over CeO_2- or SiO_2-supported Pt catalysts, we conclude that $Pt\text{-}O_x(OH)$-M species is the active site, irrespective of what M is chosen. To further support this conclusion, the turnover frequency (TOF) of the reaction over different Pt-based catalysts was calculated. Usually, TOF is calculated by normalizing the reaction rates by the total amount of surface metal species, which cannot distinguish the active/non-active sites on

the surface. Here, the TOFs were calculated by normalizing the rates by the amount of active hydroxyl groups on the surface as determined by the CO-TPR data. This resulted in the same value of TOF over the various Pt-based catalysts used for the WGS reaction. As shown in Figure 3.14, Pt species on different supports, in different structures, with different alkali-promoters [15], all had TOF values that fitted the same line in an Arrhenius-type plot. This result points to a common active site for all the Pt-based catalysts in the WGS reaction. It will be important mechanistically and useful practically to add other such ligands to extend this finding to other additives and supports.

3.4 Summary

In this chapter, the catalytic activity and stability of encapsulated platinum catalysts for the WGS reaction was presented. The Na-free Pt@SiO_2 is not active for the reaction up to 300 ^oC, while addition of Na, either in the synthesis step or by impregnation of the core-shell sample, renders the corresponding Pt-Na@SiO_2 or Na(IMP)-Pt@SiO_2 a very active catalyst for the WGS reaction, comparable to Pt/CeO_2. The active Pt-O_x(OH)-Na species in the mesoporous silica shell of the Pt-Na@SiO_2 and Na(IMP)-Pt@SiO_2 catalysts dissociate water and regenerate surface hydroxyl groups. Incorporation of sodium on these encapsulated Pt catalysts enhances their catalytic activity similar to that of Na-promoted, open Pt/SiO_2 catalysts. An oxidized Pt-O_x(OH) species associated with alkali ions or cerium ions is concluded to be the active site for the low-temperature WGS reaction, which can be manifested on any support.

The Pt-Na@SiO_2 is a very stable catalyst as was demonstrated in this work. However, the tradeoff is the lower rates measured over these encapsulated catalysts, as some of the active sites are inaccessible to reactants. Further improvement in the design of these structured catalysts is needed to solve the pore collapsing problem and improve the active site utilization.

Table 3.1 Physical properties of the examined catalysts

Catalysts	Bulk Composition (at.%)		Surface Area
	Pt	Na	(m^2/g)
SiO_2	--	--	210
Na-SiO_2	--	3	203
Na-SiO_2 washed	--	--	203
Pt/SiO_2	1	--	187
Na(IMP)-Pt/SiO_2	1	3	172
Na(IMP)-Pt/SiO_2 washed	1	1.6	172
Pt@SiO_2	1.1	--	400
Na(IMP)-Pt@SiO_2	1.1	6.1	157
Na(IMP)-Pt@SiO_2 washed	1.1	2.4	157
Pt-Na@SiO_2	1	4.4	198
Pt-Na@SiO_2 washed	1	2.7	198
Pt@SiO_2-2%CeO_2 [a]	0.8	--	223
Pt/CeO_2 [a]	0.8	--	145

a. Data of Pt/CeO_2 and Pt@SiO_2-CeO_2 are from Pierre's thesis [14].

Table 3.2 Porosity of the core-shell structured samples

Catalysts	Pore Volume (mL/g)	Pore Diameter (Å)
Pt@SiO_2	0.55	40
Pt-Na@SiO_2	0.18	48

Table 3.3 Platinum particle size distribution and metal dispersion

Catalysts	Pt Particle Size (nm) [a]		Pt Dispersion [b]
	dispersed	at the core	(%)
Pt/SiO_2	4.8±1.2	--	24
Na(IMP)-Pt/SiO_2	1.6±0.4	--	71
Na(IMP)-Pt/SiO_2 washed	1.6±0.4	--	93
$Pt@SiO_2$	2.8±0.5	6.5	22
Na(IMP)-$Pt@SiO_2$	2.4±0.8	6.5	5
Na(IMP)-$Pt@SiO_2$ washed	2.4±0.8	6.5	8
Pt-$Na@SiO_2$	2.6±0.5	7.0	6
Pt-$Na@SiO_2$ washed	2.6±0.5	7.0	11

a. Measured by TEM; particle size distribution of dispersed platinum throughout the shell was calculated from a survey of 50 particles; this does not include the TEM-invisible sub-nm clusters and atoms of Pt in the mesoporous silica shell; platinum particle size at the core is listed separately.
b. Calculated by CO chemisorption measurements at ambient temperature, assuming a linear CO adsorption on Pt [22].

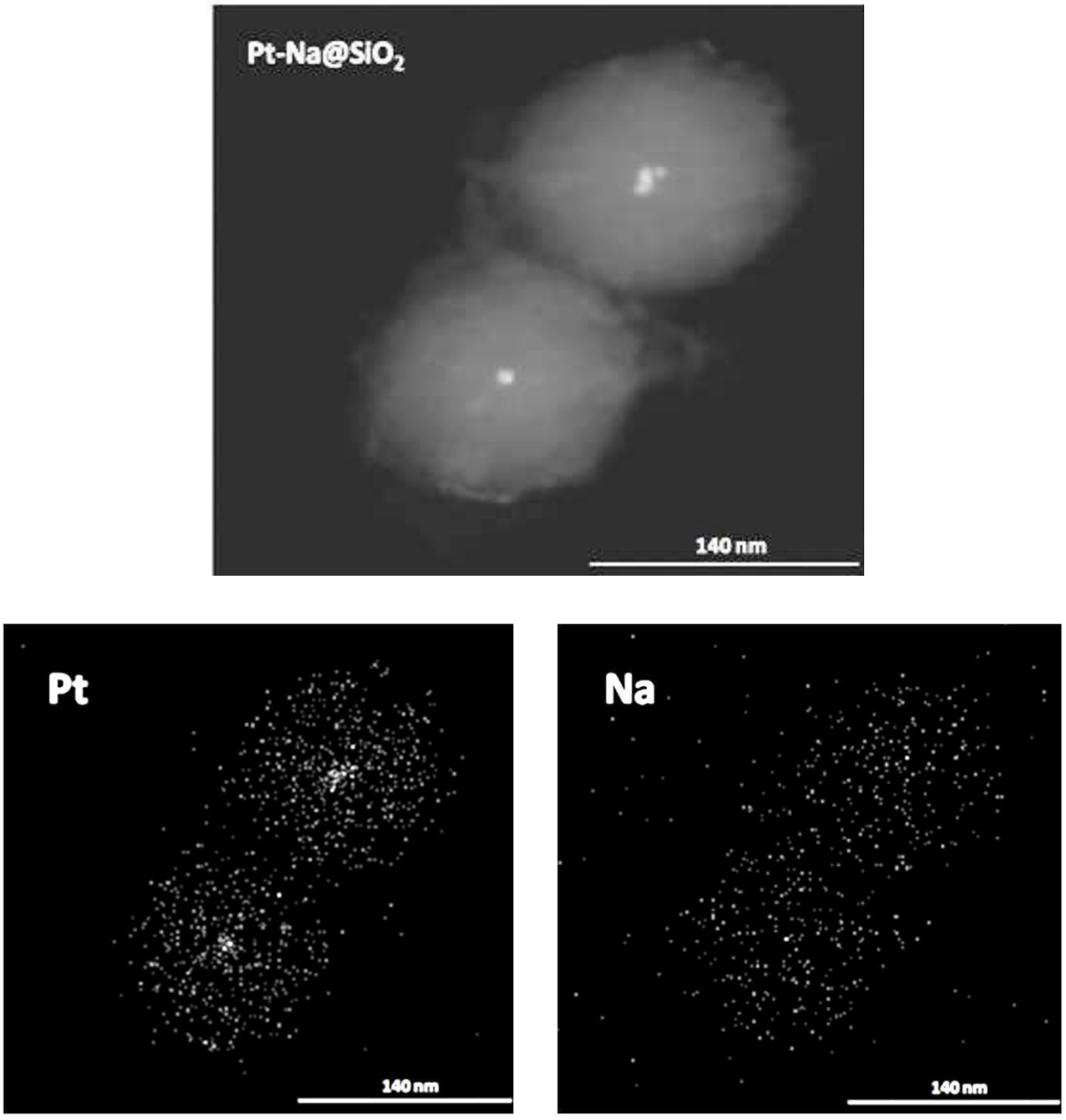

Figure 3.1 STEM image of Pt-Na@SiO_2 sample and elemental maps of Pt and Na [a]

a. STEM images are reproductions of Figure 4.1 from Pierre's thesis [14].

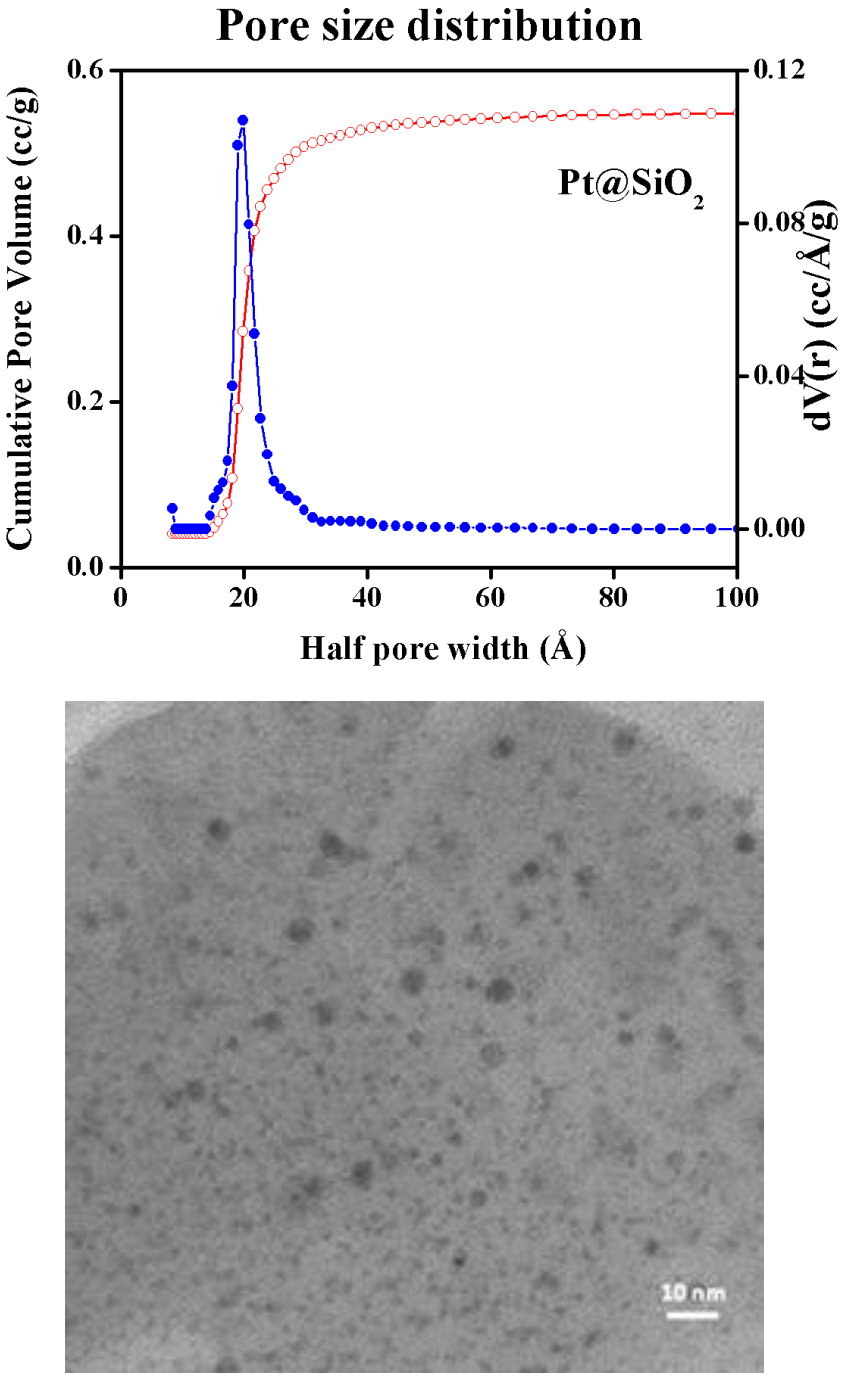

Figure 3.2 Pore size distribution of $Pt@SiO_2$ sample and HRTEM image of the dispersed platinum nanoparticles in the pores of silica shell

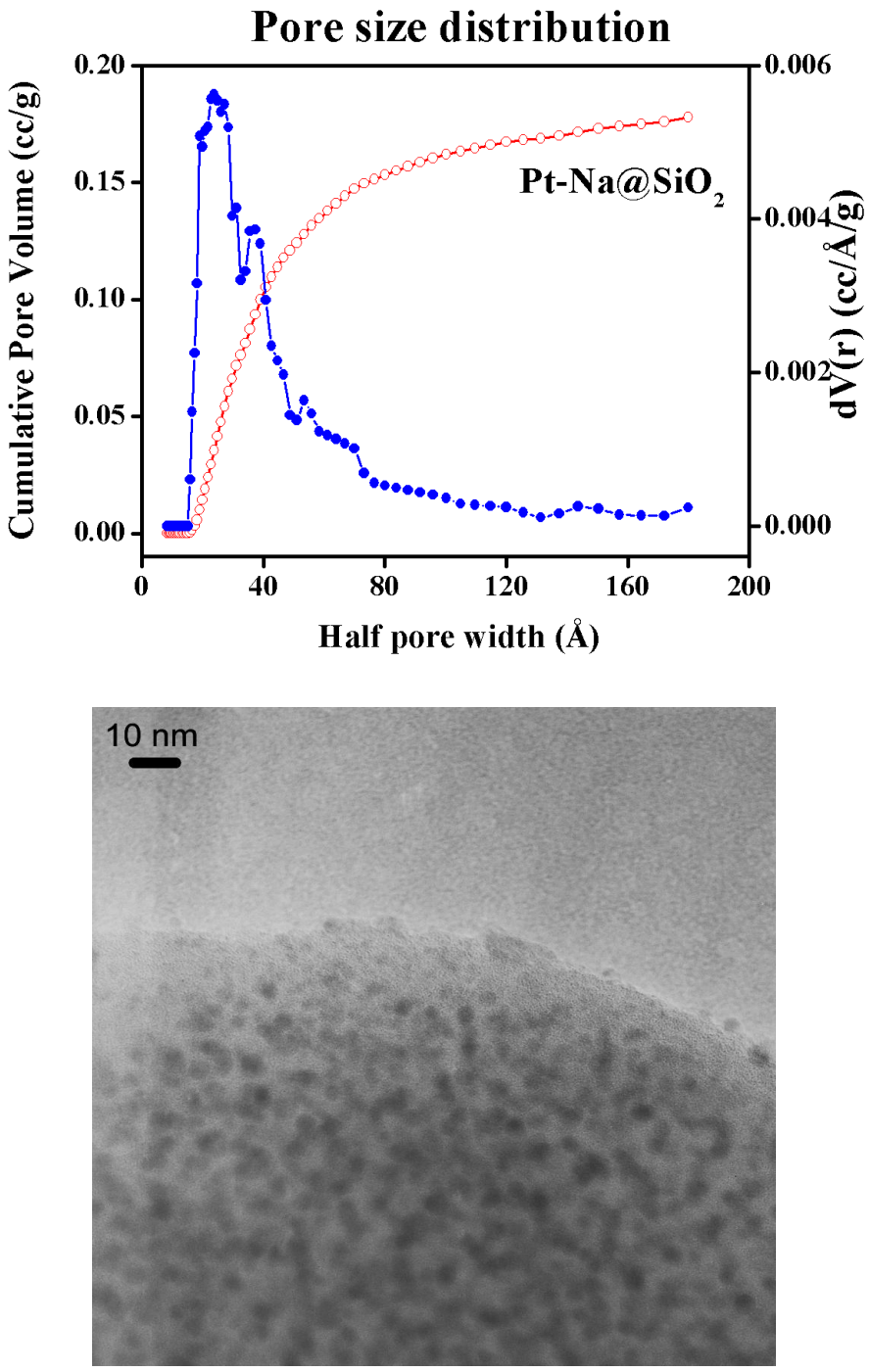

Figure 3.3 Pore size distribution of Pt-Na@SiO_2 sample and HRTEM image of the dispersed platinum nanoparticles in the pores of the silica shell

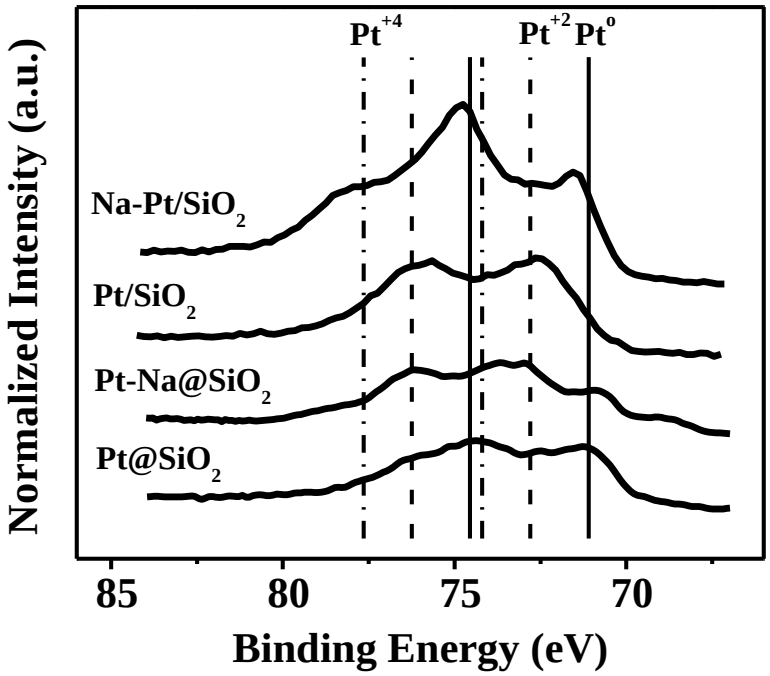

Figure 3.4 XP spectra of Pt_{4f} in $Pt@SiO_2$ and Pt/SiO_2 samples with or without Na-modification

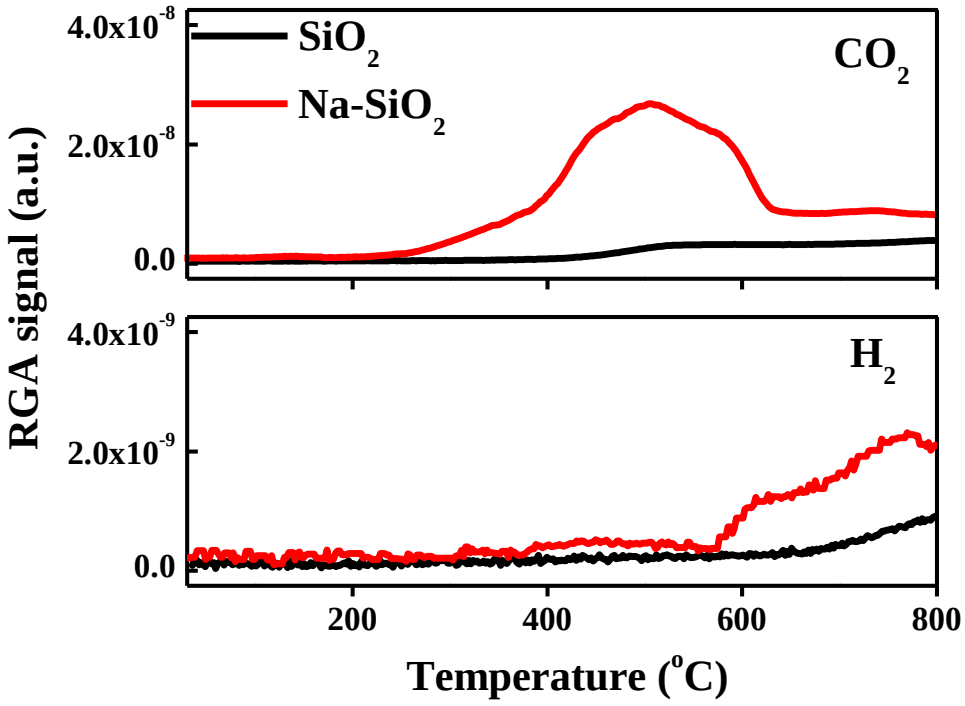

Figure 3.5 CO-TPR of bare and Na-modified silica supports

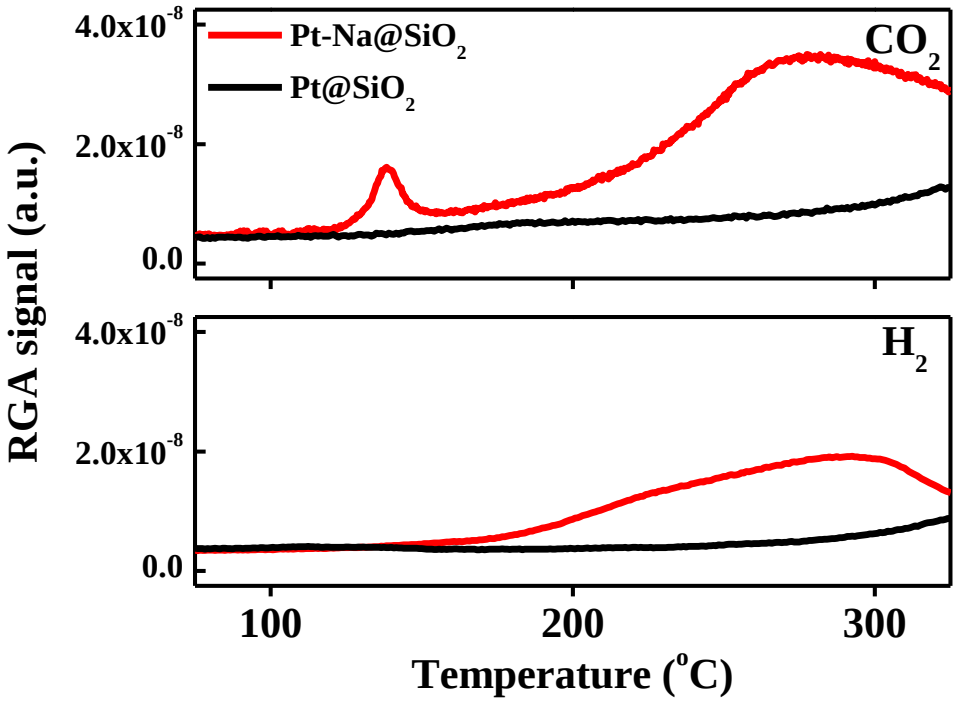

Figure 3.6 CO-TPR of $Pt@SiO_2$ and $Pt\text{-}Na@SiO_2$ catalysts

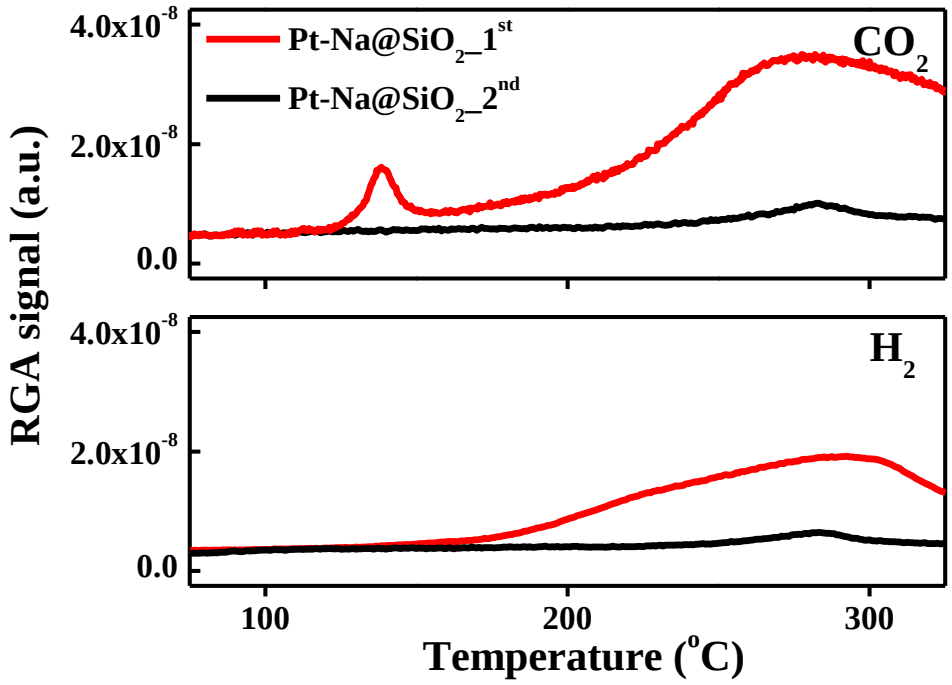

Figure 3.7 CO-TPR of Pt-Na@SiO_2 catalyst in two consecutive cycles with no intermittent rehydration

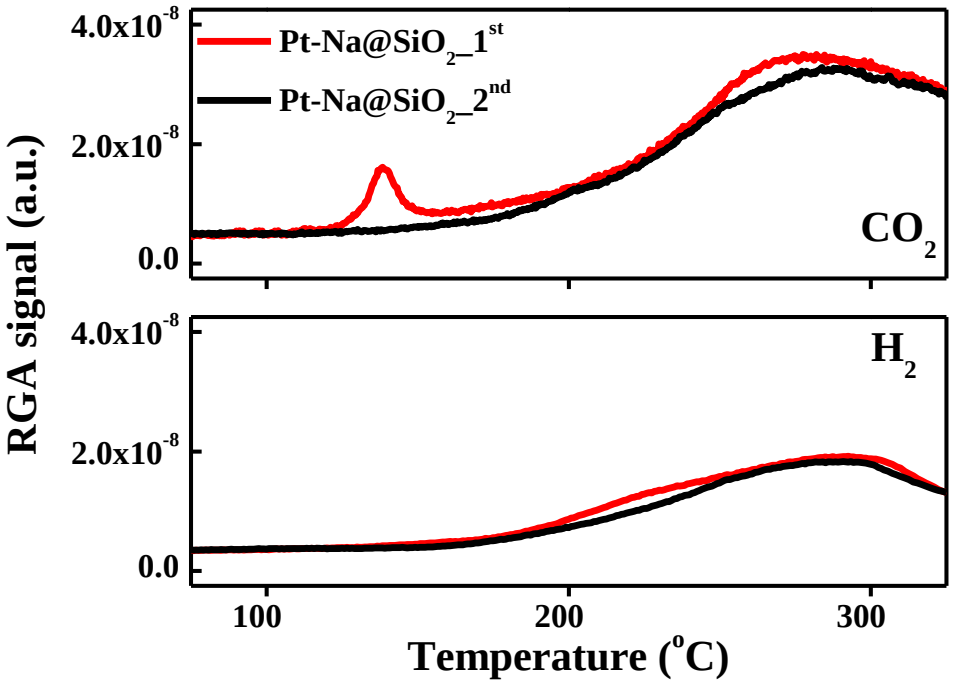

Figure 3.8 Cyclic CO-TPR of Pt-Na@SiO_2 catalyst with intermittent rehydration at room temperature

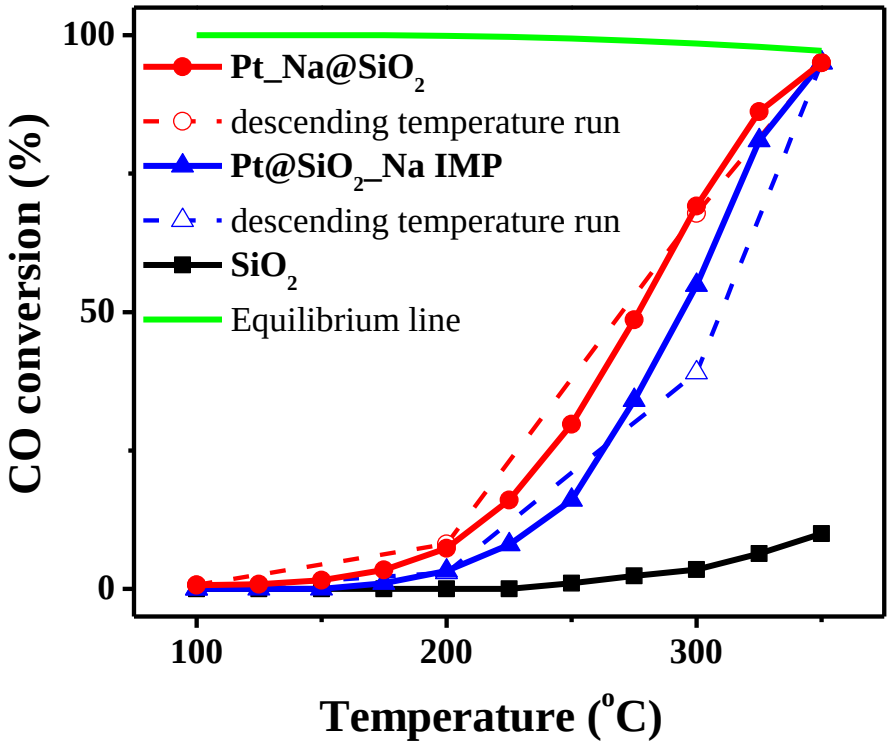

Figure 3.9 CO conversion profiles of WGS reaction equilibrium and in steady-state tests over Na-free and Na-modifed $Pt@SiO_2$ catalysts

(2%CO-10%H_2O-He, 70 mL/min, contact time = 0.09 g·s/mL)

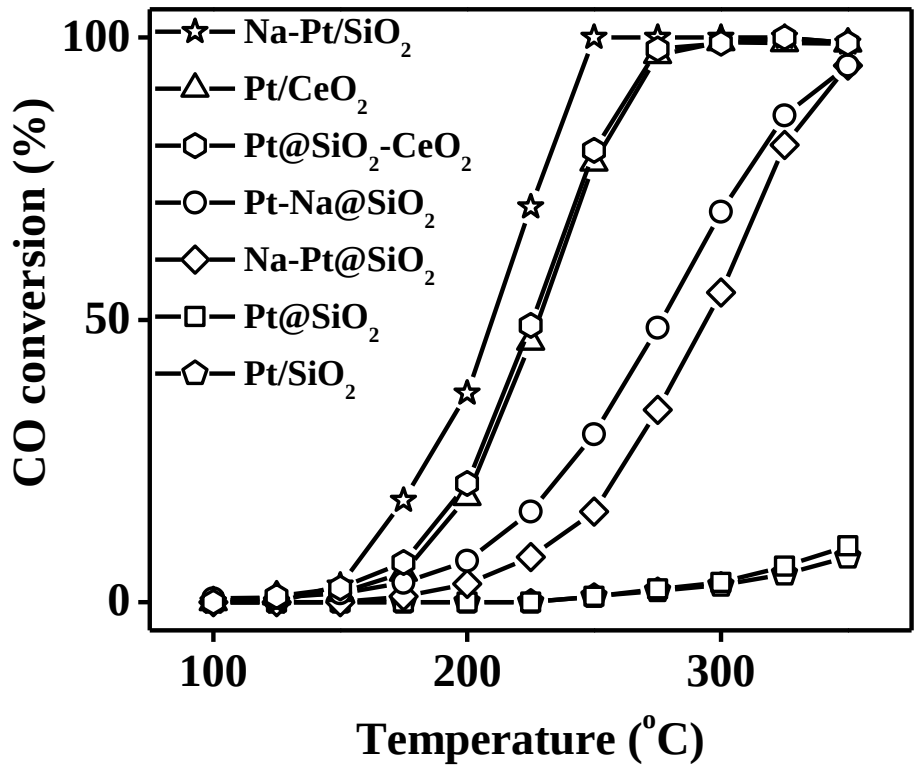

Figure 3.103 CO conversion profiles in steady-state tests of WGS reaction over $Pt@SiO_2$, Pt/SiO_2 and Pt/CeO_2 [a] catalysts

(2%CO-10%H_2O-He, 70 mL/min, contact time = 0.09 g·s/mL)

a. Data on Pt/CeO_2 and $Pt@SiO_2$-CeO_2 are from Pierre's thesis [14].

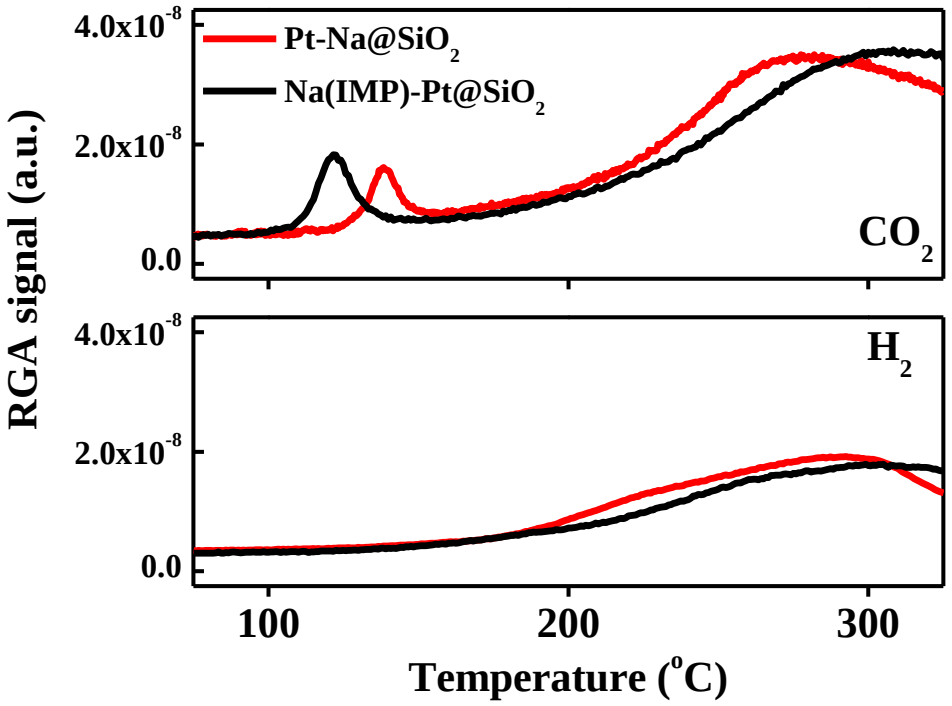

Figure 3.11 CO-TPR of Pt-Na@SiO_2 and Na(IMP)-Pt@SiO_2 catalysts

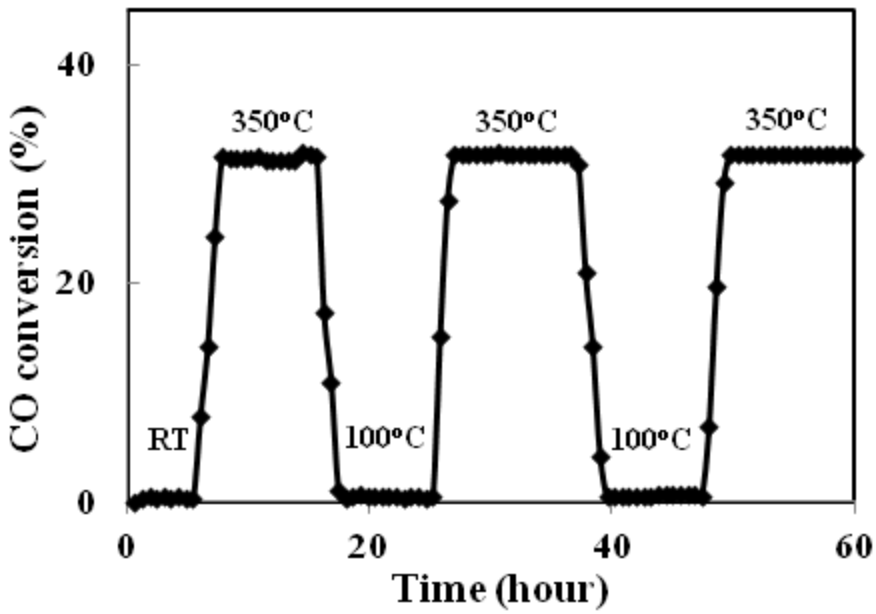

Figure 3.12 Stability test over Pt-Na@SiO_2 catalyst at 350 ^oC

(11%CO–26%H_2O–26%H_2–7%CO_2–He, 207 mL/min, contact time = 0.03 g·s/mL)

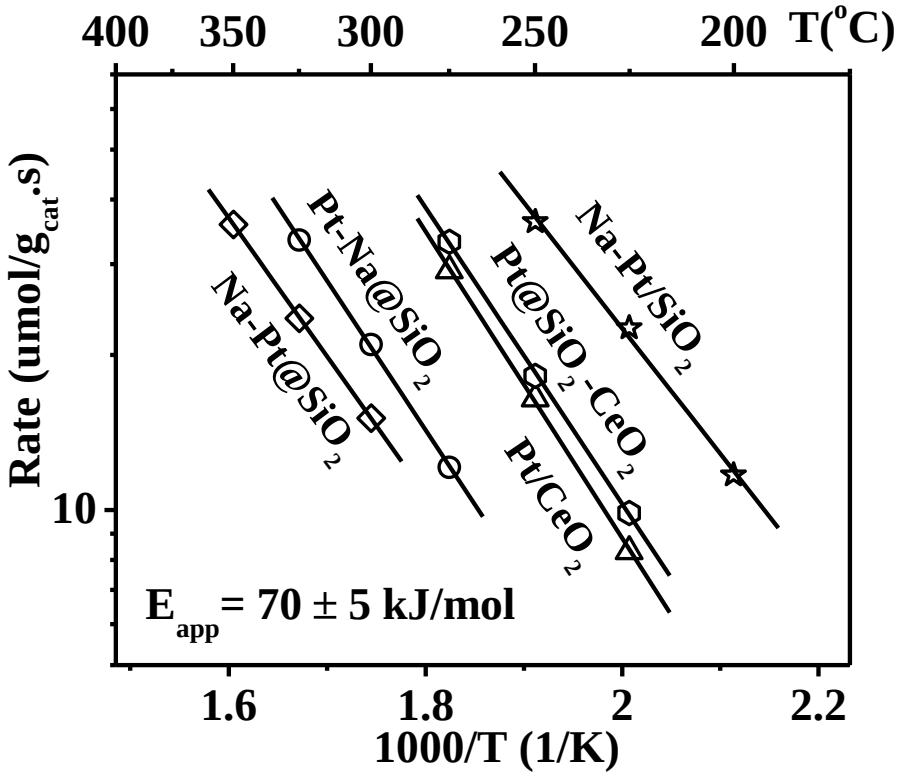

Figure 3.13 WGS reaction rates over $Pt@SiO_2$, Pt/SiO_2 and Pt/CeO_2 [a] catalysts (11%CO–26%H_2O–26%H_2–7%CO_2–He, 207 mL/min, contact time = 0.03 g·s/mL)

a. Data on Pt/CeO_2 and $Pt@SiO_2$-CeO_2 are from Pierre's thesis [14].

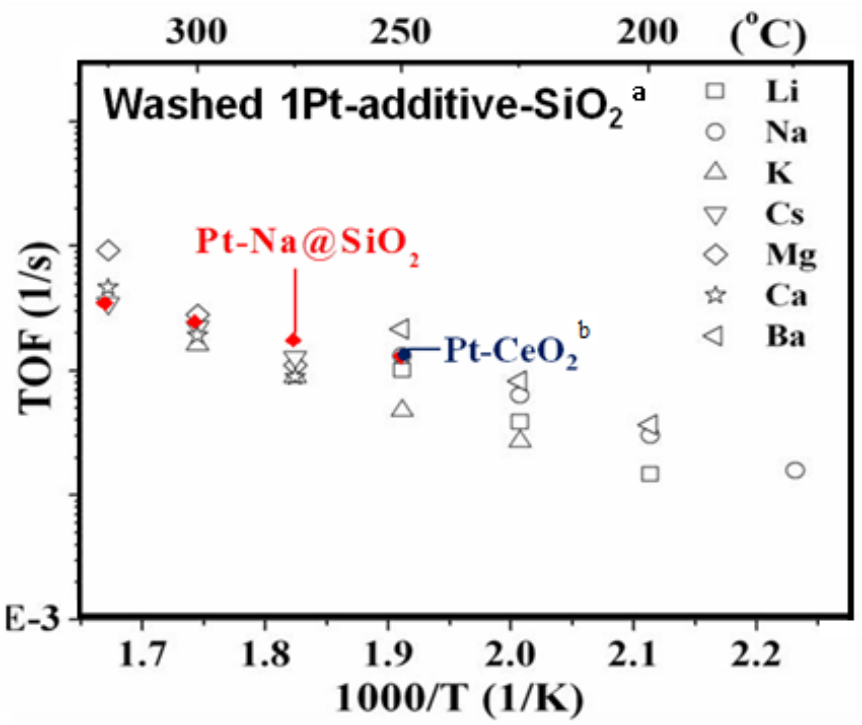

Figure 3.14 TOF of WGS reaction over various Pt-Based catalysts

(11%CO–26%H_2O–26%H_2–7%CO_2–He, 207 mL/min, contact time = 0.03 g·s/mL)

a. Data of washed 1Pt-additive-SiO_2 are from Zhai's thesis [15]
b. Data of Pt/CeO_2 was from Pierre's thesis [14]

References

[1] D. Tibiletti, A. Goguet, F.C. Meunier, J.P. Breen, R. Burch, ***Chemical Communications*** (2004) 1636-1637.

[2] K.G. Azzam, I.V. Babich, K. Seshan, L. Lefferts, ***Journal of Catalysis*** 251 (2007) 163-171.

[3] Y. Sato, K. Terada, S. Hasegawa, T. Miyao, S. Naito, ***Applied Catalysis A: General*** 296 (2005) 80-89.

[4] H. Iida, A. Igarashi, ***Applied Catalysis A: General*** 303 (2006) 48-55.

[5] Y. Bi, W. Zhang, H. Xu, W. Li, ***Catalysis Letters*** 119 (2007) 126-133.

[6] C.M.Y. Yeung, K.M.K. Yu, Q.J. Fu, D. Thompsett, M.I. Petch, S.C. Tsang, ***Journal of the American Chemical Society*** 127 (2005) 18010-18011.

[7] A. Hagemeyer, R.E. Carhart, K. Yaccato, A. Lesik, C.J. Brooks, ***United States Patent Application*** 20040175325 (2004).

[8] X. Zhu, M. Shen, L.L. Lobban, R.G. Mallinson, ***Journal of Catalysis*** 278 (2011) 123-132.

[9] P. Panagiotopoulou, D.I. Kondarides, ***Applied Catalysis B: Environmental*** 101 (2011) 738-746.

[10] P. Panagiotopoulou, D.I. Kondarides, ***Journal of Catalysis*** 267 (2009) 57-66.

[11] Y. Zhai, D. Pierre, R. Si, W. Deng, P. Ferrin, A.U. Nilekar, G. Peng, J.A. Herron, D.C. Bell, H. Saltsburg, M. Mavrikakis, M. Flytzani-Stephanopoulos, ***Science*** 329 (2010) 1633-1636.

[12] J.M. Pigos, C.J. Brooks, G. Jacobs, B.H. Davis, ***Applied Catalysis A: General*** 319 (2007) 47-57.

[13] H. Evin, G. Jacobs, J. Ruiz-Martinez, U. Graham, A. Dozier, G. Thomas, B. Davis, ***Catalysis Letters*** 122 (2008) 9-19.

[14] D. Pierre, ***M.S. Thesis, Department of Chemical and Biological Engineering, Tufts University*** (2006).

[15] Y. Zhai, ***Ph.D. Dissertation, Department of Chemical and Biological Engineering, Tufts University*** (2011).

[16] D. Pierre, W. Deng, M. Flytzani-Stephanopoulos, ***Topics in Catalysis*** 46 (2007) 363-373.

[17] P.B. Weisz, C.D. Prater, V.I.K. W.G. Frankenburg, E.K. Rideal, ***Advances in Catalysis*** 6 (1954) 143-196.

[18] M.A. Vannice, ***Kinetics of Catalytic Reactions***, Springer Science+Business Media, New York (2005), pp. 63-65.

[19] V. Calderone, J. Schütz-Widoniak, G. Bezemer, G. Bakker, C. Steurs, A. Philipse, ***Catalysis Letters*** 137 (2010) 132-140.

[20] Q. Fu, H. Saltsburg, M. Flytzani-Stephanopoulos, ***Science*** 301 (2003) 935-938.

[21] Q. Fu, W. Deng, H. Saltsburg, M. Flytzani-Stephanopoulos, ***Applied Catalysis B: Environmental*** 56 (2005) 57-68.

[22] C.R. Henry, ***Surface Science Reports*** 31 (1998) 231-325.

[23] H. Tanaka, M. Kuriyama, Y. Ishida, S.-i. Ito, T. Kubota, T. Miyao, S. Naito, K. Tomishige, K. Kunimori, ***Applied Catalysis A: General*** 343 (2008) 125-133.

[24] R.P.H. Gasser, ***An introduction to chemisorption and catalysis by metals***, Clarendon Press, Oxford University Press, Oxford, New York (1985).

[25] J. Radnik, C. Mohr, P. Claus, ***Physical Chemistry Chemical Physics*** 5 (2003) 172-177.

[26] ***National Institute of Standards and Technology X-ray Photoelectron Spectroscopy Database*** Version 3.5 (2003), http://srdata.nist.gov/xps/.

[27] A.C. Gluhoi, X. Tang, P. Marginean, B.E. Nieuwenhuys, ***Topics in Catalysis*** V39 (2006) 101-110.

[28] A.C. Gluhoi, B.E. Nieuwenhuys, ***Catalysis Today*** 122 (2007) 226-232.

Chapter 4

Alkali-Promoted, Alumina-Supported Gold Catalysts for the Low-Temperature Water-Gas Shift Reaction

4.1 Introduction

A variety of supported gold catalysts such as Au/CeO_2, Au/TiO_2 and Au/Fe_2O_3 have been reported to be highly active for the low-temperature WGS reaction [1-3]. It has been concluded that the catalytic activity depends strongly on the dispersion, chemical state and structure of the gold particles [4].

The reducible oxides supports can supply and store oxygen, which is beneficial to gold stabilization and activity, whereas the non-reducible Al_2O_3 and SiO_2 are classified as inert oxide supports. The promotion effect of alkali (earth) metals on the Au-based catalysts is of great interest in many reactions. It has been reported that alkali/alkaline earth metals can be used as structural promoters to stabilize gold clusters in the preferential oxidation of CO reaction in H_2-rich gas stream [5]. According to the literature, the addition of alkali (earth) metal oxides can be beneficial or detrimental to the gold catalyst performance. Haruta and co-workers reported that Au supported on $M(OH)_x$, where M could be Mg, Be or La, displays a high catalytic activity in CO oxidation, especially if the average size of the Au particles is around 1.5-2 nm [6, 7]. Moreover, for the Au on non-reducible Al_2O_3 support, the addition of MO_x (M: Rb, Li, Ba) is beneficial for low-temperature CO oxidation [8]. But a negative effect of alkali ions has been also reported, i.e.

K acted as a poison to Au-Pt/CeO_2 catalyst for the WGS reaction when the atomic ratio of K/Au was higher than 2.5 [9].

Gold mobility and agglomeration at high temperatures or in humid atmospheres result in loss of the gold active sites. It has been reported that Au destabilization, *e.g.* on TiO_2, takes place even with storage [10]. A great volume of research has also been devoted to understanding the gold metal-support interaction. Recent studies have focused on the modification of supports to keep the Au dispersed, primarily for the dry CO oxidation reaction. A surface of rich hydroxyl groups was essential for stabilizing the gold clusters. Veith *et al.* found that the gold clusters were stabilized against coarsening by surface hydroxyl groups on TiO_2 under ambient conditions [10, 11]. Also, the hydroxide gold species, i.e. isolated $Au(OH)_3$ well-mixed with $La(OH)_3$, showed markedly high catalytic activity for CO oxidation at a temperature as low as 193 K [7].

γ-Alumina (Puralox, SBa-200) is one of the most widely used commercial oxide supports. In this work, this type alumina was subjected to hydrothermal treatment in basic solutions in order to create an OH-rich surface for gold deposition. Addition of alkali ions was also applied to examine whether they can promote the catalytic activity and stability of Au/Al_2O_3 catalysts for the WGS reaction. Pt/modified-Al_2O_3 was also briefly examined and compared to Au/modified-Al_2O_3. Samples were characterized by BET surface area, UV-Visible Spectroscopy (UV-Vis), X-ray diffraction (XRD), ICP, and high resolution transmission electron microscopy (HRTEM). Temperature-programmed reduction (TPR) measurements and cyclic tests were conducted using the reactant, CO, as the reductant. Samples were also activated by heat pretreatment in different gas atmospheres. Catalytic activities of Au/Al_2O_3 were evaluated for the WGS reaction under various gas conditions (TPSR, steady-state) and compared with other Au-based catalysts on various oxide supports.

4.2 Materials and methods

4.2.1 Catalyst Preparation

Aluminum oxide support was first modified by hydrothermal treatment. γ-Alumina powder (Puralox, SBa-200, S_{BET} = 210 m^2/g, V_p = 0.55 mL/g) was immersed either in water or sodium hydroxide aqueous solution at 100^oC for 20 hours in an autoclave, then filtered, washed and dried at room temperature under vacuum overnight. The modified supports are denoted as Al_2O_3-H_2O and Al_2O_3-OH. Another support, aluminum hydroxide-Boehmite (AlOOH), containing –OH in its crystalline lattice was examined as reference.

1 at.% Pt/Al_2O_3 catalyst was prepared by incipient wetness impregnation (IMP). γ-Al_2O_3 was impregnated with a solution of $(NH_3)_4Pt(NO_3)_2$, the volume of which equaled the total pore volume of γ-Al_2O_3 (0.55 mL/g) under constant stirring. After impregnation, the sample was dried in vacuum at 60^oC overnight and further calcined at 400 °C at a heating rate of 2 °C/min in static air for 4 h. Pt/Al_2O_3-OH was also synthesized by the above methods on surface modified- γ-alumina supports.

1 at.% Au/Al_2O_3 catalyst was prepared by deposition-precipitation (DP) with urea. The γ-Al_2O_3 powder was immersed in 0.5 mM of $HAuCl_4$ aqueous solution and 0.42 M urea was added drop wise to adjust the pH to 8-9. The mixture was stirred at 80^oC for 4 hours. After loading the gold, the mixture was held quiescent for a while until the upper solution was decolorized, which indicates that all the gold was bound on the alumina support. All samples were recovered by filter and washed three times with hot water, then dried under vacuum at room temperature overnight. Au/Al_2O_3-OH was also synthesized by the above methods on surface modified- γ-

alumina supports. The dried samples were further treated at 200 ^{o}C for 2 h at a heating rate of 1 °C/min in different gas atmospheres to investigate heat treatment effects.

With the Au/Al_2O_3-OH catalyst, Na ions were added to the dried samples (before calcination) by IMP as well, using sodium nitrate as the precursor (Sigma-Aldrich). The Na-modified sample was dried under vacuum at room temperature overnight, then calcined in two steps, first in 10%H_2-He at 200 ^{o}C for 2 h, then in 10%O_2-He at 300 ^{o}C for 2 h, both at a heating rate of 1 ^{o}C/min. The sample was washed after calcination, then dried under vacuum at room temperature overnight, without further calcination. This sample is denoted as Na-Au/Al_2O_3-OH.

4.2.2 Hydrothermal treatment of support

Aluminium oxide is an amphoteric oxide. In the Bayer process [12], alumina is converted to aluminum hydroxide, $Al(OH)_3$, which dissolves in the hydroxide solution according to the chemical reactions:

$$Al_2O_3 + 2\ OH^- + 3\ H_2O \rightarrow 2\ [Al(OH)_4]^-$$

$$Al_2O_3 + 3\ H_2O \rightarrow 2\ Al(OH)_3$$

Next, the hydroxide solution is cooled, and the dissolved aluminum hydroxide precipitates as a white, fluffy solid.

As stated in the thesis objectives, our approach to studying effect of surface hydroxyl groups and the alkali promotion of both platinum and gold catalysts was to prepare numerous active hydroxyl groups on the alumina surface and investigate it as a suitable support for a highly-active WGS reaction catalyst. For the hydrothermal treatment, the commercial alumina

power was immersed in hot water and a sodium hydroxide solution. It was expected that many hydroxyl groups would thus be formed on the alumina surface.

Four supports were used and analyzed by XRD, namely γ-Al_2O_3, Al_2O_3-H_2O, Al_2O_3-OH and AlOOH, the resulting patterns shown in Figure 4.1 a-d. γ-Al_2O_3 and AlOOH in Figure 4.1 (a) and (b), respectively, were used as two reference materials. The γ-Al_2O_3 with hydrothermal treatment in NaOH (0.5 M, 100 ^oC for 20 h in the autoclave), as shown in Figure 4.1 (c), was almost totally converted to gibbsite, i.e. aluminum hydroxide, $Al(OH)_3$. When the same γ-Al_2O_3 was treated hydrothermally in water alone (100 ^oC for 20 h in the autoclave), all three phases of γ-alumina, gibbsite and boehmite were present in Figure 4.1 (d). Thus, the desired hydroxyl groups were created on the γ-Al_2O_3 supports by these treatments.

To further investigate the effect of the above modification of the alumina support surfaces, these untreated and modified γ-alumina supports were tested in temperature-programmed reduction, using similar protocols. CO-TPR was used to probe the onset of the WGS reaction by activation of the surface hydroxyls to produce CO_2 and H_2. As shown in Figure 4.2, untreated γ-alumina powder gave out the lowest amount of CO_2 and the signal is detectable at the highest temperature, ~ 400 ^oC; for the γ-alumina support after hydrothermal treatment by NaOH, the onset temperature of CO_2 and H_2 production is at 300^oC and the first CO_2 peak appears at 200^oC, which is due from the reaction of CO and adsorbed oxygen species on the surface. Thus, the alkali-modified alumina became an effective high-temperature shift catalyst. In early work with alkalized alumina, Amenomiya and co-workers reported that excess surface oxygen was added by the alkali and the modified alumina surface became a good high-temperature shift catalyst [13]. Our results are in agreement with that study. The catalytic properties of the hydrothermally

treated alumina, Al_2O_3-H_2O, were not as promising, however, its performance being intermediate between the untreated and the NaOH-modified alumina surfaces.

The boehmite support was not chosen in this work for Au-based WGS reaction catalysts due to the following reasons: (i) the -OH groups of AlOOH belong to the lattice of the sample, which cannot be replenished by surface hydration treatment, even with alkali additives; (ii) the fine boehmite powder forms colloid with water and cannot be recovered, which means it cannot be used in solution-based preparation methods for Au-based sample in this thesis. But it may work in dry preparation methods, i.e. vapor deposition or ALD of gold precursor is highly recommended.

On the basis of the above characterizations, the γ-alumina support with hydrothermal treatment in NaOH was the most promising, and thus Al_2O_3-OH was selected as the most suitable support for deposition of gold catalysts. The onset temperature of CO_2 and H_2 production is lower than for the untreated sample; also the increased amounts of H_2 and CO_2 production over the NaOH-treated alumina support indicate that more surface oxygen and hydroxide groups are available on this surface. But the activity is still negligible for low-temperature WGS reaction; addition of gold or platinum or another metal is necessary to interact with the Na-O surface species, adsorb CO, and activate the –OH groups at low temperatures. This is discussed in detail in the following.

4.2.3 Gold addition by urea-assisted deposition/precipitation

The precursors used in preparing supported gold catalysts are salts or complexes where gold is usually in the +3 oxidation state. The Au^{III} precursor used in this work is tetrachloroauric

acid hydrate ($HAuCl_4.3H_2O$), which is a commercially available orange solid; in aqueous solution it is a strong acid. Moreover, the speciation of the gold ions depends strongly on the concentration, pH and temperature of the solution. When $HAuCl_4$ is dissolved in water, the chloroauric anion hydrolyses to form anionic hydroxylchloro gold(III) complexes $[Au(OH)_xCl_{4-x}]^-$, where x = 0-4 (see Table 4.1) [14]. The increase in pH induces color changes of the solution from yellow to colorless, indicating the changes in gold speciation (see Figure 4.3) [15]. A UV-vis investigation of solution thermodynamics has reported that under increasing pH, Cl ligands of $AuCl_4^-$ in solution substitute with hydroxyl ligands as shown in Figure 4.4. This experiment guides us to identify the level of hydrolysis in gold preparation.

In the deposition-precipitation (DP) method, urea was selected in this work as a base to slowly increase the pH value to prepare more homogeneous materials [16]. Urea acts as a delay base since there is no reaction when it is dissolved in a suspension of the support in the aqueous metal salt solution at room temperature; hydrolysis only occurs when this is heated above 333 K, according to the reaction:

$$CO(NH_2)_2 + 3H_2O \rightarrow CO_2 + 2NH_4^+ + 2OH^-$$

whereby there is a gradual and homogeneous release of hydroxyl ions and increase of pH throughout the solution. As described above, the increase of pH results in deeper hydrolysis of the $[AuCl_4]^-$ complex; the ageing time of a gold solution at fixed pH also influences the concentrations of the gold complexes, because equilibration of the speciation is established slowly [15, 17, 18]; the increase of temperature of $HAuCl_4$ solution increases the rate of hydrolysis of the gold species.

In a previous study, it was found that small gold particles could be obtained on titania, alumina, and ceria providing that the DP time at 353K was long enough, at least 4 hours (see Table 4.2) [16, 19]. Moreover, it was found that the gold in solution (8 wt.%) was deposited onto these supports within the first hour, while the pH of the suspension was still acidic (pH ~ 3). Thereafter samples matured while the pH continued to rise, reaching a plateau at pH around 7 after 4 hours, remaining the same even after 16 hours. After careful washing with water, drying at 300 or 363K under vacuum, and calcination in air at 573K, the gold particles were found to decrease in size as the DP time was increased. In this case, all the gold in solution was deposited on the support.

Beginning with $HAuCl_4$ as a precursor, the presence of chloride is detrimental to obtaining small gold particle size and good catalytic activity. DP is usually performed at quite high pH values, so that most of the Au-Cl bonds are hydrolyzed, and thorough washing with water at the end of the preparation removes the remaining chloride. Otherwise, the complex still contains chloride in its coordination sphere; this results in sintering to form rather large gold particles during calcination, as is the case with impregnation and anion adsorption methods, where much lower pH is used [20].

4.3 Results and discussion

4.3.1 Characterization

4.3.1.1 Surface area measurements

As shown in Table 4.3, the various treated alumina samples all maintained high surface areas. The commercial γ-alumina powder has a surface area of 210 m^2/g. The modified support

Al_2O_3-OH and samples after gold deposition Au/Al_2O_3-OH have surface areas of 250-270 m^2/g. This surface area increase is due to immersing the alumina support in the basic solution during hydrothermal treatment with NaOH. The deposition-precipitation procedure at high pH and high temperature may also increased in surface area, as shown in Au/Al_2O_3 sample (see Table 4.3). On the other hand, surface modification of the Au/Al_2O_3-OH sample with subsequent addition of Na ions (by IMP of $NaNO_3$) decreased the surface area considerably, from 246 to 216 m^2/g. No further change was observed after washing the sample with DI water to remove excess Na from the surface. This drop in surface area may be a result of partial pore collapsing upon the applied impregnation and heat treatment. However, from Table 4.4, we can see the beneficial effect of Na addition on suppressing the Au particle growth on the Na-Au/Al_2O_3-OH sample. After heat treatment at 200 ^oC, the mean particle size of gold on the Al_2O_3-OH alumina supports was decreased from 3.2 nm (alkali-free) to 1.2 nm (alkali-modified). Furthermore, we examine below whether the alkali addition is necessary to produce an active WGS catalyst, even in the case of the gold supported on the hydrothermally modified Al_2O_3-OH support.

4.3.1.2 Bulk Compositional Analysis

In Chapter 3, it was established that Na-promoted Pt on open and encapsulated silica supports, well-dispersed Pt-O_x species can associate with Na ions and retain the Na ions during a water-washing step [21, 22]. Absent the Pt, all of Na washes away from the silica surface [21]. A similar result was found here with the Na-modified Au/Al_2O_3-OH sample; *i.e.* some Na remained in the sample even after several washings. The ICP result is shown in Table 4.3 for Au/Al_2O_3-OH samples both with and without Na-addition, before and after water washing treatment (sample was dried at room temperature under vacuum overnight after washing, no further

calcination). No Au was found in the washing solution as checked by ICP. The residual alkali is then attributed to the interaction of the alkali with the atomically dispersed Au species, *i.e.* to strong Au-O_x-Na interaction, resisting washing.

4.3.1.3 Electron microscopy

Transmission electron microscopy (TEM) is used to image the metal and oxide phases. It is the most effective way to investigate the metal dispersion and establish the mean size of Au nanoparticles. In the recent literature, Na-promoted Pt atoms and clusters on fumed silica [21] as well as Na-promoted Pt over bare γ-alumina [23] were observed by atomic resolution scanning transmission electron microscopy techniques. In this work, high resolution transmission electron microscopy (HR-TEM) was used to examine the prepared catalysts, which is not good for detecting atoms and nanoclusters of gold, but it can be used to survey the effect of additives and support modifications on the gold particle size distributions. The results from this comparison are shown in Table 4.4 and in Figure 4.5 a-f. In Figure 4.5 a-c, we observe Au nanoparticles on the γ-alumina, the hydrothermally modified alumina support, and with Na-addition in the fresh catalysts before WGS reaction (the fresh catalyst Au/Al_2O_3 and Au/Al_2O_3-OH were calcined in 10%H_2-He at 200 ^oC for 2 h; the Na-Au/Al_2O_3-OH sample was calcined in two steps, first in 10%H_2-He at 200 ^oC for 2 h, then in 10%O_2-He at 300 ^oC for 2 h; sample was washed after calcination, then dried under vacuum at room temperature overnight, no further calcination). The Na-Au/Al_2O_3-OH sample has the smallest average gold particle size with narrow size distribution (1.2 ± 0.3 nm), while Au/Al_2O_3 and Au/Al_2O_3-OH had similar but bigger (3.2 ± 0.8 nm) gold nanoparticles. Thus, the modification (hydroxylation) of the support alone cannot be used to control the gold particle size.

The above findings are important in guiding the catalyst design and can be used to investigate the alkali effect on gold species supported on non-reducible oxide supports. The samples were imaged again after the WGS reaction up to 350 ^{o}C for a total of 10 h on stream, whereupon only the Na-Au/Al_2O_3-OH used catalyst was found to maintain 14% of its gold particles below 2 nm (and presumably had also a fraction of gold in sub-nm size, TEM-invisible), as shown in Figure 4.5 d. The used Au/Al_2O_3 and Au/Al_2O_3-OH samples, however, were found to contain all gold in > 2 nm size particles, as shown in Figures 4.5 e and f. This observation is in agreement with the WGS activity results which are discussed in the next section. Combining these two results, it is concluded that the –OH species alone on the surface are not enough to stabilize the gold; the presence of the alkali is absolutely necessary. The residual alkali ions (after washing) may be thought to bind to the dispersed Au species on the modified Al_2O_3-OH support surface and suppress the sintering of Au nanoparticles during the WGS reaction.

4.3.1.4 Metal oxidation states

XPS analysis is usually applied to study the surface concentration of Au, Pt, Na and O, and the oxidation states of the precious metal in the sample. For Pt/Al_2O_3, Au/La_2O_3 and gold on many other oxide supports, XPS has been a very useful tool to check their chemical properties before and after reaction. But Au/Al_2O_3 is challenging to analyze by XPS. Using the Au_{4f} XP spectra to characterize gold, the binding energies for Au^0 are at 87.7 and 84.0 eV, for Au^+ at 88.3 and 84.6 eV, and for Au^{3+} at 90.2 and 86.5 eV, respectively [24]. However, the Al_{2p} XP spectra have strong signal in the same energy range. This binding energy overlap (between 70-100 eV) makes it difficult to characterize gold by XPS. Here, we only used XPS to follow the different Al states of the untreated γ-alumina and modified alumina supports, as shown in Figure 4.6.

Catalyst pretreatment in different gas atmospheres was introduced as a qualitative method to investigate the gold chemical properties, as discussed in a following section where the effect of various gas pretreatments on the activity is examined. While this is not a substitute for XPS, it allowed us to follow the activity as a function of modification of the gold state on the surface of the various supports.

4.3.2 Reducibility and Regeneration

4.3.2.1 Reducibility

Alumina does have hydroxyl groups of different type and amount depending on its type and preparation conditions. CO-TPR was used here to identify reducible surface oxygen species and probe the onset of the WGS reaction by activation of the surface hydroxyls to produce CO_2 and H_2. On the basis of the CO-TPR results in Figure 4.2, hydrothermal treatment of the γ-alumina with NaOH changes its reducibility by the addition of alkali and attendant extra surface oxygen and OH groups. But as discussed above, addition of alkali alone, while adding more OH to the surface, renders the alumina a high-temperature shift catalyst but does not make it a low-temperature one. It takes a metal, e.g. Pt or Au, to combine with the hydroxyls on the surface and create a low-temperature shift catalyst.

Platinum is needed to activate the OH groups for low-temperature WGS. This was first shown in the Ph.D. thesis work of Zhai at Tufts [25]. The results from Pt/Al_2O_3 catalysts indicate that the surface properties of the alumina support were modified by hydrothermal treatment, and hydroxyl groups were created on the support. We can follow this here, first with Pt addition. Comparing the CO-TPR results in Figures 4.2 and 4.7, the onset of the CO_2 and H_2 production

shifts to much lower temperature (~ 150 ^{o}C) over the Pt/Al_2O_3 and Pt/Al_2O_3-OH samples, compared to the metal-free aluminas. The higher amount of hydroxyl groups on the surface of the hydrothermally treated alumina was beneficial and used in the reaction, as was found by the correspondingly higher H_2 production on the Pt/Al_2O_3-OH sample than from Pt/Al_2O_3, as shown in Figure 4.7.

Since the alumina modification is a good way to promote the platinum-based catalysts, we set out to investigate the potentially similar activation of Au/Al_2O_3 catalysts for the WGS reaction in this work. Three samples, Au/Al_2O_3, Au/Al_2O_3-OH and Na-Au/Al_2O_3-OH (washed) were tested in CO-TPR under the same conditions. Comparing the results in Figure 4.8, an increase of H_2 and CO_2 productions at high temperature (above 200 ^{o}C) over Au on the modified alumina support indicated that more surface oxygen and hydroxide groups were available on the surface, but the most significant improvement was found on the Na-Au/Al_2O_3-OH sample, where the surface oxygen and hydroxide groups were activated at a temperature as low as 50 ^{o}C. The fact that the activation of surface OH groups was promoted so dramatically is promising for developing alkali-modified gold catalysts for the low-temperature WGS reaction. Below we examine the regenerability of the –OH groups which is crucial for stable catalyst activity.

4.3.2.2 Regeneration

Cyclic CO-TPR is a good way to investigate the stability of the active sites and the regenerability of the hydroxyl groups. As shown in Figure 4.9, the Au/Al_2O_3 surface was largely depleted of hydroxyl groups in the second cycle, as expected by their consumption by CO in the first TPR cycle. Introduction of water vapor after the second CO-TPR cycle, was unsuccessful to

reproduce the first-cycle production of H_2 or CO_2 production. Hence these catalysts should not be stable, since the active –OH groups cannot be regenerated. As we will see in the activity tests, this prediction holds true. Similar results were observed over the Au/Al_2O_3-OH sample as shown in Figure 4.10. Thus, the much higher amount of hydroxyl groups on the surface of Au/Al_2O_3-OH were also not able to be fully recovered. This all points to the need for the presence of a promoter/stabilizer, such as the alkali-ions found earlier for the Pt-based catalysts.

As discussed before, alkali additives can stabilize the Pt ions and clusters on silica. They were found here to promote the activation of hydroxyl groups on the surface of the Au/Al_2O_3-OH sample. Thus, cyclic CO-TPR tests were conducted to evaluate of reversibility of the hydroxyl groups on the surface of Na-Au/Al_2O_3-OH. If a second cycle of CO-TPR was carried out without any treatment after the first cycle, negligible CO_2 and H_2 productions were detected, which means that most of the reducible species had been consumed and surface OH groups were depleted during the first cycle. If a rehydration treatment was introduced after the 2^{nd} cycle at room temperature for an hour, a full regeneration of the OH groups was found even for those at low temperature, as shown in Figure 4.11 by the almost full recovery of H_2 production along with CO_2 production. These cyclic CO-TPR tests demonstrate that the activation of water and the regeneration of OH groups take place on the Na-promoted Au sites at close to ambient temperatures. This is the feature that renders the Au-O_x(OH)-Na cluster active for the low-temperature WGS reaction, which is in agreement with the study of the Na-Pt/SiO_2 catalyst in [22]. This is a significant result that may be used to design stable gold catalysts on non-reducible supports, such as alumina.

4.3.3 WGS reaction activity

4.3.3.1 Effect of pretreatment

Proper pretreatment is necessary and important to achieve a good catalytic activity. Several approaches were examined in this work. Prior to the activity measurement, Au/Al_2O_3 sample was heated at 200 °C for 2 h at a heating rate of 1 °C/min in different gas atmospheres, followed by cooling down to the room temperature. Five samples were tested in dynamic TPSR mode, as-prepared (dried at room temperature under vacuum overnight, no calcination), after pretreatment in He, or in 10% H_2, or in 10% O_2, or in 10% CO_2 (balanced with He) as shown in Figure 4.12. As-prepared and H_2-pretreated Au/Al_2O_3 showed similar highest activities; the CO_2-pretreated sample came next; and the ones with He- or O_2-pretreatment had the lowest activity. This result is in agreement with Lessard's Master thesis research of Au/La_2O_3 [26]. Recently, Gates and co-workers investigated Au/La_2O_3 for CO oxidation and found that oxidized gold sites play a role in the catalytic CO oxidation reaction [27]; it was determined that CO_2 was capable of oxidizing Au^0 through a dissociation mechanism:

$$2\ Au^0 + CO_2 \rightarrow Au^+\text{-}O^{2-}\text{-}Au^+ + CO$$

The presence of cationic gold (Au^+) results from CO_2 oxidizing the gold sites at room temperature, and activation of O_2 requires cationic gold. In this work, Au/Al_2O_3 was also heated in 10% CO_2 (with He) and followed by a TPSR test. The activity is better than the O_2-pretreated sample. This finding may indicate that Au^{1+} is part of the acitve site for the WGS catalyst, but not Au^0 or Au^{3+}. This approach thus compensates in part the difficulty of XPS characterization of the Au/Al_2O_3 catalysts, as mentioned above.

4.3.3.2 WGS reaction activity

In the WGS steady-state tests, shown in Figure 4.13, Na-addition had a great promotion effect on the activity of the Na-Au/Al_2O_3-OH catalyst, while the Na-free samples, Au/Al_2O_3 and Au/Al_2O_3-OH, showed lower activity for the reaction up to 300 ^oC and poor stability above 300 ^oC. These results confirm the discussion in CO-TPR experiments and observations by TEM in the previous section. Gold species associated with Na ions maintained good dispersion during the WGS reaction. But the gold species on the bare alumina surfaces, even if surrounded by –OH groups as in the Al_2O_3-OH surface, easily sinter at high temperatures, as shown in Figure 4.5 e and f, and they cannot regenerate the –OH on the alumina surface, which explains why activity decreased above 300 ^oC in the reaction gas mixture. The Na addition is therefore crucial for a stable gold catalyst.

The Na-promotion effect of the WGS reaction activity over the Au/Al_2O_3 catalysts was further confirmed in activity tests conducted in the full reformate gas mixture, as depicted in Figure 4.14. The reaction rate over Na-promoted Au/Al_2O_3-OH catalyst is higher than those over the Na-free samples. Na ions stabilize the Au ions and facilitate the regeneration of the active -OH groups, continuously providing OH to complete the reaction pathway. These -OH groups are not regenerable on the alkali-free Au/Al_2O_3 or Au/Al_2O_3-OH surfaces, but they are on ceria. This result might demonstrate that Na-promotion has a similar function as the interaction between Au and reducible supports, i.e. CeO_2, Fe_2O_3, and TiO_2 [3, 25, 26, 28].

The Na-Au/Al_2O_3-OH sample was also tested at as low a temperature as 100 ^oC for up to 10 h, as depicted in Figure 4.15. It shows stable activity for the WGS reaction. This is in agreement with the cyclic CO-TPR result in Figure 4.11, which shows that the sodium additive greatly improves the regenerability of the active hydroxyl groups even at room temperature.

Moreover, this low-temperature activity is stable, since no deactivation was observed during the 10 h test; and this is an important finding for catalyst design.

4.3.3.3 Kinetic Measurements

The WGS reaction activity over the Au-based catalysts is confirmed in activity tests conducted in the full reformate gas mixture, as depicted in Figure 4.14. The apparent activation energies of the WGS reaction, E_{app}, over all these Au/Al_2O_3 samples fall into the same range of 45 ± 5 kJ/mol (see Figure 4.14), no matter on what support the gold catalyst were prepared and whether or not Na promoters were used. Moreover, the activation energies over these catalysts are close to those over other Au-based samples on different supports, as listed in Table 4.5. This finding supports our initial hypothesis that the Au-O_x(OH)-M species is the active site for the WGS, irrespective of what M is chosen. We still need further investigations, i.e. DFT calculation and EXAFS analysis, to support this hypothesis, and guide catalyst design and mechanistic studies of the low-temperature WGS reaction in future work.

4.4 Summary

In this work, the catalytic activity and stability of alumina-supported gold catalysts for the WGS reaction was investigated. Alumina is a non-reducible oxide support and, unlike CeO_2 or Fe_2O_3, it cannot provide active surface oxygen. Hydrothermal treatment with NaOH can modify the properties of this support by adding excess oxygen and hydroxyl groups on the surface. Gold species, deposited on the surface by DP with urea, render the reducible oxygen and surface hydroxyl groups active at low temperatures. However, these are non-regenerable, as

shown here by cyclic CO-TPR tests. The gold catalyst is not stable. Alkali additives greatly improve the regenerability of these active hydroxyl groups even at room temperature. The catalyst stability is now also greatly improved. In the WGS reaction, the Na-free Au/Al_2O_3 and Au/Al_2O_3-OH samples have low activity and poor stability especially at high temperature; while addition of Na can maintain atomically dispersed gold on the supports, probably Au^{1+}, thus improving the activity and stability of the $Na\text{-}Au/Al_2O_3$ catalyst. A partially oxidized $Au\text{-}O_x(OH)$-Na species is concluded to be the active site for the low-temperature WGS reaction on the alkali-modified supports. It will be interesting to extend this finding to silica supports in future work.

Table 4.1 Gold speciation in $HAuCl_4$ solutions at room temperature as a function of pH [14]

$HAuCl_4$ solution		10^{-2} M in NaCl (1M) [a]	10^{-1}-10^{-3} M [a]	2×10^{-2} M [b]	1-2.5×10^{-3} M
pH or range of pH of predominance of Au^{III} speciation	$[AuCl_4]^-$	pH 1.4-6.2	pH 2	pH 1-3.8	pH ≦ 4
	$[Au(OH)Cl_3]^-$	pH 6.2-8.1	pH 7.5	pH 3.8-5.2	
	$[Au(OH)_2Cl_2]^-$	pH 8.1-11	pH 9.2	pH 5.2-6.6	
	$[Au(OH)_3Cl]^-$	pH 11-12		pH 8.2-11.2	
	$[Au(OH)_4]^-$	pH 12		pH 11.2-12	pH 7
Characterization technique		Raman UV-visible	XANES EXAFS	Raman	EXAFS
Reference		[29]	[30]	[31]	[32]

a. pH range of predominance of the various Au^{III} species
b. Each pH range corresponds to a single species except at pH 6.6-8.2: mixture of $[Au(OH)_2Cl_2]^-$ and $[Au(OH)_3Cl]^-$

Table 4.2 Au/oxide samples prepared by DP with urea at 353K

Oxide support	Surface area (m^2/g)	PZC	DP time (h)	Final pH	[Au] [a] (wt.%)	d_{Au} (nm)	Reference
CeO_2	256	~ 6	1	4.4	7.9	8.1 [b]	[19]
			16	6.6	8.2	< 5	
TiO_2	45	~ 6	1	3	7.2	7.1	[19]
			2	6.2	6.5	3.2	
			4	7	7.7	2.7	
			16	7.3	6.8	2.5	
SiO_2	250	~ 2	1	5.2	2.9	< 20	[19]
			16	7	3.7	> 20	
γ-Al_2O_3	100	~ 7.5	1	4.3	6.9	6.9	[19]
			16	7.1	7.2	2.3	
γ-Al_2O_3 [c]	210		4	7.5	1.1 [e]	3.4	this work
Al_2O_3-OH [d]	251		4	7.7	1.2 [e]	3.2	this work

a. A nominal gold loading is 8 wt.%
b. Estimated by XRD (poor contrast between gold particles and CeO_2 by TEM)
c. γ-alumina powder, commercial (Puralox, SBa-200, S_{BET} = 210 m^2/g, V_p = 0.55 mL/g)
d. γ-alumina after hydrothermal treatment in NaOH (0.5 M, 100 ^oC for 20 h in the autoclave), washed
e. Values are in at.%. The designed gold loading on these alumina supports was 1 at.% in this work

Table 4.3 Physical properties of the examined catalysts

Catalysts	Bulk Composition (at.%)			BET Surface Area
	Pt	Au	Na	(m^2/g)
Al_2O_3 [a]	--	--	--	210
Al_2O_3-OH [b]	--	--	1.4	251
Pt/Al_2O_3 [c]	1.0	--	--	178
Pt/Al_2O_3-OH [c]	1.0	--	1.4	175
Au/Al_2O_3 [d]	--	1.1	--	269
Au/Al_2O_3-OH [d]	--	1.2	0.05	246
Na-Au/Al_2O_3-OH [d]	--	1.1	3.0	216
Na-Au/Al_2O_3-OH [d] washed	--	1.1	2.4	216

a. γ-alumina powder, commercial (Puralox, SBa-200, S_{BET} = 210 m^2/g, V_p = 0.55 mL/g)
b. γ-alumina after hydrothermal treatment in NaOH (0.5 M, 100 ^oC for 20 h in the autoclave), washed
c. 1% Pt loading on alumina supports by IMP method
d. 1% Au loading on alumina supports by DP with urea method

Table 4.4 Au particle size distribution on different alumina supports

Catalysts	Au particle size distribution (nm) [a, b]	
	Fresh [c]	Used [d]
Na-Au/Al_2O_3-OH	1.2 ± 0.3 [e]	2.5 ± 0.7 [f]
Au/Al_2O_3-OH	3.2 ± 0.8	4.5 ± 1.1
Au/Al_2O_3	3.4 ± 1.1	5.3 ± 1.2

a. Measured by HR-TEM, size distribution was done from a survey of ~ 50 particles
b. The sub-nanometer Au clusters (TEM-invisible) was not included
c. Pretreated in 10%H_2-He at 200 ^oC for 2 h at a heating rate of 1 °C/min, before WGS reaction
d. After the WGS reaction up to 350 ^oC for a total of 10 h on stream (2%CO-10%H_2O-He)
e. ~ 30% of particles counted were < 1 nm
f. ~ 1% of particles counted were < 1 nm

Table 4.5 Comparison of the activation energy over Au-based catalysts on various oxides

Catalysts	Preparation	Bulk composition		E_{app} [a] (kJ/mol)	References
		Au (at.%)	Na (at.%)		
Au/CeO_2	DP	1.0	--	41.0	[28]
$Na\text{-}Au/CeO_2$	DP+IMP	1.0	3.0	49.7	[28]
Au/Fe_2O_3	DP	1.7	--	46.1	[25]
$K\text{-}Au/Fe_2O_3$	DP+IMP	1.7	1.5 [b]	41.9	[25]
Au/TiO_2	DP+UV	1.2	--	43.5	[3]
Au/La_2O_3	AA	1.0	--	49.0	[26]
Au/Al_2O_3	DP	1.1	--	44.2	this work
$Au/Al_2O_3\text{-}OH$	DP	1.2	--	53.2	this work
$Na\text{-}Au/Al_2O_3\text{-}OH$	DP+IMP	1.1	3.0	48.1	this work

a. Measured in 11%CO-26%H_2O-26%H_2-7%CO_2-He (207 mL/min, contact time = 0.03 g·s/mL)
b. Concentration of K-additive

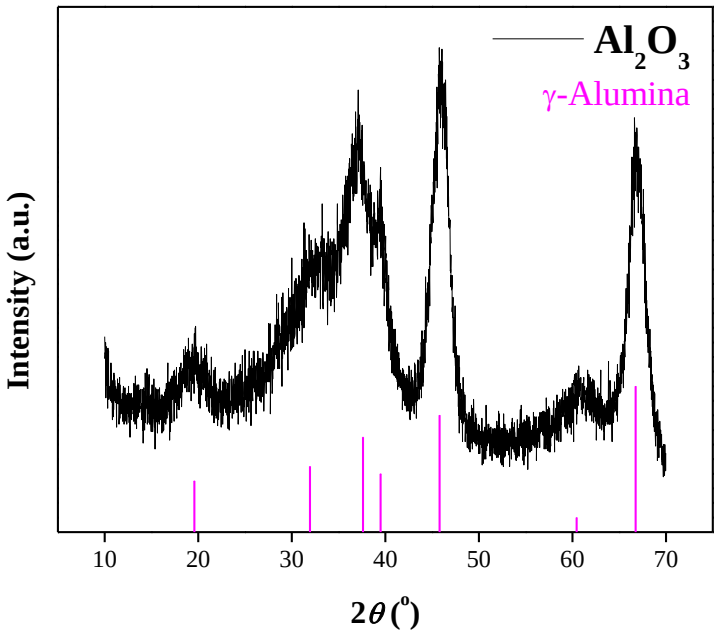

Figure 4.1 (a) XRD patterns of commercial γ-alumina powder (Puralox, SBa-200)

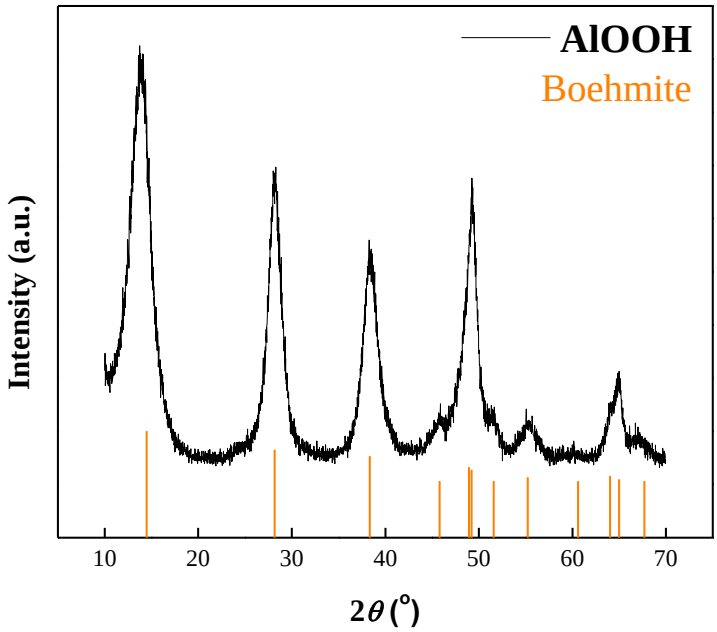

Figure 4.1 (b) XRD patterns of commercial boehmite powder (Pural, SCF-55)

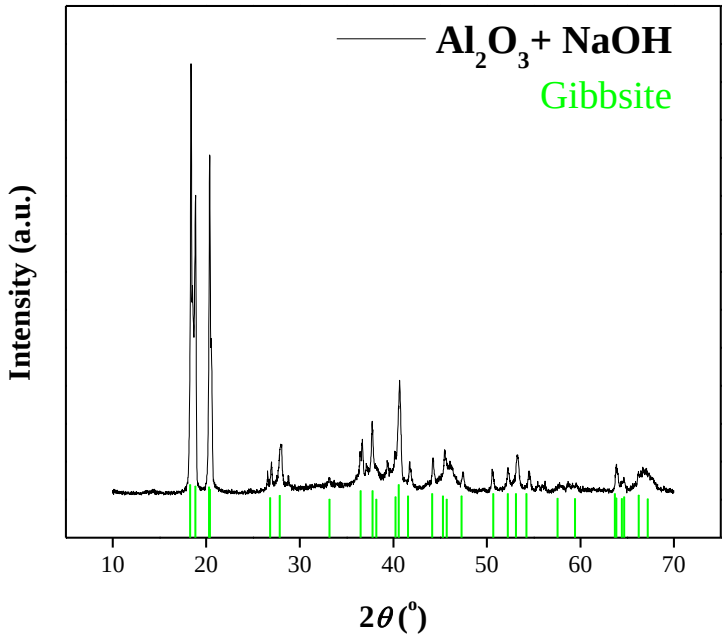

Figure 4.1 (c) XRD patterns of γ-alumina after hydrothermal treatment in NaOH [a]

a. Hydrothermal treatment in NaOH (0.5 M, 100 ^{o}C for 20 h in the autoclave), washed, no calcination

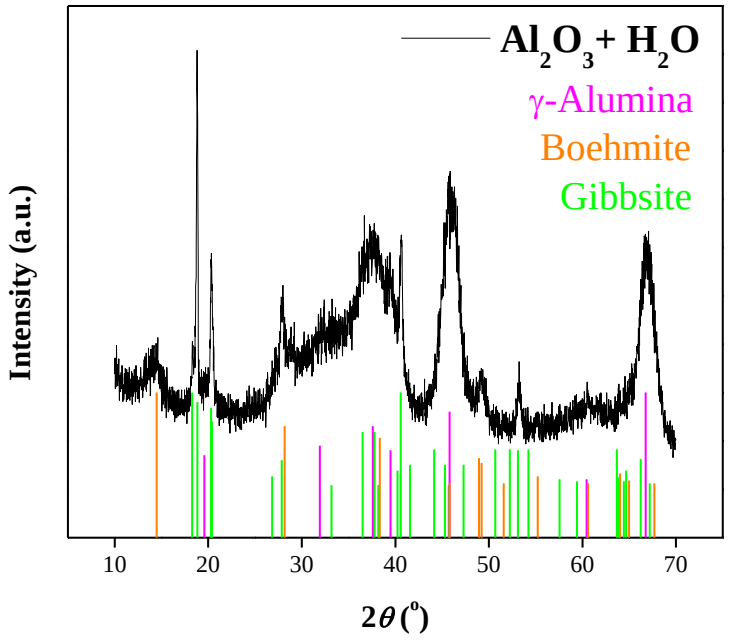

Figure 4.1 (d) XRD patterns of alumina after hydrothermal treatment in water [a]

a. Hydrothermal treatment in H_2O (100 ^oC for 20 h in the autoclave), washed, no calcination

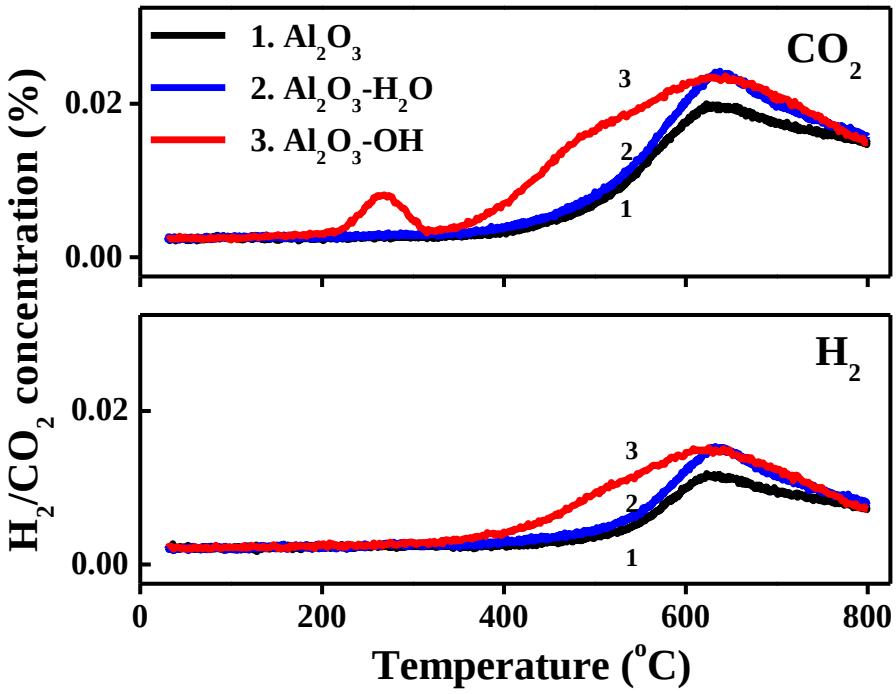

Figure 4.2 CO-TPR tests of untreated and hydrothermally modified γ-alumina supports [a-c]

a. γ-alumina powder, commercial (Puralox, SBa-200, S_{BET} = 210 m^2/g, V_p = 0.55 mL/g)
b. Hydrothermal treatment in NaOH (0.5 M, 100 °C for 20 h in the autoclave), washed, no calcination
c. Hydrothermal treatment in H_2O (100 °C for 20 h in the autoclave), washed, no calcination

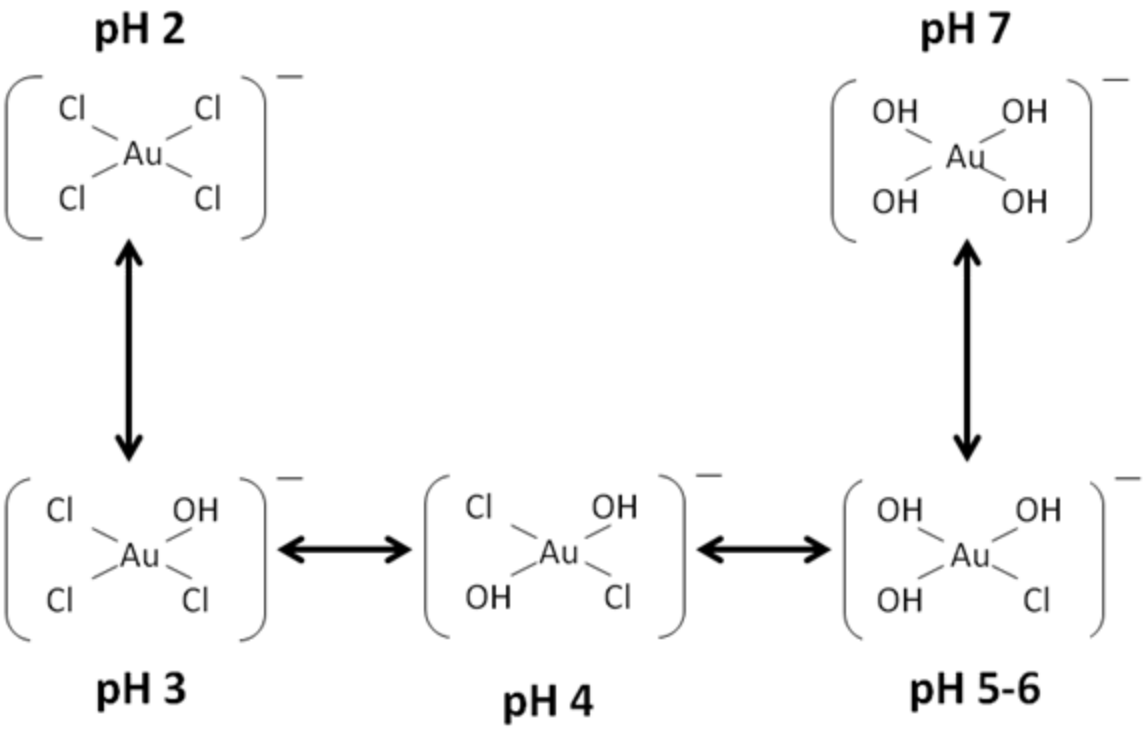

Figure 4.3 Gold species present in the solution as a function of pH [20]

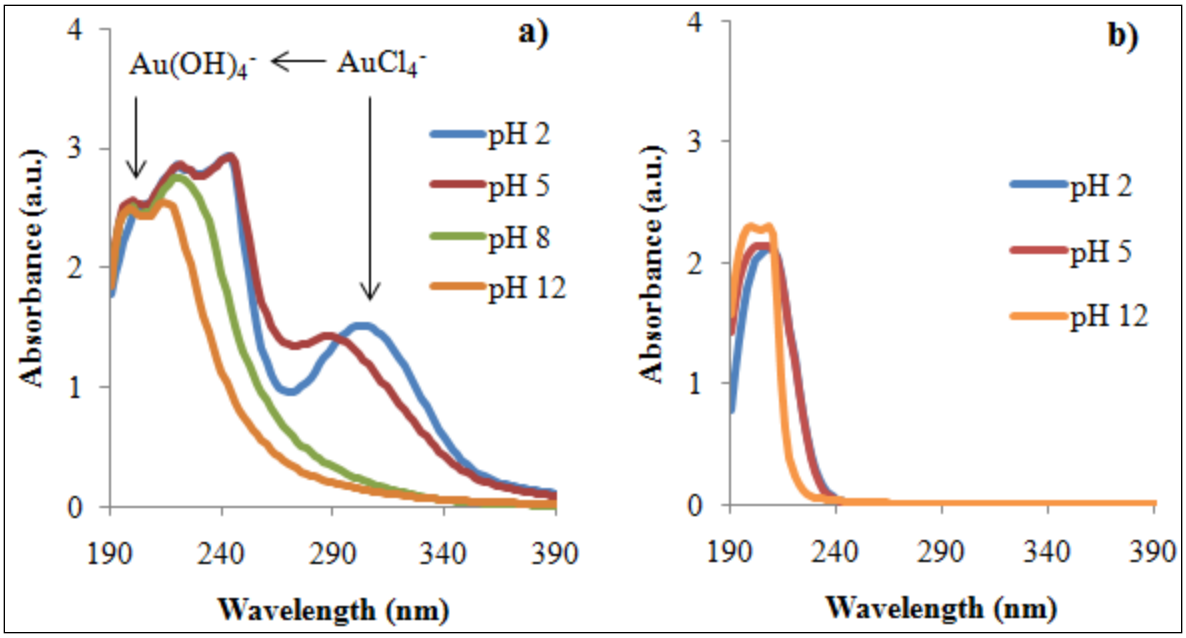

Figure 4.4 UV-Vis spectra of 4×10^{-4} M Au precursor solutions at different pH (a) before $AgNO_3$ addition (b) after $AgNO_3$ addition

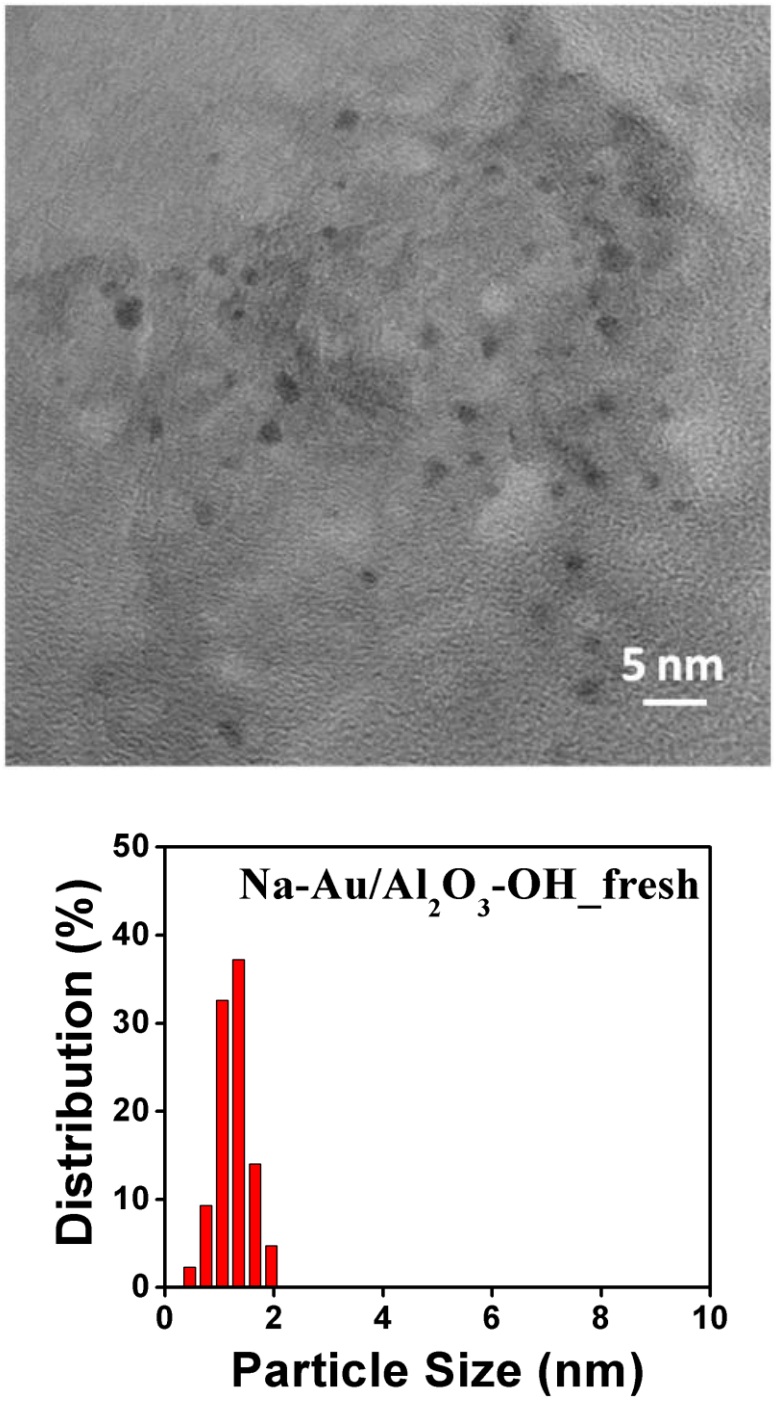

Figure 4.5 (a) TEM image of the fresh Na-Au/Al_2O_3-OH catalyst [a] and Au particle size distribution

a. Calcined in 10%H_2-He at 200 ^oC for 2 h, and then in 10%O_2-He at 300 ^oC for 2 h

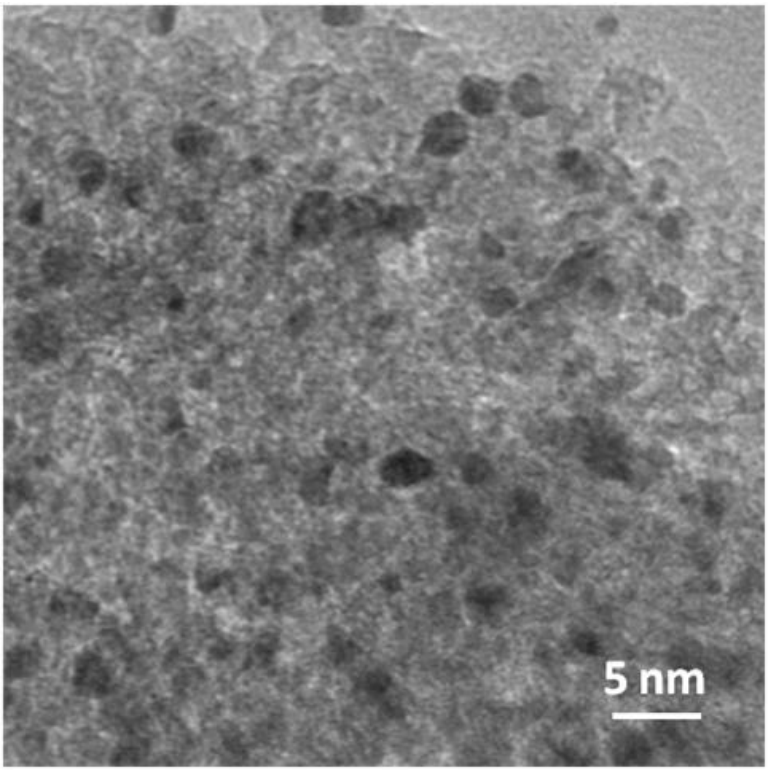

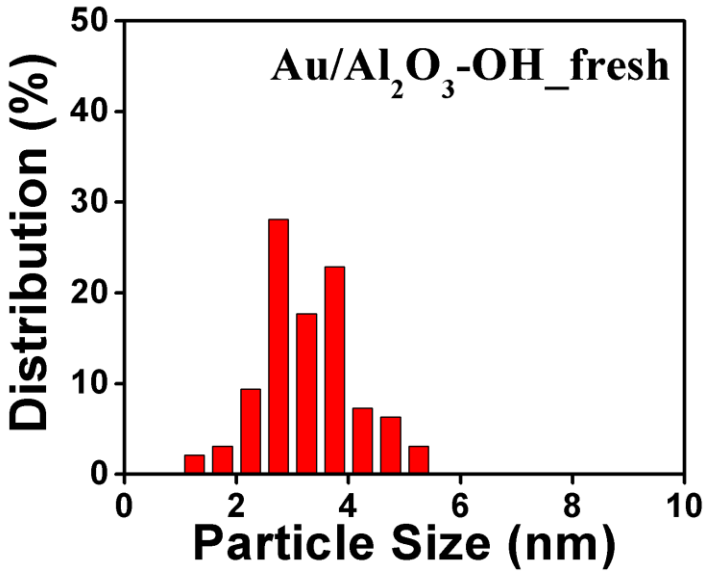

Figure 4.5 (b) TEM image of the fresh Au/Al_2O_3-OH catalyst [a] and Au particle size distribution

a. Calcined in 10%H_2-He at 200 ^oC for 2 h

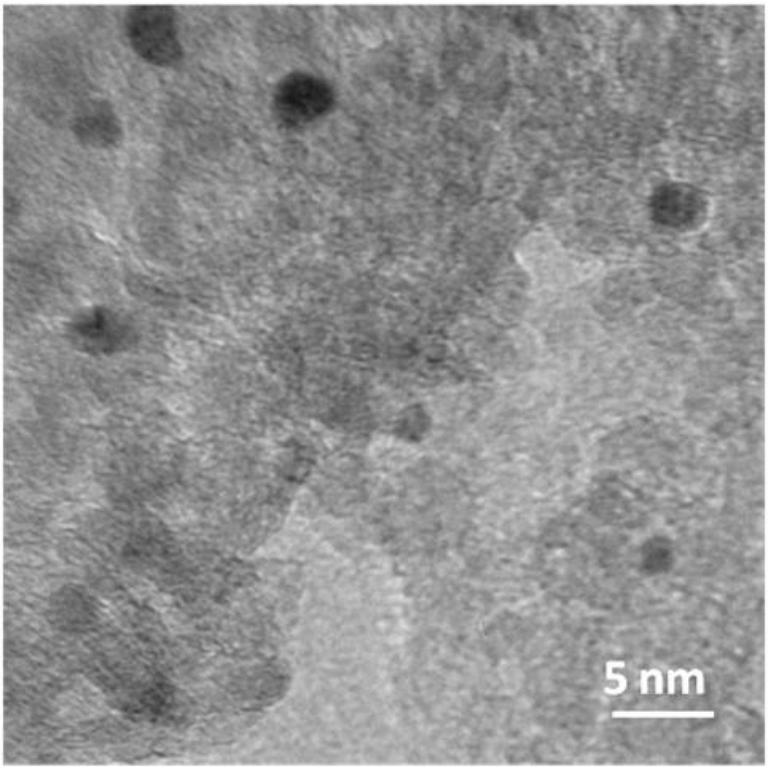

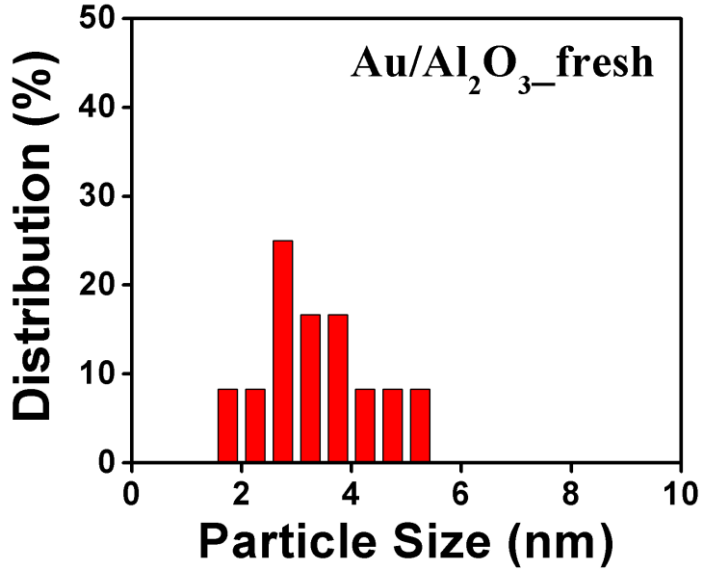

Figure 4.5 (c) TEM image of the fresh Au/Al_2O_3 catalyst [a] and Au particle size distribution

a. Calcined in 10%H_2-He at 200 ^oC for 2 h

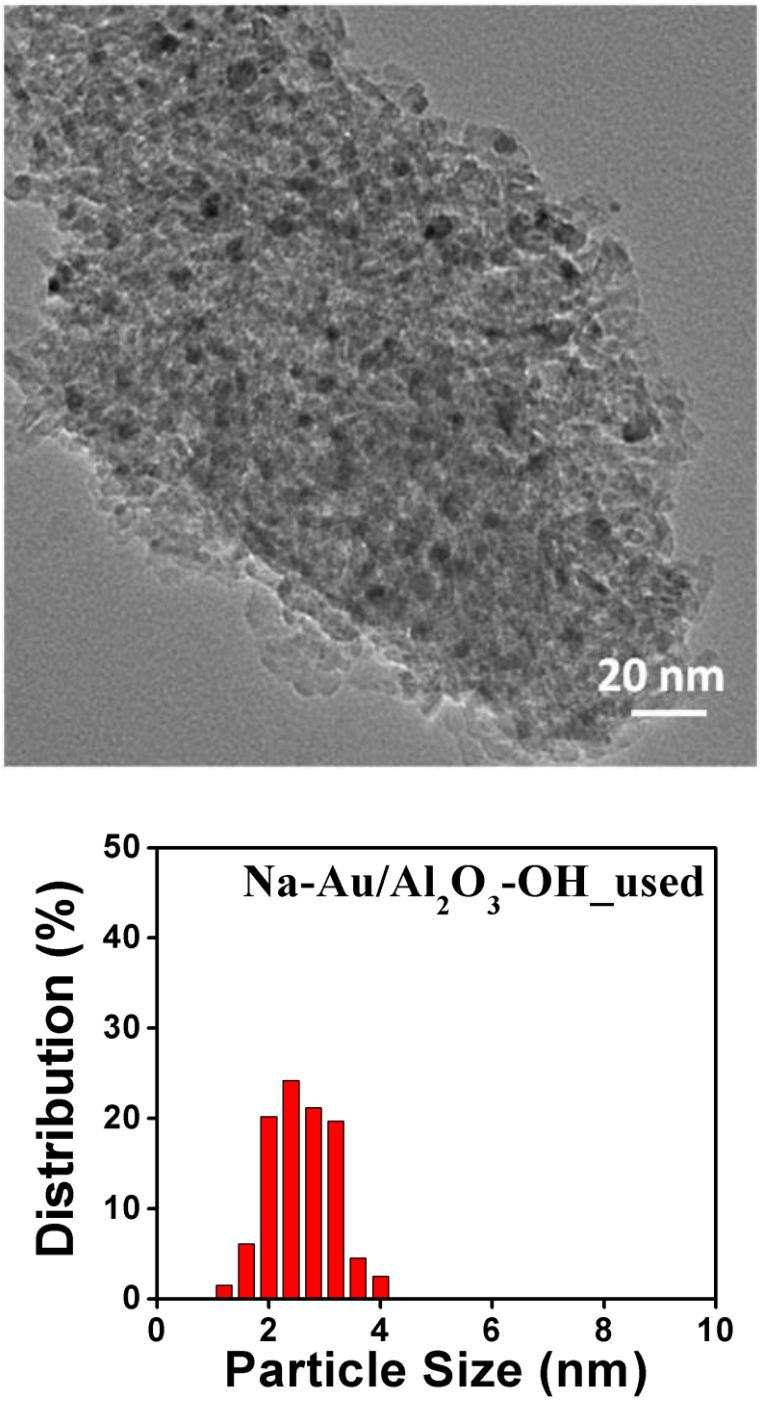

Figure 4.5 (d) TEM image of the used Na-Au/Al_2O_3-OH catalyst [a] and Au particle size distribution

a. After the WGS reaction for a total of 10 h on stream (2%CO-10%H_2O-He, 70 mL/min, 350 ^oC)

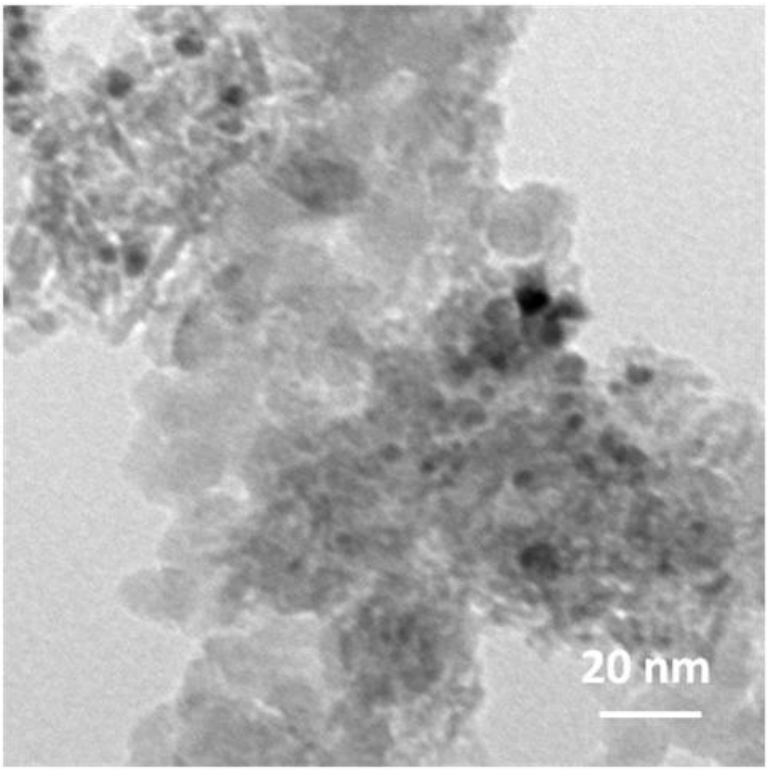

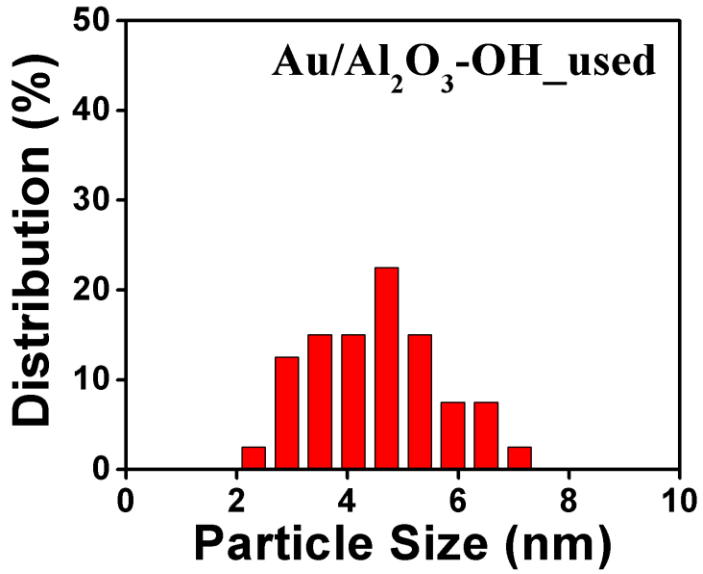

Figure 4.5 (e) TEM image of the used Au/Al_2O_3-OH catalyst [a] and Au particle size distribution

a. After the WGS reaction for a total of 10 h on stream (2%CO-10%H_2O-He, 70 mL/min, 350 ^oC)

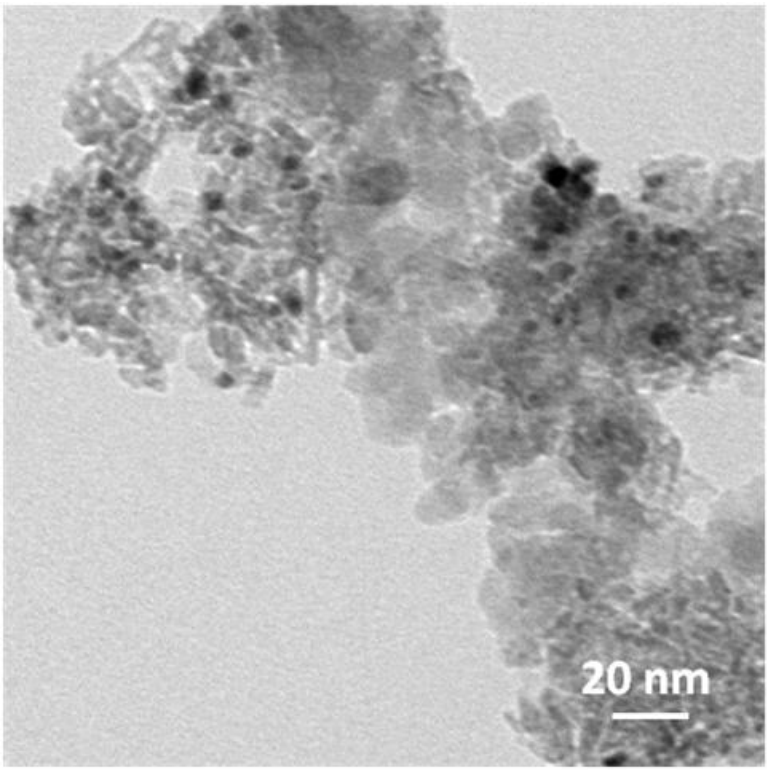

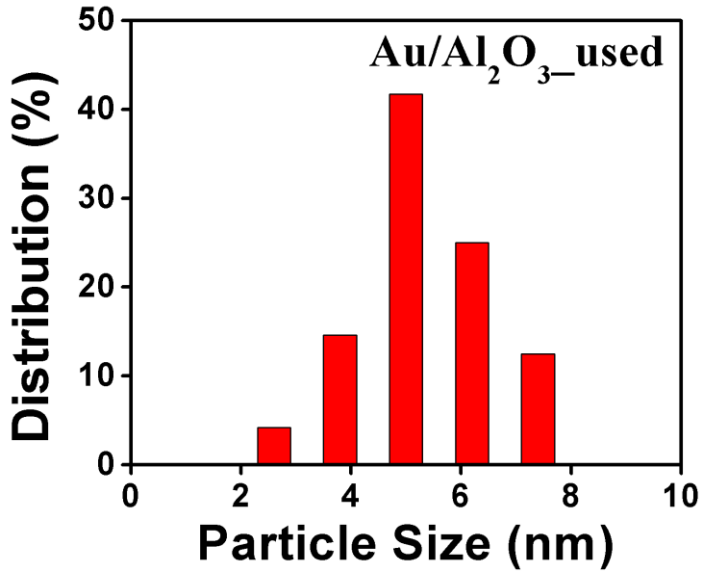

Figure 4.5 (f) TEM image of the used Au/Al_2O_3 catalyst [a] and Au particle size distribution

a. After the WGS reaction for a total of 10 h on stream (2%CO-10%H_2O-He, 70 mL/min, 350 ^oC)

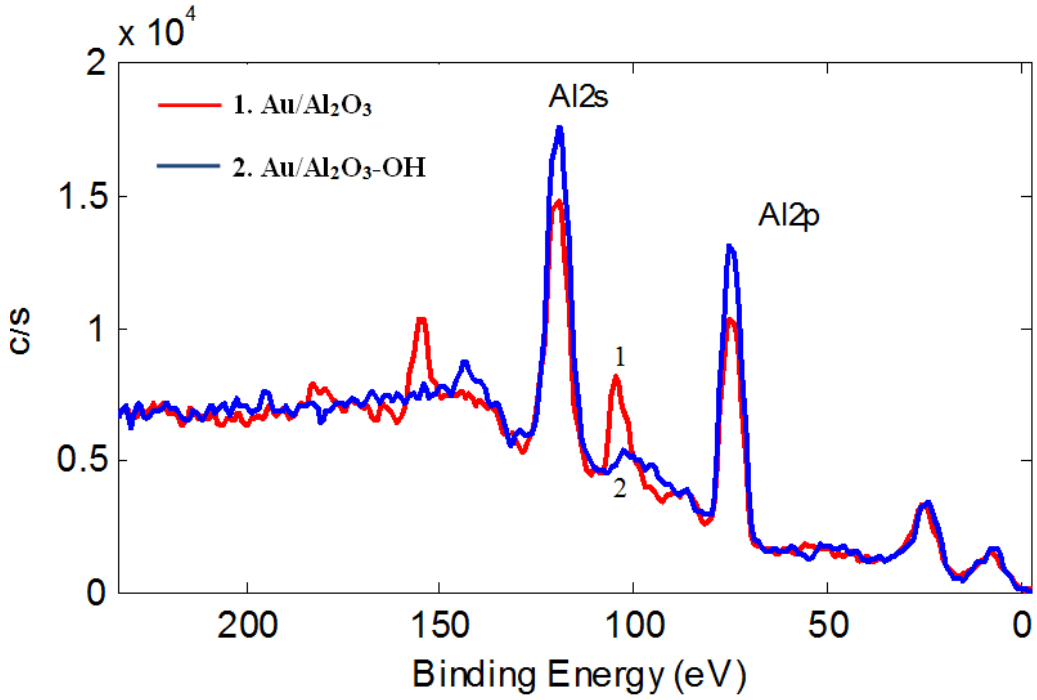

Figure 4.6 X-ray photoelectron spectra of Au/Al_2O_3 and Au/Al_2O_3-OH samples

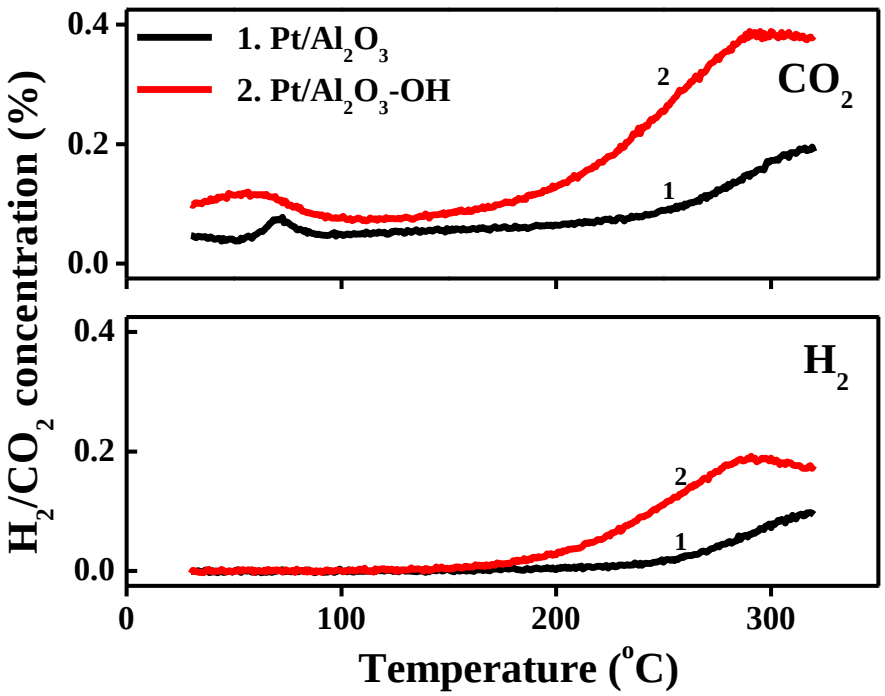

Figure 4.7 CO-TPR of Pt/Al_2O_3 and Pt/Al_2O_3-OH

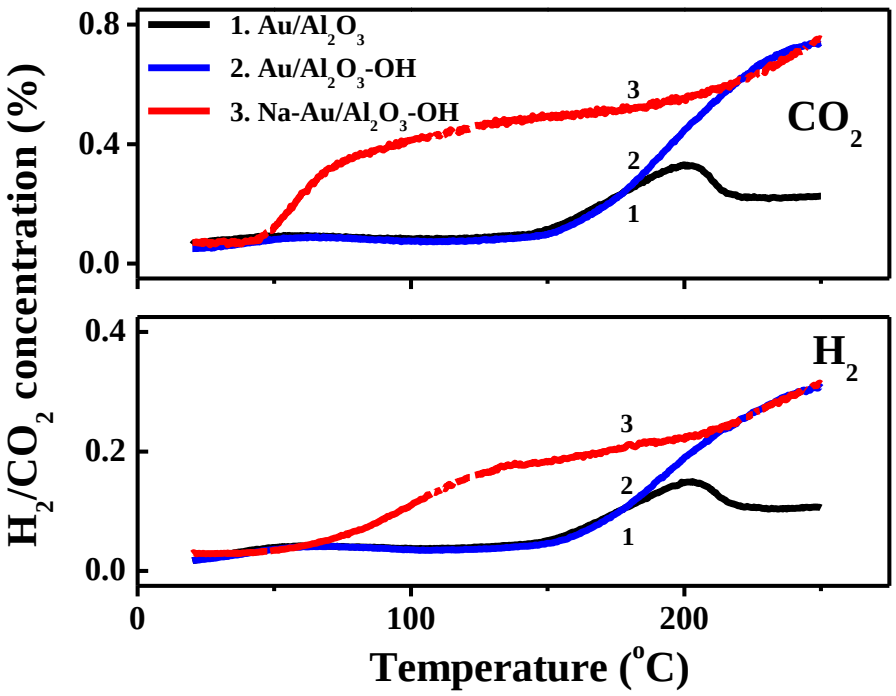

Figure 4.8 CO-TPR of Au/Al_2O_3, Au/Al_2O_3-OH and Na-Au/Al_2O_3-OH washed samples

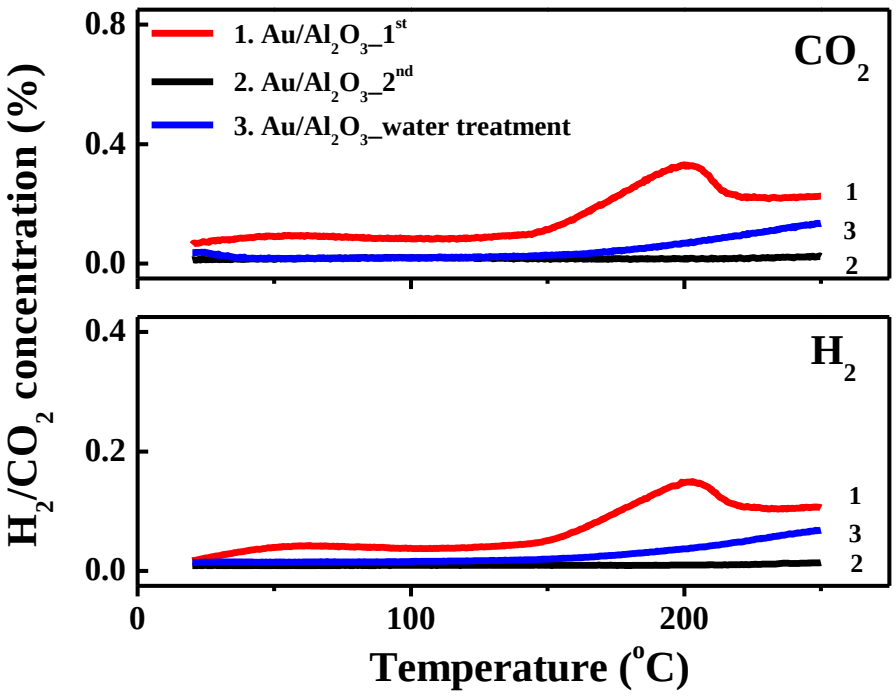

Figure 4.9 CO-TPR of Au/Al_2O_3 catalyst in three consecutive cycles with and without intermittent rehydration at room temperature

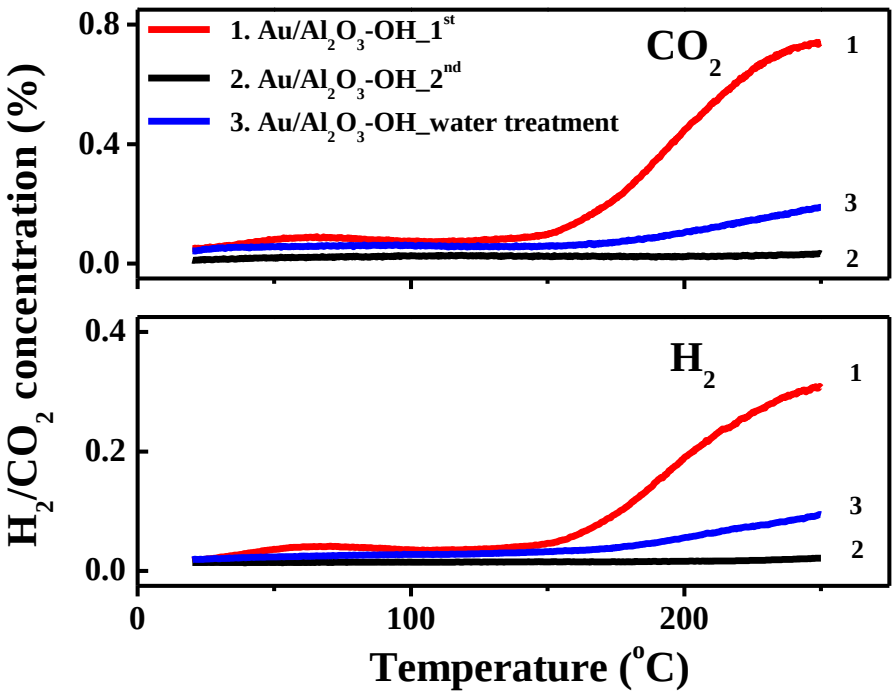

Figure 4.10 CO-TPR of Au/Al_2O_3-OH catalyst in three consecutive cycles with and without intermittent rehydration at room temperature

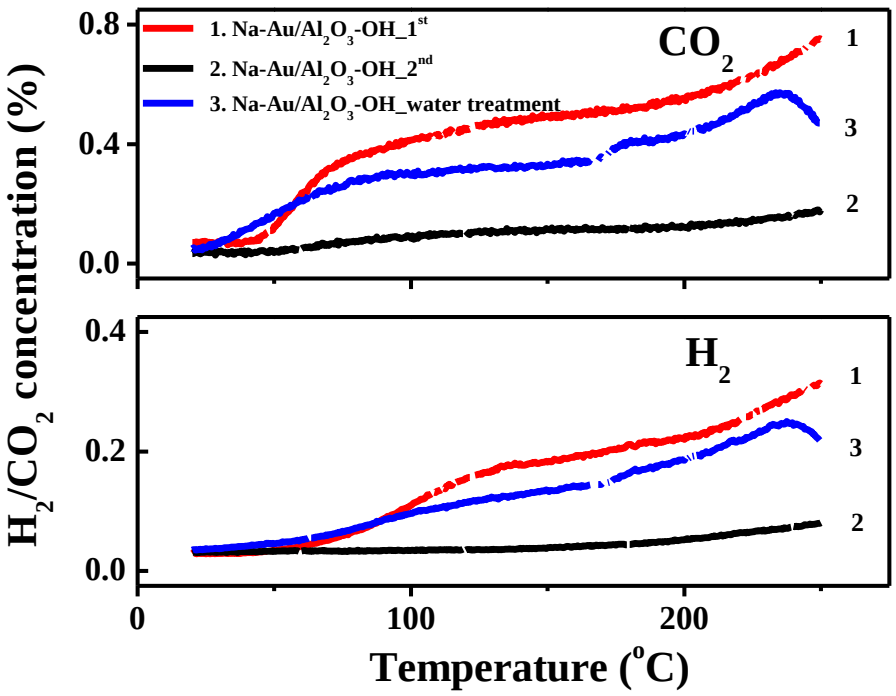

Figure 4.11 CO-TPR of Na-Au/Al_2O_3-OH catalyst in three consecutive cycles with and without intermittent rehydration at room temperature

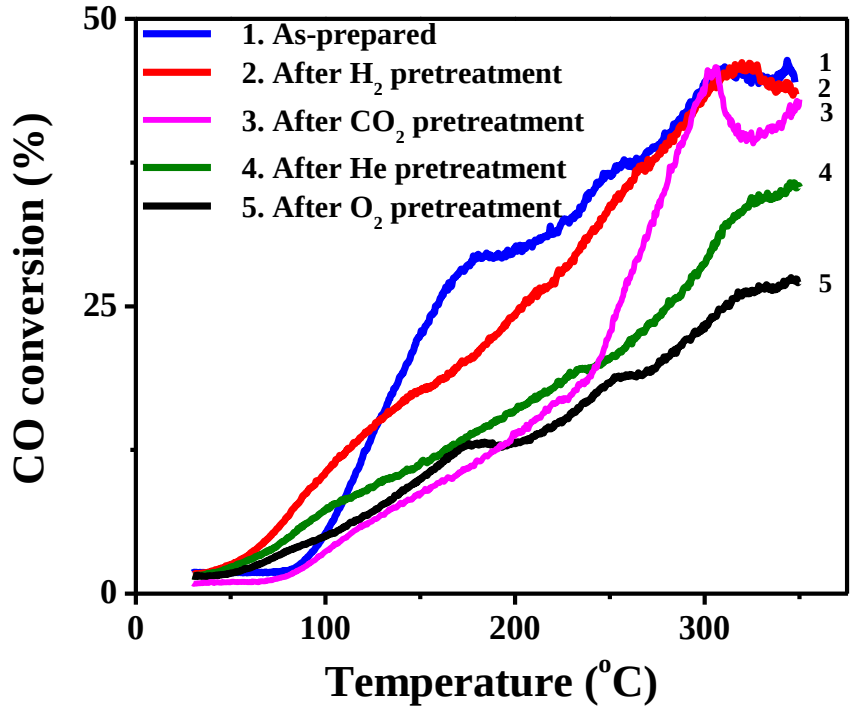

Figure 4.12 CO conversion profiles in TPSR of WGS reaction over Au/Al_2O_3 catalyst after pretreatment [a] in different gas atmospheres

a. Heated at 200 °C for 2 h at a heating rate of 1 °C/min in different gas atmospheres followed by cooling down to the room temperature before test

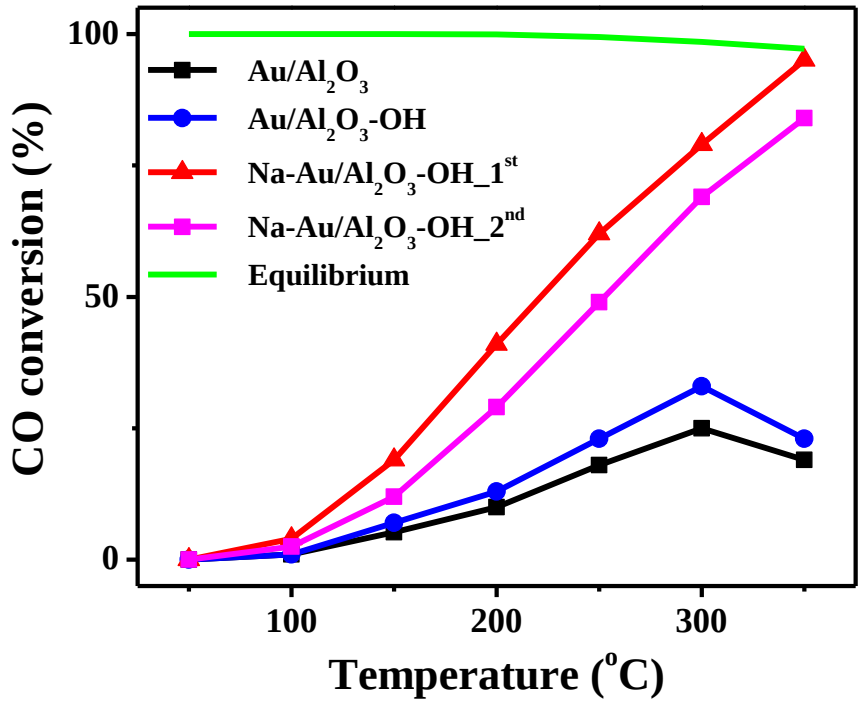

Figure 4.13 CO conversion profiles in steady-state tests of WGS reaction over Au/Al_2O_3 Au/Al_2O_3-OH and Na-Au/Al_2O_3-OH catalysts

(2%CO-10%H_2O-He, 70 mL/min, contact time = 0.09 g·s/mL)

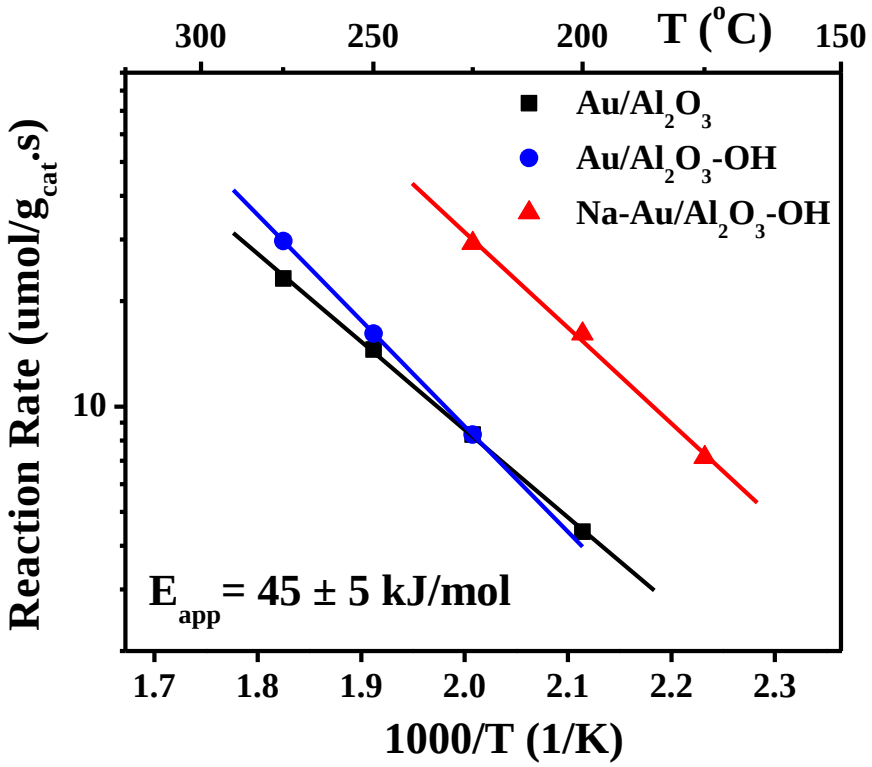

Figure 4.14 WGS reaction rates and activation energies over Au/Al_2O_3 Au/Al_2O_3-OH and Na-Au/Al_2O_3-OH catalysts

(11%CO–26%H_2O–26%H_2–7%CO_2–He, 207 mL/min, contact time = 0.03 g·s/mL)

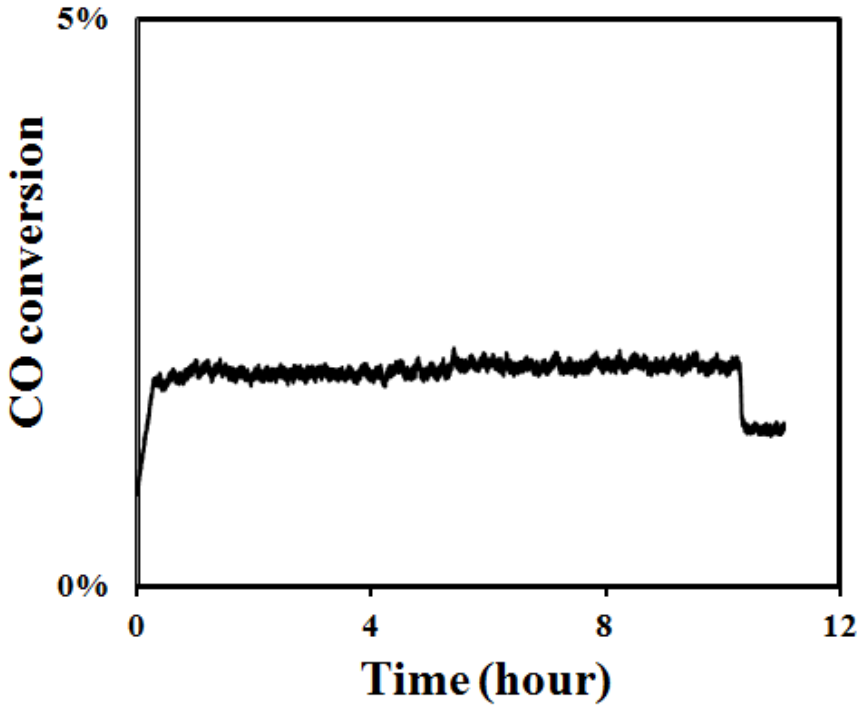

Figure 4.15 Low-temperature stability test of Na-Au/Al_2O_3 at 100 ^oC (10%CO-3%H_2O-He, 30 mL/min, contact time = 0.03 g·s/mL, 10 h)

References

[1] Q. Fu, H. Saltsburg, M. Flytzani-Stephanopoulos, ***Science*** 301 (2003) 935-938.

[2] W. Deng, C. Carpenter, N. Yi, M. Flytzani-Stephanopoulos, ***Topics in Catalysis*** 44 (2007) 199-208.

[3] M. Yang, L.F. Allard, M. Flytzani-Stephanopoulos, ***Angewandte Chemie International Edition*** (2012) submitted.

[4] T. Tabakova, V. Idakiev, D. Andreeva, I. Mitov, ***Applied Catalysis A: General*** 202 (2000) 91-97.

[5] A.C. Gluhoi, B.E. Nieuwenhuys, ***Catalysis Today*** 122 (2007) 226-232.

[6] S. Tsubota, M. Haruta, T. Kobayashi, A. Ueda, Y. Nakahara, P.A.J.P.G. G. Poncelet, B. Delmon, ***Studies in Surface Science and Catalysis***, Elsevier, 1991, pp. 695-704.

[7] T. Takei, I. Okuda, K.K. Bando, T. Akita, M. Haruta, ***Chemical Physics Letters*** 493 (2010) 207-211.

[8] A.C. Gluhoi, X. Tang, P. Marginean, B.E. Nieuwenhuys, ***Topics in Catalysis*** V39 (2006) 101-110.

[9] Y. Li, Q. Yu, X. Zou, H. Zhuo, Y. Yao, Z. Suo, ***Chinese Journal of Catalysis (Chinese Version)*** 31 (2010) 671.

[10] G.M. Veith, A.R. Lupini, N.J. Dudney, ***The Journal of Physical Chemistry C*** 113 (2008) 269-280.

[11] G.M. Veith, A.R. Lupini, S.J. Pennycook, N.J. Dudney, ***ChemCatChem*** 2 (2010) 281-286.

[12] F. Habashi, ***Hydrometallurgy*** 79 (2005) 15-22.

[13] Y. Amenomiya, G. Pleizier, ***Journal of Catalysis*** 76 (1982) 345-353.

[14] G.C. Bond, C. Louis, D.T. Thompson, ***Catalysis by Gold***, Catalytic Science Series 6 (2006)

[15] S. Ivanova, V. Pitchon, Y. Zimmermann, C. Petit, ***Applied Catalysis A: General*** 298 (2006) 57-64.

[16] R. Zanella, S. Giorgio, C.R. Henry, C. Louis, ***The Journal of Physical Chemistry B*** 106 (2002) 7634-7642.

[17] S.-J. Lee, A. Gavriilidis, ***Journal of Catalysis*** 206 (2002) 305-313.

[18] F. Moreau, G.C. Bond, A.O. Taylor, ***Chemical Communications*** (2004) 1642-1643.

[19] R. Zanella, L. Delannoy, C. Louis, ***Applied Catalysis A: General*** 291 (2005) 62-72.

[20] S. Ivanova, C. Petit, V. Pitchon, ***Applied Catalysis A: General*** 267 (2004) 191-201.

[21] Y. Zhai, D. Pierre, R. Si, W. Deng, P. Ferrin, A.U. Nilekar, G. Peng, J.A. Herron, D.C. Bell, H. Saltsburg, M. Mavrikakis, M. Flytzani-Stephanopoulos, ***Science*** 329 (2010) 1633-1636.

[22] Y. Wang, Y. Zhai, D. Pierre, M. Flytzani-Stephanopoulos, ***Applied Catalysis B: Environmental*** (2012) submitted.

[23] J.H. Kwak, J. Hu, D. Mei, C.-W. Yi, D.H. Kim, *e. al.*, ***Science*** 325 (2009) 1670-1673.

[24] ***National Institute of Standards and Technology X-ray Photoelectron Spectroscopy Database*** Version 3.5 (2003), http://srdata.nist.gov/xps/.

[25] Y. Zhai, ***Ph.D. Dissertation, Department of Chemical and Biological Engineering, Tufts University*** (2011).

[26] J.D. Lessard, ***M.S. Thesis, Department of Chemical and Biological Engineering, Tufts University*** (2012).

[27] M. Mihaylov, E. Ivanova, Y. Hao, K. Hadjiivanov, B.C. Gates, H. Knozinger, ***Chemical Communications*** (2008) 175-177.

[28] N. Yi, R. Si, H. Saltsburg, M. Flytzani-Stephanopoulos, ***Energy & Environmental Science*** 3 (2010) 831-837.

[29] J.A. Peck, C.D. Tait, B.I. Swanson, G.E. Brown Jr, ***Geochimica et Cosmochimica Acta*** 55 (1991) 671-676.

[30] F.o. Farges, J.A. Sharps, G.E. Brown Jr, ***Geochimica et Cosmochimica Acta*** 57 (1993) 1243-1252.

[31] P.J. Murphy, M.S. LaGrange, ***Geochimica et Cosmochimica Acta*** 62 (1998) 3515-3526.

[32] J.H. Yang, J.D. Henao, C. Costello, M.C. Kung, H.H. Kung, J.T. Miller, A.J. Kropf, J.G. Kim, J.R. Regalbuto, M.T. Bore, H.N. Pham, A.K. Datye, J.D. Laeger, K. Kharas, ***Applied Catalysis A: General*** 291 (2005) 73-84.

Chapter 5

Conclusions and Recommendations

5.1 Conclusions

In this thesis, I have investigated the synthesis of platinum and gold species on non-reducible oxides supports using alkali ions promoters which render them active and stable catalysts for the low-temperature water-gas shift reaction. The following are the major conclusions from this thesis work.

First, silica-encapsulated platinum species, $Pt@SiO_2$, were prepared by a reverse microemulsion technique. This core-shell structure is effective to support the platinum clusters throughout the porous silica shell (of thickness 60-70 nm). This accounts for most of the platinum, only a minor portion of which resides at the particle core (7-10 nm). The silica shell is mesoporous. The platinum species in the porous shell were well dispersed, especially if associated with alkali additives and they were accessible to reactant gases, except for those which were buried inside collapsed pores. The accessible Pt sites were active and very stable, as verified by cyclic shutdown/startup operation and isothermal testing at 350 ^{o}C.

Alumina-supported gold species were prepared by a deposition-precipitation method using urea to control the precipitation. Unlike CeO_2 or Fe_2O_3 supports, alumina is a non-reducible oxide which cannot provide active surface oxygen. Hydrothermal treatment with NaOH was found to modify the surface properties of the alumina with a

large number of –OH groups. The subsequent deposition of gold at high pH afforded a high number of dispersed Au-OH_x species on the surface. Since almost no alkali remained on the surface after the gold deposition and subsequent washings, this preparation allowed us to examine whether –OH alone was sufficient for an active catalyst. The answer to this question was negative. While initially the activity of the Au/Al_2O_3-OH was good, the catalyst was not stable; gold particle growth and eventual loss of –OH took place, as found by cyclic CO-TPR with intermittent surface rehydration.

The major finding of this thesis is that alkali ions are absolutely necessary to stabilize the Au-OH_x species, even on surfaces previously enriched with -OH species, as the hydrothermally treated alumina that was examined here. Thus, the alkali ions are the promoters of the Pt- and Au-based catalysts for the low-temperature WGS reaction when the Pt or Au species is supported on inert oxide supports, such as SiO_2 or Al_2O_3. The promoted species has the following properties: i) it contains an ensemble of Au- (or Pt-)O-Na species; which stabilize both the metal cation and the sodium cation on the surface; the latter being non-washable in repeated washings; ii) the –OH associated with the active species are now regenerable; i.e. they are replenished with intermittent rehydration during cyclic CO-TPR, and are thus directly involved in the WGS reaction pathway.

These findings apply also to the alkali-promoted Pt@SiO_2. Indeed, while the Na-free Pt@SiO_2 is not active for the reaction up to 300 ^oC, addition of Na, either in the synthesis step or by impregnation of the core-shell sample, renders the corresponding Pt-Na@SiO_2 or Na(IMP)-Pt@SiO_2 a very active catalyst for the WGS reaction, comparable to Pt/CeO_2. While the reaction rates on the core-shell Pt are lower than on the open silica support due to limited accessibility of some of the Pt during the pore collapsing when

sodium was added on the former, the apparent activation energies were the same, 70 ± 5 kJ/mol. The TOFs were also the same on both supports; and on Pt/CeO_2. To estimate the TOFs, the rates were normalized by the amount of active –OH as measured by CO-TPR. Hence, the same platinum species are active on all supports.

As an overall conclusion, oxidized $Pt\text{-}O_x(OH)$ species associated with alkali ions or cerium ions are the active sites for the low-temperature WGS reaction. The same conclusion has been reached for the partially oxidized $Au\text{-}O_x(OH)$ species on the alumina supports examined in this thesis. The presence of Na (or another alkali) is necessary to provide the regenerable –OH groups and stability to the active site. The apparent activation energies for the Na-promoted Au on alumina are the same (45 ± 5 kJ/mol) as for Au/CeO_2 and Au/Fe_2O_3 catalysts, hence again we conclude that a $Au\text{-}O_x(OH)$-M species, where M: Na, Ce, Fe, etc., is the active site for the water-gas shift reaction. What M is does not matter, as was already concluded for the WGS reaction on Au-O-Ce and Au-O-Fe sites [1].

In summary, these findings are useful for the design of novel precious metal catalysts for the water-gas shift reaction in the absence of a reducible oxide support. With a clear identification of the active site, and ways to stabilize it under realistic operating conditions, only trace amounts of a noble metal will be needed for the next generation of highly active and stable catalysts for the water-gas shift reaction.

5.2 Recommendations

Based on the findings described in this thesis, gold on modified aluminum oxide support shows the potential of being prepared as an active catalyst for the WGS reaction. However, the long-term stability of gold-based catalysts in the reaction, and even with storage, is a lingering problem, limiting its industrial application. Thus, future work should focus on ways to stabilize the gold clusters and small nanoparticles to prevent deactivation during the reaction.

Gold mobility and agglomeration at high temperatures or in humid atmospheres result in loss of the gold active sites. The melting-point of gold particles depends on its size, and drops quickly for small nanoparticles < 5nm [2] (see Figure 5.1). Tsang and his group have introduced the reverse microemulsion technique to prepare Pt/CeO_2 core-shell structured catalysts [3] and compared the properties of platinum on ceria and encapsulated in ceria ($Pt@CeO_2$) [4]. Zaera and his group use dendrimers to control the metal nanoparticle size and deposit them inside the pores of SBA-15 silica support to improve their stability. They have also reported the prevention of metal nanoparticle migration and coalescence by using encapsulation and the "yolk-shell" structure for gold particles [5] , which achieve a special photocatalytic microreactor.

In order to stabilize the dispersed gold species on the alumina support, we may further coat the particles with a thin outer layer or shell for protection. Building a layer of a few nanometer thickness of oxide shell or another material can effectively prevent coalescence of the metal [6, 7]. Silica is widely reported in the literature as a shell material, and has been used to coat metals [5]. In the early part of this thesis, attempts to use the reverse microemulsion technique to prepare $Au@SiO_2$ were unsuccessful because of the

difficulty in controlling the rapid gold precipitation during the reduction step. In the literature we find successful preparations of $Au@SiO_2$ through colloid methods, where the gold colloids have been first prepared and then coated with a silica shell. However, this method results in big gold particle size (15-20nm) [8]. Since the desired gold ions and clusters have already been prepared on the surface of alumina supports, I propose that these surfaces are now further protected by the encapsulation method; alternatively, atomic layer deposition (ALD) techniques are recommended below to further protect the Au/Al_2O_3 catalyst.

An outer silica shell can be prepared through tetraethylorthosilicate (TEOS) hydrolysis, along with surfactant PVP (or TTAB, CTAB) as a capping agent. The desirable mesoporous structure of silica shell can be achieved through the PVP burning [9] or a sodium hydroxide etching procedure [5, 8] to increase the accessibility of active gold species to the reactant gases (see Figure 5.2). Meanwhile, additional sodium ions can be added through the porous shell to the gold catalyst. Alternatively, Al_2O_3 layers can be coated onto the catalyst particles by ALD, and proper heat treatment can effectively form a porous structure, as was demonstrated in a recent paper [13]. This additional alumina protection layer improves the coking- and sintering-resistance of a Pd-based catalyst [10] (see Figure 5.3). Here, we expect that the silica or alumina outer layers will improve the stability of gold nanoparticles against aggregation.

Many good results are expected from the recommended future work: (1) in heat treatment or in the reaction atmosphere, small gold clusters will be kept well dispersed under the protection layers; (2) during the NaOH-etching process, the liquid phase will bridge the gap and enhance the interaction between gold species and hydroxyl groups on

alumina support; (3) along with the sodium hydroxide solution flowing into the porous shell, the liquid phase will penetrate through the permeable silica and reach the gold-alumina catalysts core, this may leave residual sodium ions inside the shell and give a better contact with dispersed gold species. Here, different alkali ions (Na, K, Cs) will be considered in terms of their size and electronegativity to serve as Au-O_x(OH) promoters and stabilizers. An alkali-promoted ionic gold cluster associated with hydroxyl groups and immobilized inside the porous protection layers is the final goal in the design of active and stable gold catalyst configuration for the low-temperature water-gas reaction.

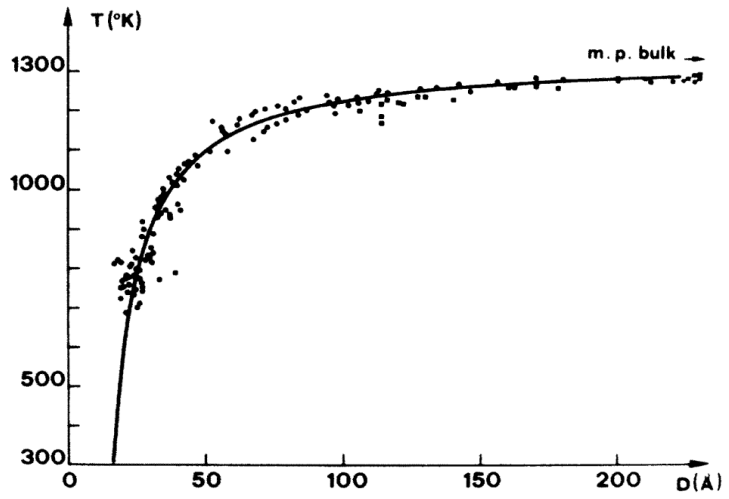

Figure 5.1 Experimental and theoretical value of melting-point of gold particles [2]

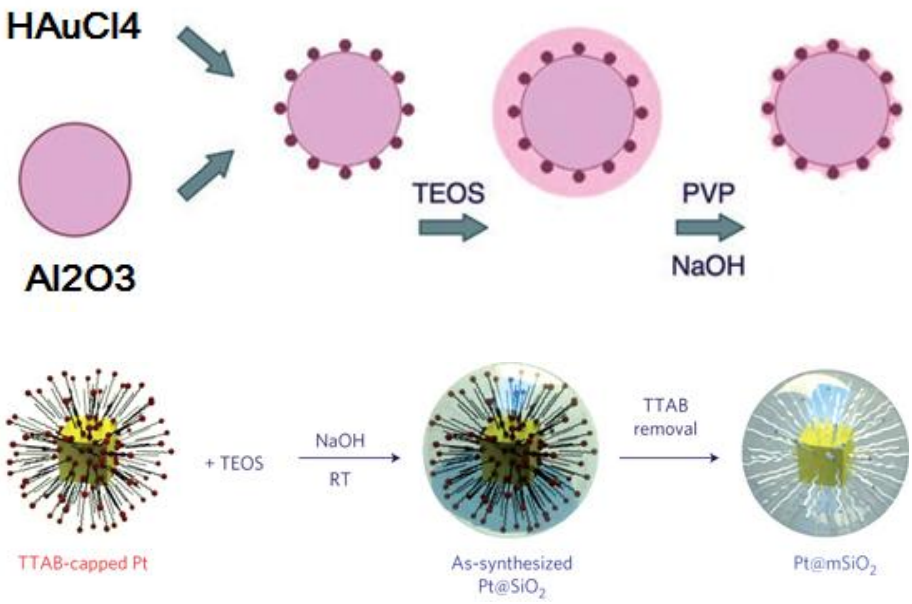

Figure 5.2 Schematic illustration of the mesoporous silica sphere preparation process [5, 9]

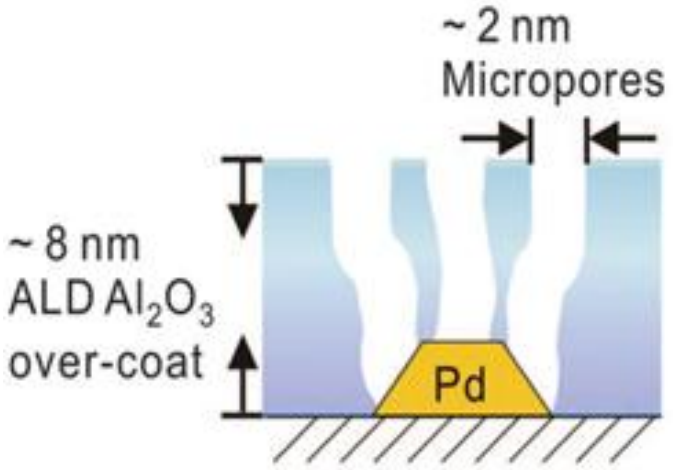

Figure 5.3 Schematic illustration of the porous alumina layers prepared by ALD process and calcination [10]

References

[1] W. Deng, C. Carpenter, N. Yi, M. Flytzani-Stephanopoulos, ***Topics in Catalysis*** 44 (2007) 199-208.

[2] P. Buffat, J.P. Borel, ***Physical Review A*** 13 (1976) 2287-2298.

[3] K.M.K. Yu, C.M.Y. Yeung, D. Thompsett, S.C. Tsang, ***Journal of Physical Chemistry B*** 107 (2003) 4515-4526.

[4] C.M.Y. Yeung, F. Meunier, R. Burch, D. Thompsett, S.C. Tsang, ***Journal of Physical Chemistry B*** 110 (2006) 8540-8543.

[5] I. Lee, M.A. Albiter, Q. Zhang, J. Ge, Y. Yin, F. Zaera, ***Physical Chemistry Chemical Physics*** 13 (2011) 2449-2456.

[6] C. Graf, D.L.J. Vossen, A. Imhof, A. van Blaaderen, ***Langmuir*** 19 (2003) 6693-6700.

[7] L.M. Liz-Marzán, M. Giersig, P. Mulvaney, ***Langmuir*** 12 (1996) 4329-4335.

[8] Q. Zhang, T. Zhang, J. Ge, Y. Yin, ***Nano Letters*** 8 (2008) 2867-2871.

[9] S.H. Joo, J.Y. Park, C.-K. Tsung, Y. Yamada, P. Yang, G.A. Somorjai, ***Nat Mater*** 8 (2009) 126-131.

[10] J. Lu, B. Fu, M.C. Kung, G. Xiao, J.W. Elam, H.H. Kung, P.C. Stair, ***Science*** 335 (2012) 1205-1208.